Summer 2015

Thermodynamic and chemical kinetic coupled modeling for the determination of cyclic combustion phasing in HCCI engines

Krishawn Michele Goodwin

Department:

THERMODYNAMIC AND CHEMICAL KINETIC COUPLED MODELING FOR THE DETERMINATION OF CYCLIC COMBUSTION PHASING IN HCCI ENGINES

by

KRISHAWN MICHELE GOODWIN

A THESIS

Presented to the Faculty of the Graduate School of the

MISSOURI UNIVERSITY OF SCIENCE AND TECHNOLOGY

In Partial Fulfillment of the Requirements for the Degree

MASTER OF SCIENCE IN MECHANICAL ENGINEERING

2015

Approved by

James A. Drallmeier, Advisor
Kelly O. Homan
Douglas A. Bristow

ABSTRACT

Homogeneous charge compression ignition (HCCI) is a low temperature combustion mode that contains great potential for decreasing emissions while increasing efficiency in internal combustion engines. The limitation is in that it is inherently difficult to control based on the lack of an external combustion trigger. This thesis outlines the potential of using the combustion residual species of carbon monoxide as a method of controlling the location of combustion by using data from a computer model. The model is a nonlinear five-state thermodynamic model that is coupled with a skeletal chemical kinetic model for PRF96. The model computes the amount of carbon monoxide within the cylinder during partial burn, which is when the engine is most difficult to control, and also calculates the amount of carbon monoxide residual that will be fed forward into the next cycle. The model is verified by comparing experimental data at the steady state and at the onset of partial burn collected from a Hatz 1D50Z engine located on the Missouri S&T campus. The impact of the carbon monoxide on the cyclic dynamics of the engine is observed through return maps displaying cyclic dependence generated by using data from the model. These return maps are created to determine the effects of the naturally produced amounts of carbon monoxide during partial burn, artificially increased amount of carbon monoxide during partial burn and complete combustion, and the effects of the intake temperature on several important engine parameters. These effects observed can be used to determine the relevance of using carbon monoxide as a control for HCCI.

ACKNOWLEDGMENTS

First, I would like to thank my advisor, Dr. James Drallmeier, for all of the time, effort, and support that he has provided me with. Without him, I never would have been provided such excellent opportunities to further my educational and professional career. I would also like to recognize the hard work of my graduate committee, Drs. James Drallmeier, Kelly Homan, and Douglas Bristow in the critiquing of this thesis, and in their desire and dedication to pass on their knowledge.

My friends and colleagues also deserve heartfelt thanks for the inspiration, support, and good times that they have provided me with. My partner in the engines lab, Allen Ernst, helped explain many things to me that significantly aided in my research. Furthermore, Jim Hoff aided with the answering of countless questions regarding verification of engine events and provided much expertise with the creation of testing apparatuses. Joshua Bettis, whose work I based this model off of, supported me through email correspondence. Several others, including Dave Macke and Jesse Hoemann helped me to better create intricacies within the code.

I would also like to thank my husband, Brandon Goodwin, for all of the moral support that he has provided me with during the entirety of this endeavour and many others.

Finally, I would like to thank my family for all the love and support that they have shown me throughout the years. Without the faith and determination that they instilled within me at a younger age, I never could have made it as far as I have. I am blessed beyond measure to have you all in my life.

TABLE OF CONTENTS

LIST OF ILLUSTRATIONS

LIST OF TABLES

NOMENCLATURE

Symbol	Description
ATDC	After Top Dead Center
BDC	Bottom Dead Center
BTDC	Before Top Dead Center
C_7H_{16}	n-Heptane
C_8H_{18}	iso-Octane
CA10	10% Heat Release Location in CAD
CA50	50% Heat Release Location in CAD
CA90	90% Heat Release Location in CAD
CFD	Computational Fluid Dynamics
CI	Compression Ignition
CO	Carbon Monoxide
EGR	Exhaust Gas Recirculation
EVC	Exhaust Valve Closing
EVO	Exhaust Valve Opening
HCCI	Homogeneous Charge Compression Ignition
IMEP	Indicated Mean Effective Pressure
IVC	Intake Valve Closing
IVO	Intake Valve Opening
LLNL	Lawrence Livermore National Laboratory
LHV	Lower Heating Value
LTC	Low Temperature Combustion
NO_x	Nitrogen Oxide
NVO	Negative Valve Overlap
OF	Overlap Factor
P_i	Pressure at State i
PM	Particulate Matter
PRF	Primary Reference Fuel
PRR	Pressure Rise Rate

RGI	Residual Gas Injector
SI	Spark Ignition
SOC	Start of Combustion
T_i	Temperature at State i
TDC	Top Dead Center
UTG	Universal Test Gas
V_i	Volume at State i
W_{ig}	Gross Indicated Work
α_e	Mass Fraction of External Residual
α_i	Mass Fraction of Internal Residual
α_{unb}	Mass Fraction of Unburned Residual
β	Percentage of Chemical Energy Lost to Heat Transfer
Γ	Molar Amount of CO
γ	Specific Heat Ratio
$\Delta\theta$	Combustion Duration
θ_{23}	Crank Angle Location of Combustion
θ_{SOC}	Crank Angle of SOC
ϕ	Equivalence Ratio

1. INTRODUCTION

1.1. HOMOGENEOUS CHARGE COMPRESSION IGNITION

Homogeneous Charge Compression Ignition, henceforth referred to as HCCI, is an emerging form of technology that could provide a solution to surpassing the increasingly stringent regulations on emissions and efficiency facing the automotive industry today. HCCI is a hybrid type engine that combines aspects from both Spark Ignition (SI) and Compression Ignition (CI) engines. The four-stroke process is initiated with the intake of a pre-mixed fuel and air charge followed by the compression of the mixture by the piston. A nearly instantaneous combustion occurs when the in-cylinder chemical properties attain the conditions necessary for ignition. The energy produced pushes the piston, generating work, followed by the occurrence of the exhaust stroke. HCCI is a Low Temperature Combustion (LTC) mode, which allows for a marked improvement in efficiency over SI engines along with a reduction in the amount of Particulate Matter (PM) and Nitrogen Oxide (NO_x) emissions when compared to CI engines [1]. HCCI is also beneficial to investigate because of the wide variety of fuel types that it can operate on including, but not limited to, gasolines, diesel fuels, and ethanols. Despite all of these benefits, HCCI is not without its challenges. One of the largest obstacles to be faced is the control of the Start of Combustion (SOC). There is no clear instigation of combustion by a spark or injection; it occurs when the chemical conditions are favorable. Factors that impact the chemical conditions are in-cylinder chemical composition, temperature, and pressure which change on a cyclic basis. Furthermore, HCCI is only stable in a limited operating range and can have high CO

emissions due to the low temperature at low loads being insufficient to complete the oxidation process [2]. The operating range is bounded by high pressure rise rates that threaten the structural integrity of the engine at the most advanced SOC timing, and a partial burn/misfire regime when the SOC timing is retarded [3]. The partial burn/misfire regime is characterized by high cyclic variation in output and product species. These obstacles have been approached in a number of ways which will be addressed below.

1.2. CONTROL METHODS

Several different methods of control have been investigated to determine how to best affect SOC, thus stabilizing the combustion process. Many methods use residual affected HCCI to increase the sensible energy of the mixture [4]. One method, Exhaust Gas Recirculation (EGR), can be used to affect both in-cylinder chemical composition and temperature. External EGR can be used to raise the temperature of the chemical mixture to advance SOC. Another method uses Negative Valve Overlap (NVO) to trap the exhaust gas in the cylinder by closing the exhaust valve before the piston reaches Top Dead Center (TDC) [1]. The control method of greatest significance for this study uses residual CO to affect SOC. Many studies have shown that CO has an accelerating impact on SOC [5-6]. Since the HCCI process results in higher CO emissions relative to conventional combustion [2], recycling this chemical by-product to positively affect engine operation would be beneficial. The timing advance of SOC caused by CO has potential to widen the range where stable combustion can occur. In order for this ability to be fully realized, cyclic variation of the in-cylinder properties must be understood, along with the exact effect of CO on the timing. Thus, an accurate model depicting the

cyclic variation of the in-cylinder chemical composition, temperature, and pressure especially during the onset of the partial burn/ misfire regime is necessary.

1.3. HCCI MODELING

Many different approaches have been taken by various scholars in order to model the HCCI process. Many models focus purely on the chemical kinetic aspect. Single and multi-zone models ranging from zero-dimensional to multi-dimensional with detailed chemistry have been used to investigate the chemical transformation and in-cylinder stratification that happens within the engine on a cyclic basis. Yao et al. describe these models and their distinct purposes in detail in their study [2]. Additionally, there are a variety of chemical kinetic mechanisms, from skeletal and reduced to highly detailed, that purely focus on the evolution of chemical species during the combustion process [7]. The mechanism of greatest importance in this case is the skeletal mechanism of Tsurushima [8] which considers the chemical kinetics of the combustion process of any Primary Reference Fuel (PRF). This model was selected for use because through its 33 species and 38 reactions, it accurately describes the chemical reaction without a heavy computational load, so that it can be paired with a thermodynamic model to evaluate the cyclic effect of CO on the start of combustion.

Other models focus on the control of the HCCI process in order to predict the thermodynamic states that the engine will attain. With the assumption of an instantaneous, constant volume combustion process, an ideal model can be used to estimate the in-cylinder thermodynamic properties [9]. A nonlinear model will be more indicative of the actual HCCI process, and can allow for a control model approach

whereas a CFD model would be computationally burdensome and unsuitable for real-time control [1]. The thermodynamic properties can be used in congruence with an Arrhenius reaction rate expression to calculate SOC thus determining whether the engine has attained complete combustion, partial burn, or misfire for each cycle [4].

It is the focus of this study to unite the skeletal chemical kinetic mechanism of Tsurushima [8] to a discrete time nonlinear five-state thermodynamic model described in detail in [4]. The intent is to create a model that can determine the amount of CO present in the cylinder during the partial burn regime based on when SOC occurs to predict the effect of the CO on the following cycle. This model will be validated by experimental data collected from the 1D50Z Hatz Engine at Missouri University of Science and Technology, with the purpose of evaluating CO as a form of control for HCCI.

In the next chapter, a thorough review shall be conducted on HCCI literature as it pertains to thermodynamic modeling and the effect of CO and explain why this current work is necessary for progress in this field. Chapter three will discuss the derivation of equations pertaining to the HCCI process and describe how the CHEMKIN code was coupled with the discrete-time nonlinear five-state thermodynamic model. It will further detail the residual gas fraction model, the onset of combustion model, and other key correlations. Chapter four will review the single cylinder 1D50Z Hatz assembly at Missouri S&T where the data is acquired for the model validation that will occur in chapter five. For this validation, the trends between the code and the acquired data will be compared and analyzed to demonstrate the capabilities of the model. A presentation and discussion of the results demonstrating the degree of control that the residual CO has on

the SOC will occur in chapter six, followed by a final chapter that summarizes the information presented here-in and proposes ideas for future work.

2. LITERATURE REVIEW

2.1. DISCOVERY AND DEVELOPMENT OF HCCI TECHNOLOGY

HCCI combustion was first researched in 1979 by Onishi et al. to increase the combustion stability of two-stroke gasoline engines [10] and was referred to as Active Thermo-Atmosphere Combustion. By 1983, the concept of HCCI had been applied to four-stroke engines [11], and it was noted that the combustion process was controlled by the in-cylinder charge composition, temperature, and pressure. From this point onward, researchers have been determined to develop a control method to improve the robustness of HCCI combustion to expand the operating regime so that this technology can be integrated into commercial applications.

2.2. CONTROL METHODS

Several different methods have been considered for the expansion of the operating regime with varying levels of success. One of these methods uses Negative Valve Overlap (NVO) to trap residual gases in the cylinder to influence the start of combustion during each subsequent cycle. In a study performed by Olesky et al. [12], NVO was used to explore the limits of HCCI combustion phasing in a single cylinder research engine operated with 87 octane research grade gasoline. Two separate engine sweeps of internal Exhaust Gas Recirculation (EGR) and intake air temperature were performed to determine the limits of operation and the effect on the Start of Combustion (SOC). It was found that with increased amounts of residual gas trapped in the cylinder, combustion phasing was advanced. A similar effect was noticed with increased intake air temperatures. However, the advancing effect of intake air temperature was relatively low

when compared to the effect of the trapped residual gas. This was credited to the higher thermal energy content of the residual gases. Thus, the conclusion was that cyclic feedback, as well as chemical and thermal effects of air dilution, has a significant impact on combustion behavior. A similar study conducted by Hellström et al. [13] analyzed cyclic variability in an HCCI engine with high residuals due to NVO. The main focus of the study was to investigate the dominant effects of cyclic evolution in a four cylinder HCCI engine. Initially, through symbolic time-series analysis, it was determined that combustion phasing is dominated by coupling between cycles and not between cylinders. The results of the experiment determined that cyclic variability is highly influenced by the amount of residual gas present in the cylinder.

Another method to control the auto-ignition process is through the use of external EGR. A study by Zhao et al. [14] examines external EGR and analyzes dilution, chemical, thermal, and charge heating effects. Dilution effects are defined by the reduction of inlet air available in the cylinder due to the presence of EGR. This reduces the specific heat capacity of the mixture which in turn affects the ignition timing and duration. The reaction of the combustion products present in the EGR with the freshly inducted mixture was evaluated as the chemical effect. The new chemical reactions occurring due to an altered chemical composition influence the ignition process. The thermal effect is identified by the rise in total heat capacity of the in-cylinder components due to EGR. The dilution, chemical, and thermal effects were evaluated together in this study, and it was found that they retard the ignition timing and lengthen the combustion duration. The thermal effects were the most dominant among these, because the temperature of the charge has a great impact on when the chemical reactions occur and

what products are created. The charge heating effect is defined as the increase in temperature of the intake charge due to the addition of hot EGR. This study determined that charge heating effects impact the subsequent combustion process by altering temperature requirements to reach full combustion. Overall, the study showed that hot EGR advances the start of combustion during the complete combustion regime. The partial burn and misfire regimes were not evaluated.

A third method considered by scholars for the control of the auto-ignition process is to have a dual mode engine by coupling SI with HCCI. A study by Yang and Zhu [15] discusses the difficulties with transitioning between these two modes and the control thereof. The challenges lie in the distinct operating parameters required for the two modes in combination with the cyclic dynamics during the transition period. The intent for the coupling of these two modes is to extend the boundaries of operation by switching from the more efficient HCCI to SI when instability starts to occur, e.g. cold start, high load, idle, etc. In order to accomplish this, many obstacles need to be overcome, especially considering that favorable thermodynamic conditions for one mode are adverse to the other. Therefore, the control mechanism used needs to be precise and have the capability of rapid adjustability. In this study, the goal was to switch from one mode to another without detectable torque fluctuation as measured by indicated mean effective pressure (IMEP). A multi-step mode transition was chosen so that the SI combustion could be used to increase the temperature of the unburned gas mixture to achieve HCCI combustion. The study determined that smooth transition between the two modes is achievable but there is a lack of controllability while in the HCCI mode that impedes improvement of IMEP fluctuation that can lead to misfire.

2.3. THE EFECT OF INDIVIDUAL SPECIES

Although much of the research in this field considers EGR as a control method as §2.2 demonstrates, up until recently very few articles cover the individual species that the exhaust gas is comprised of. EGR has been shown to affect the combustion process and ignition timing, but not every species therein has the same effect. Therefore it is imperative to determine which species plays the largest role to obtain more precise control of combustion so that the HCCI process can become more robust. The most prevalent species are CO_2, H_2O, N_2, O_2, and CO. There are also trace amounts of particulate matter (PM) and NO_x present, however in such small quantities they do not impact the chemical reactions that occur during the combustion process [6, 16]. Another exhaust gas species to consider is the amount of residual fuel present. This appears in increased amounts when a Negative Valve Overlap (NVO) strategy [12] is used, and the effects of this species are accounted for as will be shown in §3.2.1. Finally, there are transient products within the gas like short-chain hydrocarbons, aldehydes, alcohols, and other species that a recent study by Xie et al. [17] suggests have a role in advancing auto-ignition. However, for this work their effects are not further analyzed because the amounts at which they are naturally produced in the engine are small. A study completed by Anderlohr et al. [5] investigated the effect of CO, CO_2, and H_2O on the oxidation of the exhaust gases. The main focus of the study was to understand the reaction kinetics inside the exhaust line, and therefore the results of this study are very pertinent to external EGR. Since the thermodynamic conditions of the gases in the exhaust line apply to all residuals, these results can be used to estimate the condition of the internal EGR as well. Numerous simulations were run with various combinations of the three selected

species to determine the effect of each species alone and how they interacted with each other. For the case where all three species were simulated, ignition delays varied between 60 and 80 percent of the reference case as determined with pure N_2. Thus, a significant impact is caused by at least one of these species. In the mono-dilutant cases, CO and H_2O were determined to have much stronger accelerating effects than CO_2. It was also established that CO directly participates in and influences chemical reactions. Additionally, since N_2 was used in the reference case, it can be eliminated as a possible species that could be used to control auto-ignition. Another relevant study by Subramanian et al. [6] focused on the impact of CO and H_2 on the auto-ignition delay during HCCI combustion. In this work, the chemical species were added to the initial charge; they were not recycled from the exhaust gases as in the previous studies. The effects of these species on the intermediate reactions were examined using three separate detailed reaction mechanisms created by Lawrence Livermore National Laboratory (LLNL) and Department of Physical Chemistry of Reactions (DCPR) [6]. Additionally, it was observed that residual fuel in the cylinder had a less than 0.5% impact on ignition delay relative to the change in equivalence ratio, and therefore it can be considered as negligible. However, residual fuel is retained in the unburned residual part of the model for completeness, since although the effect on ignition delay is negligible, it is still a large component of the unburned residual. Another observation is that CO addition does not change the qualitative behavior of the ignition process; it only impacts the ignition delay. The reaction mechanisms show a 5-10% increase of the ignition delay when CO is added when the intake temperature is around 600 K. On the other hand, the mechanisms show a 20% decrease of the ignition delay time due to CO when the intake temperature is greater

than 1,000 K. These effects are less noticeable for a rich mixture, however the nature of HCCI is lean and therefore the rich case does not apply. The study observed that as the equivalence ratio gets leaner, CO has an increasing chemical impact on ignition delay. H_2 was discovered to increase ignition delay at temperatures between 600-1,000 K but has a negligible effect at higher temperatures. Furthermore, H_2 has the greatest effect in rich mixtures. Since the current work focuses on naturally produced products in lean combustion, H_2 is not pertinent to this study. Evidence supporting that CO_2 has a negligible effect is shown by He et al. [18]. Additionally, it is revealed that H_2O has a minimal effect on ignition delay time. The last major species that constitutes EGR is O_2. Zhao et al. [14] observed that while auto-ignition timing could be advanced with an increase in throttling, the engine efficiency is greatly reduced by this method due to pumping losses. Hence, CO is shown to have a significant impact on ignition timing with no currently observed detrimental effects and is chosen to be the species of interest in this current work.

2.4. THERMODYNAMIC AND CHEMICAL MODELING

There are many types of thermodynamic models that have been considered for the simulation of the HCCI process from simplified zero-dimensional thermo-kinetic models to complex multi-dimensional fluid mechanic models with coupled kinetics. The different varieties of modeling depend largely upon the intent of the study. Shaver [19] describes these different types of models in detail, and explains how when trying to develop a model suitable for control, a simplified model is best. It is necessary to include all important characteristics to create an accurate model but not extraneous data that would

create computational inefficiencies. Very few models have considered cyclic dynamics in residual-affected HCCI. Shaver [19] created a single-zone ten-state simulation model with cyclic coupling as a central focus by using a physics-based control approach. This model accurately captured the dependence of the system outputs (e.g. in-cylinder conditions, work output, exhaust gas temperature, etc.) on the controllable system inputs. Additionally, it captured cyclic coupling and ignition timing while maintaining a low computational expense. Shaver's model is based on an open system first-law thermodynamic analysis, using the mass flow model with steady state compressible flow relations. The model also includes an integrated global Arrhenius rate model to determine the ignition timing and has ten states that are used to define the system. Bettis [4] further developed Shaver's model by building off of the original model to create a discrete-time non-linear five-state thermodynamic model intended to be used for controller development. The non-linear model utilized fewer assumptions than the model presented by Shaver, and thus is more representative of the actual combustion process and can be controlled for a wider range of conditions. The model focused on gasoline-type fuels and captured the behavior of an engine that used pre-heated intake air with external EGR to achieve HCCI combustion. The model was validated against experimental data obtained from a single-cylinder compression ignition engine and was found to be capable of precisely tracking many parameters, including the start of combustion. Bettis' work did not include any effect from residual gases, and therefore Attebery [3] expanded the model to investigate the effects of the internally trapped residuals on the performance of an HCCI engine. This was accomplished by using a residual gas fraction approximation to calculate the amount of exhaust gases to be carried over to the next cycle and

subsequently evaluating the effects of cyclic variability. These effects could be examined to determine the applicability of using the internal gases as a potential control mechanism to extend the operation limits of HCCI combustion. Attebery concluded that the composition of the residuals produce a much larger effect on the next cycle than the temperature of the mixed fresh and residual species. With this verdict, Ernst [7] began work developing a chemical kinetic model in CHEMKIN using Tsurushima's [8] skeletal Primary Reference Fuel (PRF) with 33 species and 38 reactions. This simplified model was selected because of its low computational load while maintaining the integrity of a more intensive chemical kinetic mechanism. The focus of this study was to use this mechanism to calculate the amounts of each chemical species present during a PRF fueled HCCI combustion process.

2.5. JUSTIFICATION OF THIS WORK

Initially, a review was completed on the different types of control methods being considered in the field of HCCI in order to expand the operating regime so that this method of combustion may be used in commercial applications. It was shown that EGR, both internal and external, has a significant effect on cyclic variability observed in the combustion process and can influence the start of combustion (SOC). Additionally, a discussion was held on the coupling of HCCI with SI so that during the extreme load conditions which are detrimental to HCCI functionality, stability could be provided by switching engine modes. While this is a viable option, the authors of the study [15] noted that during HCCI mode the controllability was dismal. Therefore, it is important to focus on the potential control that EGR can provide.

Subsequently, it was noted that recent studies have started to delve into determining the effect of the individual residual gas species on cyclic variability. Out of the major naturally produced species, CO has been shown to have the most significant effect at levels similar to those produced during the partial burn regime. This alludes to a potential boon in that the higher CO levels typical of HCCI combustion, relative to conventional combustion [2], can be recycled through the engine to control instability and lower emissions.

Lastly, different thermodynamic and chemical models were introduced. Many models of varying degrees of complexity have been created to simulate the HCCI process. A simple linear physics based model intended as a controller was created by Shaver [19], and has been expanded by additional scholars [3,4] to be a discrete-time non-linear five-state thermodynamic model that considers the cyclic effect of residual gases on the combustion process. The relative simplicity allows for a computationally inexpensive model that still accurately tracks the characteristic properties of the combustion process. Therein lies the basis of the model created in this work. The expanded Shaver model will be coupled with the skeletal chemical kinetic mechanism used by Ernst [7] in order to capture the effect of residual CO on the cyclic variability of the HCCI combustion process. Additionally, the ignition timing will be adjusted for each cycle based off of the creation of CO through its relationship with CO_2. This completed model will then be verified with data collected from the single cylinder 1D50Z Hatz engine located in the Combustion and Spray Dynamics Laboratory at Missouri S&T.

3. FIVE-STATE THERMODYNAMIC AND CHEMICAL KINETIC MODEL

3.1. THERMODYNAMIC BASIS

3.1.1. HCCI Engine Process. The HCCI process shares many similarities with a typical four-stroke internal combustion engine cycle with only a few deviations from standard spark and compression ignition strategies. The cycle begins with the induction of a lean pre-mixed homogeneous fuel and heated air mixture at intake valve opening. External EGR can also be inducted into the cylinder in this phase depending on the capabilities of the experimental set-up. The fuel, air, and external EGR are combined with any internal residual remaining in the cylinder from the previous cycle. After the intake valve closes near bottom dead center, the piston begins compressing the mixture until thermodynamic conditions are such that combustion occurs. The combustion process is nearly instantaneous and no discernible flame front is produced [2]. The auto-ignition transpires approximately around top dead center. The piston is subsequently forced downwards, creating work. Towards bottom dead center the exhaust valve opens to allow the burnt mixture to be pushed from the cylinder while the piston is traveling back up during the exhaust stroke. Depending on the valve timing of the engine, some exhaust can be trapped in the engine due to Negative Valve Overlap (NVO) which is defined by the intake valve opening near top dead center before the exhaust valve has fully closed. This timing strategy can be used in HCCI to help influence the Start of Combustion (SOC) since this process lacks the external combustion trigger that is present in other internal combustion engine strategies.

The engine being considered for this study is a one-cylinder Hatz 1D50Z CI engine operating as an HCCI engine due to alterations to the piston that change the

compression ratio. The alterations to the piston [20] and the specifics regarding the experimental set-up are discussed in detail in Chapter 4. As mentioned above, the valve timing in addition to the engine geometry can be crucial to the combustion process, and therefore the model must take these into consideration in order to accurately capture trends in the engine. The values for these important parameters are further discussed in Chapter 4.

3.1.2. Thermodynamic Assumptions. In order to accurately predict the changes that occur cyclically within the engine, a solid foundation must be the basis upon which this model is built. Therefore, with this realization and the description of the actual process above, an ideal constant-volume combustion thermodynamic model can be used to simplify the four-stroke engine into a series of five thermodynamic states.

Although state one is typically defined as the induction process, in this model state one is the compression stroke because it is based off of a model that was designed to be used for non-linear control and thus must be capable of predicting future events by information present in the current state [4]. Since the inputs occur during the induction process, state five by this naming convention, each subsequent cycle can be determined using information from the previous one. This allows the model to meet the requirements of the neural network based feedback controller as presented in [21]. The first assumption is that the compression stroke during state one is isentropic (constant entropy), which is typical of ideal thermodynamic processes. The nearly instantaneous auto-ignition process is assumed to be isochoric (constant volume) and is captured in state two. For state three, the expansion and blow-down processes are assumed to be isentropic. During the exhaust and the subsequent induction strokes, states four and five respectively, the assumptions

are that the processes are adiabatic and maintain a constant pressure. These assumptions stem from the fact that the engine used in this study is naturally aspirated and that each stroke occurs on a small time scale. These assumptions can be verified in Chapter 5 of Heywood [9]. These states and their accompanying assumptions are summarized in Figure 3.1.

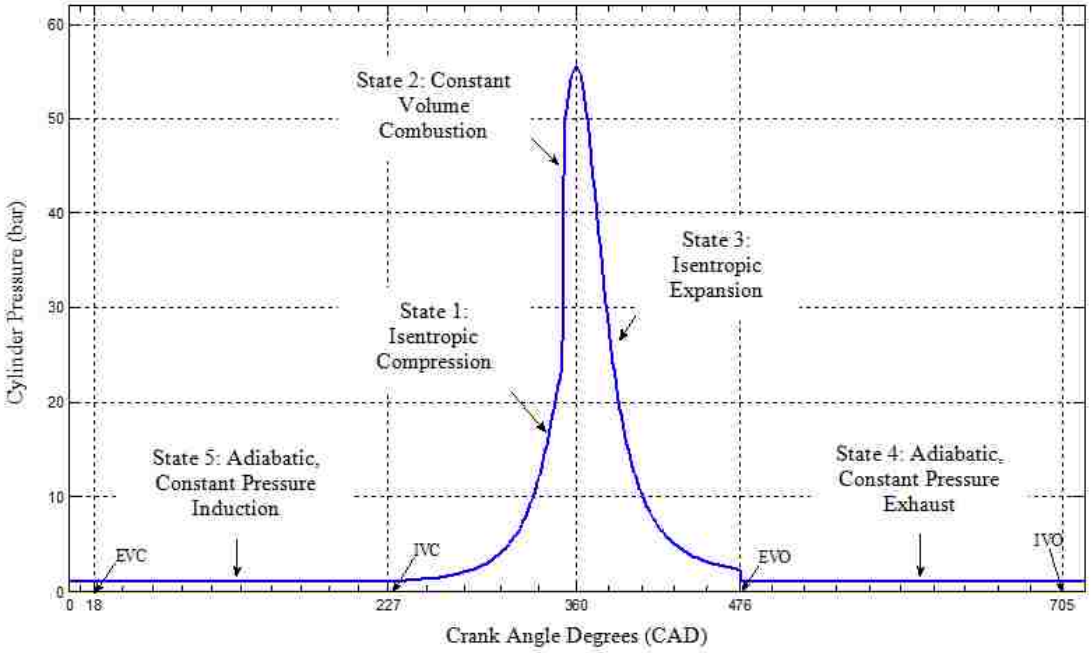

Figure 3.1. Five-State Thermodynamic Process Summary for the Hatz 1D50Z

Figure 3.1 shows the discrete process on which the remainder of the model can be built. These assumptions will allow for a mathematical representation of the progression of

events that occur within the engine for the purpose of evaluating the effects of cyclic coupling due to CO residual.

3.1.3. Inputs. There are three input values in the model that allow for the control of the engine due to their physical significance in the HCCI process [22]. The first of these input values is the intake temperature. This variable is represented by $T_{in,k}$ where k denotes the current engine cycle. The other two values are the mass fraction of external EGR, $\alpha_{e,k}$, and the flow rate of fuel in grams per minute, gpm_k. All of the inputs influence combustion timing by either temperature effects, as in the case of $T_{in,k}$, or dilution effects, as with $\alpha_{e,k}$ and gpm_k. It should be noted that external EGR is included for completeness of the model, but the results focused on in this work do not include the use of this feature.

3.1.4. Outputs. There are many outputs associated with this model that can help provide understanding for the events that are transpiring on a cyclic basis. The first of these output values is the crank angle degree where combustion occurs, as represented by $\theta_{23,k}$. In HCCI, this variable is desired to be accurately controlled so that the operating range can be extended by optimizing the combustion timing. Another important value to consider is the peak pressure, $P_{3,k}$. This value provides the basis for calculating the work, $W_{ig,k}$ which can be monitored so that optimization can occur. In order to maintain an acceptable operating range, the pressure rise rate PRR_k is another important output to consider. The pressure rise rate can determine if the integrity of the engine structure is threatened by the combustion process and if the noise levels are acceptable. The final output relates the work output to the fuel energy input, thus providing an efficiency term with which to monitor the cyclic variation of different test cases by. The efficiency for the k^{th} cycle is denoted by η_k.

3.1.5. State Variables. Since this model is based off of a model designed for controller development [4], it has retained the state variables necessary to update the next cycle based on information obtained in the current cycle. These states must be capable of describing the dynamics of the system in terms of the output variables. It is beneficial for the states to have physical significance for ease of monitoring how the process is affected by changes in the outputs. Therefore, in HCCI the states should be related to combustion. The first state variable is the mixture temperature at IVC, represented by $T_{1,k}$. This temperature can be used to predict the temperature at combustion and thus the thermodynamic condition in the cylinder. Another variable is the mass fraction of trapped residual, $\alpha_{tot,k}$. The residual from the previous cycle remaining in the cylinder contains CO which directly affects the combustion timing of the subsequent cycle. The final state variable considered is the crank angle degree of combustion, $\theta_{23,k}$, which was also determined to be an output.

Further details on the selection of these input, output, and state variables can be found in [4] and [22].

3.2. THERMODYNAMIC EQUATION DERIVATION

3.2.1. Chemical Balance Equation. The previous model as determined by Bettis [4] was developed using the fuel n-heptane, C_7H_{16}, checked with iso-octane, C_8H_{18}, and validated with a Universal Test Gas with a 96 octane rating (UTG96). In this investigation, in order to model the correct amount of CO residual within the engine, a Primary Reference Fuel (PRF) must be used in order to couple the chemical kinetic mechanism of Tsurushima [8] with the Bettis [4] model. Primary reference fuels are pure

research fuels consisting of only percentages of n-heptane and iso-octane by volume. Correspondence with Ernst [7] ascertained that the primary reference fuel to select should be based off of the octane index of fuels that had been successfully run on the Hatz 1D50Z previously. It was determined that PRF96, a fuel 96% iso-octane and 4% n-heptane by volume would be a sufficient surrogate to maintain similar combustion characteristics in engine performance.

In order to derive a chemical formulation for the primary reference fuel in terms of n-heptane and iso-octane with volume percentages known, a 100 mL solution was assumed. Using density and molar mass data from the API Technical Data Book [23], the number of moles of each fuel species was determined using Equation 3.1.

$$n = V * \rho * M \tag{3.1}$$

The number of moles can then be divided by the total number of moles. This is also known as the mole fraction. Thus, one total mole of fuel will be considered in the chemical balance. The stoichiometric chemical balance is seen in Equation 3.2.

$$0.955C_8H_{18} + 0.045C_7H_{16} + 12.4325(O_2 + 3.76N_2) \xrightarrow{yields} 7.955CO_2 + 8.955H_2O + 46.7462N_2 \tag{3.2}$$

From here onward the fuel terms will be represented as shown below.

$$PRF96 + 12.4325(O_2 + 3.76N_2) \xrightarrow{yields} 7.955CO_2 + 8.955H_2O + 46.7462N_2 \tag{3.3}$$

Additionally, accounting for the fact that HCCI is a fuel-lean process, the equivalence ratio ϕ can be added to the equation to adjust the terms as needed as well as an O_2 term on the products side. A caveat to this is that this study is trying to investigate the effect of CO on the ignition timing. Typically, in fuel-lean reactions there is no CO produced. But during the periods when the engine is in an unstable phase, there will be localized rich regions due to in-cylinder stratification [16, 24]. Therefore, a CO term will

be added that will only come into effect during incomplete combustion cycles by being equal to zero when complete combustion occurs. In order to ensure that the CO amount imported from CHEMKIN in §3.10.2 is in the same scale as the value calculated in the thermodynamic model, a scaling factor will be used as explained in §3.10.3. With all of these effects considered, Equation 3.3 becomes:

$$\phi PRF96 + 12.4325(O_2 + 3.76N_2) \xrightarrow{yields} (7.955 - \sigma)\phi CO_2 + 8.955\phi H_2O + 46.7462N_2 + \sigma\phi CO + \left[12.4325(1 - \phi) + \frac{\sigma\phi}{2}\right] O_2 \quad (3.4)$$

In Equation 3.4, ϕ is the equivalence ratio and σ is derived from the amount of CO imported from the chemical kinetic mechanism in the previous cycle and will be discussed in detail in §3.10.

In order to account for internal EGR, external EGR, and unburned residual, the reactant side of Equation 3.4 is modified to include the necessary terms as seen below.

$$\phi PRF96 + 12.4325(O_2 + 3.76N_2) + \alpha_i[(7.955 - \sigma)\phi CO_2 + 8.955\phi H_2O + 46.7462N_2 + \sigma\phi CO + \left[12.4325(1 - \phi) + \frac{\sigma\phi}{2}\right] O_2] + \alpha_e(\phi + 59.1787)N_2 + \alpha_{unb}\left(\phi PRF96 + 12.4325(O_2 + 3.76N_2)\right) \quad (3.5)$$

The fresh inducted charge is represented by the first two terms and the internal residual consists of the products from Equation 3.4 multiplied by the fraction of internal residual α_i. Likewise, the external EGR molar amount is multiplied by the fraction of EGR, α_e. The external EGR is represented by nitrogen only since nitrogen is an inert gas that will not affect combustion [4, 5], and it is the most prominent component in terms of amount when compared to the other EGR components. Furthermore, although the external EGR term is included in the chemical balance, the Hatz 1D50Z assembly from

which the experimental data will be obtained to validate this model does not currently have the capability of external EGR. Thus, the term is included not only to retain the accuracy of the prior model [19], but also to allow for this model to be used with testing systems that do have this ability. Finally, the species representing the unburned residual that is remaining in the cylinder is multiplied by the fraction of unburned residual α_{unb}. The method for determining α_{unb} is discussed in §3.3.2. The composition effect of including the unburned residual term is through the specific heat capacity of high temperature unburned reactants and not from properties of individual chemical species [3]. Even though the amount of fuel that is left in comparison to all other species after 10% of combustion has occurred is at minimum an order of magnitude smaller as can be seen in Figure 3.2, it is nevertheless retained.

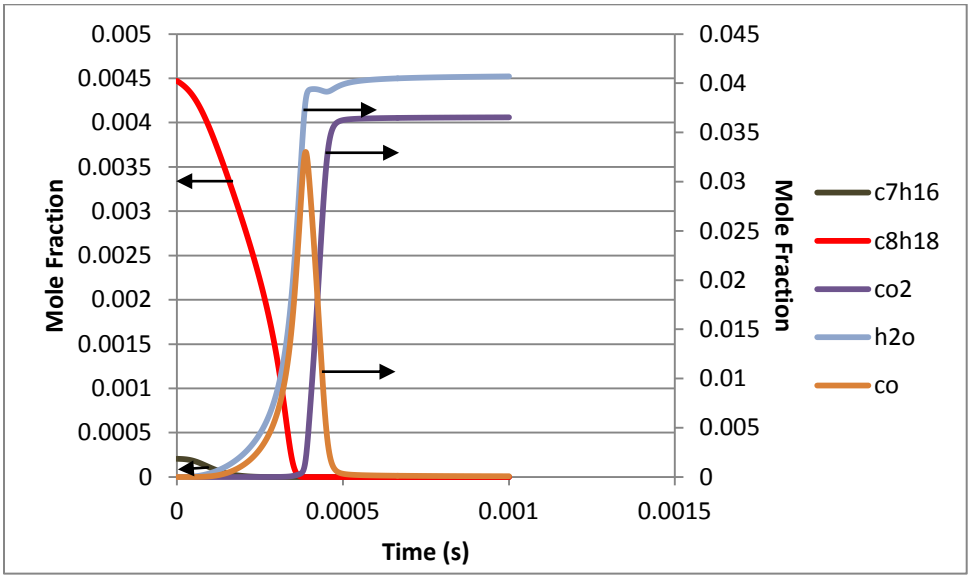

Figure 3.2. Molar Amounts of Primary Species during Combustion

Figure 3.2 was created using the chemical amounts calculated from the CHEMKIN code with inlet conditions of a fuel flow rate of 6 grams per minute (gpm), which is an equivalence ratio of 0.28, an atmospheric inlet pressure, and a temperature of 1050 K immediately after compression all of which are indicative of a stable operating point in the Hatz 1D50Z HCCI engine set up. Detailed information regarding the CHEMKIN model will be presented beginning in §3.9. In this figure it is important to note that the fuel species, which are highest on the left side and decrease as the time increases, use the primary axis on the left. The product species which increase as the combustion process occurs, with the exception of CO, are related to the right, secondary axis. For the purpose of elucidation, arrows have been added denoting the vertical axis that each curve belongs to. The nitrogen and oxygen terms are not pictured because they are much greater in magnitude than the other species and have been left off for clarity. It can additionally be seen that the amount of CO during the combustion process attains values comparable to those seen for the major products. The effect of CO on cyclic dynamics will be discussed in Chapter 6.

3.2.2. Adiabatic Induction. Now that the chemistry behind the thermodynamic process has been evaluated, the equations for the idealized cycle can be considered. The pre-heated air is mixed with fresh fuel and external EGR at atmospheric pressure, and these components are inducted into the cylinder when the intake valve opens. The first law of thermodynamics can be utilized to determine the state of the reactants upon mixing. Using T_{egr} and T_{in} as the temperatures of the external EGR and reactants respectively, and T_{prod} as the temperature of the products, internal EGR, and unburned

residual, Equation 3.6 can be used to form an expression for the temperature immediately before compression occurs.

$$\sum_{products} N_{i,k}\bar{h}_{i,k}(T_{prod,k}) + \sum_{reactants} N_{i,k}\bar{h}_{i,k}(T_{in,k}) + \sum_{EGR} N_{i,k}\bar{h}_{i,k}(T_{egr,k}) + \sum_{iEGR} N_{i,k}\bar{h}_{i,k}(T_{prod,k}) + \sum_{unb} N_{i,k}\bar{h}_{i,k}\left(T_{prod,k}\right) = \sum_{mix} N_{i,k}\bar{h}_{i,k}(T_{1,k}) \quad (3.6)$$

In this equation, $N_{i,k}$ represents the number of moles of species i during the current cycle k, $\bar{h}_{i,k}$ is the molar enthalpy of each species i, and $T_{1,k}$ is the temperature after each component has been completely mixed. Assuming that the molar enthalpy can be approximated using constant specific heats, the following formula is generated:

$$\bar{h}_i(T) = \Delta\bar{h}_{f,i} + \bar{c}_{p,i}\left(T - T_{ref}\right) \quad (3.7)$$

where $\Delta\bar{h}_{f,i}$ is the molar heat of formation of each species i, and T_{ref} is the reference temperature that corresponds to the heat of formation [4, 9]. By substituting Equation 3.7 into Equation 3.6 and applying it to Equation 3.5 at intake valve closing (IVC) immediately before compression begins, the in-cylinder mixture temperature can be found.

$$T_{1,k} = \frac{c_{1,k-1}T_{in,k-1} + c_{egr,k-1}\alpha_{e,k-1}T_{egr,k} + c_{2,k-1}\alpha_{i,k}T_{prod,k} + c_{unb,k-1}\alpha_{unb,k-1}T_{prod,k}}{c_{1,k-1} + c_{2,k-1}\alpha_{i,k} + c_{egr,k-1}\alpha_{e,k-1} + c_{unb,k-1}\alpha_{unb,k-1}} \quad (3.8)$$

In Equation 3.8, the c terms are molar averaged specific heats of the reactants, internal EGR, external EGR, and unburned residual and are used for simplification. They are respectively seen in Equations 3.9-3.12.

$$c_{1,k} = \phi_k\bar{c}_{p,PRF96,R} + 12.4325\bar{c}_{p,O2,R} + 46.7462\bar{c}_{p,N2,R} \quad (3.9)$$

$$c_{2,k} = \left[12.4325(1-\phi_{k-1}) + \frac{\sigma_{k-1}\phi_{k-1}}{2}\right]\bar{c}_{p,O2,P} + 46.7462\bar{c}_{p,N2,P} + (7.955 - \sigma_{k-1})\phi_{k-1}\bar{c}_{p,CO2,P} + \sigma_{k-1}\phi_{k-1}\bar{c}_{p,CO,P} + 8.955\phi_{k-1}\bar{c}_{p,H2O,P} \quad (3.10)$$

$$c_{egr,k} = (\phi_k + 59.1787)\bar{c}_{p,N2,E} \tag{3.11}$$

$$c_{unb,k} = \phi_{k-1}\bar{c}_{p,PRF96,U} + 12.4325\bar{c}_{p,O2,U} + 46.7462\bar{c}_{p,N2,U} \tag{3.12}$$

The subscripts R, P, E, and U on the specific heats represent the temperature of the reactants, products, EGR, and unburned residual so that the correct values can be used. Even though the temperatures vary by cycle and by set point, for defining the specific heat values the temperatures are assumed to be 430 K, 750 K, 300 K, and 750 K respectively. This helps for the model to track the trends as accurately as possible, without requiring a look-up table for the specific heat values adding to computational expense. The specific heat values can be found in [9], or calculated from [23] as is the case with PRF96.

At this point, it can be assumed that T_{prod}, the temperature of the residual, is directly related to the exhaust temperature of the previous cycle in a linear manner. The relationship is seen in Equation 3.13.

$$T_{prod,k} = \chi T_{5,k-1} \tag{3.13}$$

This relationship is a simple equation used to model heat transfer, using χ to represent the heat lost during valve overlap. Although a more complex model could be used, Shaver [19] demonstrates that this expression does a reasonable job of matching experimental observations while maintaining simplicity. The multiplier χ is determined by aligning the experimental intake temperatures with the exhaust temperatures calculated from the model [4]. For the PRF96 fuel being used in this study with the Hatz 1D50Z engine, the value for χ was determined to be 0.56. Substituting Equation 3.13 into Equation 3.8 produces a formula for the temperature of the mixture at IVC:

$$T_{1,k} = \frac{c_{1,k-1}T_{in,k-1} + c_{egr,k-1}\alpha_{e,k-1}T_{egr,k} + (c_{2,k-1}\alpha_{i,k} + c_{unb,k-1}\alpha_{unb,k-1})\chi T_{5,k-1}}{c_{1,k-1} + c_{2,k-1}\alpha_{i,k} + c_{egr,k-1}\alpha_{e,k-1} + c_{unb,k-1}\alpha_{unb,k-1}} \tag{3.14}$$

3.2.3. Isentropic Compression. Typical of ideal thermodynamic models, isentropic compression assumes an adiabatic, reversible process. For this model, compression begins immediately after IVC, when the fresh charge, external EGR, residual and unburned gases are completely mixed. Thus, the expressions shown in Equations 3.15 and 3.16 are applicable.

$$T_{2,k} = \left(\frac{V_1}{V_{23,k}}\right)^{\gamma-1} T_{1,k} \tag{3.15}$$

$$P_{2,k} = \left(\frac{V_1}{V_{23,k}}\right)^{\gamma} P_{1,k} \tag{3.16}$$

State one is defined to be the point immediately before compression at IVC. State two is after compression has occurred, right before the onset of combustion. $V_{23,k}$ is the volume at which combustion transpires for the cycle k, assumed to be constant because of the nearly instantaneous nature of combustion in HCCI. Another variable in the above equations to be discussed is γ, which represents the ratio of specific heats. For the fuel and air mixture used, this parameter is equal to 1.3, and although this number varies slightly throughout the combustion process, Heywood [9] verifies that it is acceptable to keep it as a constant.

P_1, T_1, and V_1 signify the pressure, temperature, and volume respectively as soon as the intake valve closes. The pressure is assumed to be atmospheric and the temperature is an input variable. The volume can be determined using slider-crank relations from [9], engine geometry, and the crank angle degree at which the volume is desired to be calculated. To determine V_1 the crank angle degree used would be IVC, and for V_{23} the crank angle degree at which combustion occurs, θ_{23} is used. The slider-crank relation can be seen in Equation 3.17.

$$V_{23,k} = V_c\left[1 + 0.5(r_c - 1)\left(R + 1 - \cos(\theta_{23,k}) - \sqrt{R^2 - \sin^2(\theta_{23,k})}\right)\right] \quad (3.17)$$

3.2.4. Homogeneous Constant Volume Combustion. Since HCCI combustion is typically very fast, the assumption of instantaneous combustion is justified. Auto-ignition is assumed to occur uniformly throughout the cylinder, and all in-cylinder heat transfer is assumed to happen during combustion. The location of combustion is determined by using trapezoidal integration to evaluate the Modified Arrhenius rate threshold model, and is discussed in further detail in §3.5. Rearranging the reactants from Equation 3.5 and assuming complete combustion with the inclusion of the unburned fuel and CO for when complete combustion does not occur, the combustion reaction is as follows:

$$(\phi_k + \alpha_{unb,k}\phi_{k-1})PRF96 + \left[12.4325(\alpha_{i,k+1}(1 - \phi_{k-1}) + \alpha_{unb,k} + 1) + \frac{\alpha_{i,k+1}\sigma_{k-1}\phi_{k-1}}{2}\right]O_2$$
$$+[46.746(1 + \alpha_{i,k+1} + \alpha_{unb,k}) + \alpha_{e,k}(\phi_k + 59.1787)]N_2 + (7.955 - \sigma_{k-1})\alpha_{i,k+1}\phi_{k-1}CO_2$$
$$+8.955\alpha_{i,k+1}\phi_{k-1}H_2O + \alpha_{i,k+1}\sigma_{k-1}\phi_{k-1}CO \xrightarrow{yields} [7.955(\phi_k + \alpha_{i,k+1}\phi_{k-1}) - \Gamma_k]CO_2 +$$
$$(\alpha_{unb,k}\phi_{k-1})PRF96 + \left[12.4325(\alpha_{i,k+1}(1 - \phi_{k-1}) + \alpha_{unb,k} + 1 - \phi_k) + \frac{\Gamma_k}{2}\right]O_2 +$$
$$[46.746(1 + \alpha_{i,k+1} + \alpha_{unb,k}) + \alpha_{e,k}(\phi_k + 59.1787)]N_2 + \Gamma_k CO + 8.955(\phi_k + \alpha_{i,k+1}\phi_{k-1})H_2O \quad (3.18)$$

In Equation 3.18, the fuel term on the products side of the equation has been assigned only the unburned residual term from the reactant side so that if combustion is complete, then there is no residual fuel considered. Additionally it is important to note that Γ is the imported value of CO from the CHEMKIN model, which would be zero in the case of complete combustion. It is necessary to note that upper case gamma, Γ, and lowercase gamma, γ, represent two distinct variables, with Γ being the molar amount of CO, and γ being the ratio of specific heats. Another important note is the exception to the naming

convention where the subscript k represents the current cycle. The $\alpha_{i,k+1}$ term also refers to the current cycle. The reasoning for this can be seen in Appendix B. In all other terms, k is the current cycle. Furthermore, in order for the equation to properly balance, it must be noted that:

$$\alpha_{i,k+1}\sigma_{k-1}\phi_{k-1} = \Gamma_k \tag{3.19}$$

As a check to ensure that this equation is properly balanced and is comparable to the combustion reaction seen in [4] on which this model is based, all $\alpha_{unb,k}$, σ_{k-1}, and Γ_k can be set to zero. It can clearly be seen that the equations have the same form with the only difference being the leading coefficients due to the fuel chemistry being different.

Once again, the first law of thermodynamics can be used to determine the state of the system after combustion has occurred. The analysis can use a closed system approach since the entire process happens in the cylinder with all valves closed. Thus, the first law equation applicable to this situation is:

$$\Delta U = Q - W \tag{3.20}$$

Since work, represented by W, is directly related to the change in volume and the combustion process is considered instantaneous, no work is produced during combustion. Making use of this knowledge in addition with the relation in [19] that models the amount of heat transfer as a percentage of the chemical energy available from the combustion reaction, Equation 3.20 becomes:

$$U_{2,k} = U_{3,k} + LHV_{PRF96}N_{PRF96}\beta \tag{3.21}$$

where U_2 and U_3 are the internal energies of the system prior to and after combustion, respectively, and β is the percentage of chemical energy lost to heat transfer during combustion. This term is set to 0.1, approximating the amount of energy lost to heat

transfer as seen in [9]. N_{PRF96} corresponds to the moles of fuel, and LHV_{PRF96} represents the lower heating value for PRF96. The lower heating value for this primary reference fuel is defined as seen in Equation 3.22.

$$LHV_{PRF96} = \Delta\bar{h}^{\circ}_{f,PRF96} - 7.955\Delta\bar{h}^{\circ}_{f,CO2} - 8.955\Delta\bar{h}^{\circ}_{f,H2O} \tag{3.22}$$

where $\Delta\bar{h}^{\circ}_{f}$ is the enthalpy of formation of each species and can be found in [9], or calculated from [23] as is the case with PRF96. Using Equation 3.22 in congruence with the ideal gas law, Equation 3.21 can be expressed in terms of enthalpy.

$$\sum_{2} N_{i,k}\bar{h}_{i,k} - N_{i,k}R_uT_{2,k} = \sum_{3} N_{i,k}\bar{h}_{i,k} - N_{i,k}R_uT_{3,k} + LHV_{PRF96}N_{PRF96}\beta \tag{3.23}$$

Using the chemical expression for the combustion reaction in Equation 3.18 and noting that the species summation for state two is the reactants side, and state three is the products side, an expression for the in-cylinder temperature immediately after combustion can be derived. This expression is shown in Equation 3.24.

$$T_{3,k} = \frac{\left(c_{1,k-1} + c_{2,k-1}\alpha_{i,k} + c_{egr,k-1}\alpha_{e,k-1} + c_{unb,k-1}\alpha_{unb,k-1} - R_uN_{2,k}\right)T_{2,k} + c_{3,k-1} + c_{5,k-1}T_{ref}}{c_{2,k-1}\alpha_{i,k} + c_{egr,k-1}\alpha_{e,k-1} + c_{unb,k-1}\alpha_{unb,k-1} + c_{4,k-1} - R_uN_{3,k}} \tag{3.24}$$

where

$$c_{3,k} = \phi_k\bar{h}^{\circ}_{f,PRF96} + \left(\Gamma_k - \alpha_{i,k+1}\phi_{k-1}\sigma_{k-1} - 7.955\phi_k\right)\bar{h}^{\circ}_{f,CO2} + \left(\alpha_{i,k+1}\phi_{k-1}\sigma_{k-1} - \Gamma_k\right)\bar{h}^{\circ}_{f,CO} - 8.955\phi_k\bar{h}^{\circ}_{f,H2O} - LHV_{PRF96}\beta \tag{3.25}$$

$$c_{4,k} = \left(7.955\phi_k + \alpha_{i,k+1}\phi_{k-1}\sigma_{k-1} - \Gamma_k\right)\bar{c}_{p,CO2} + \left(\Gamma_k - \alpha_{i,k+1}\phi_{k-1}\sigma_{k-1}\right)\bar{c}_{p,CO} + 8.955\phi_k\bar{c}_{p,H2O} + 46.7462\bar{c}_{p,N2} + \left[12.4325(1-\phi_k) + \frac{\Gamma_k}{2} - \frac{\sigma_{k-1}\phi_{k-1}\alpha_{i,k+1}}{2}\right]\bar{c}_{p,O2} \tag{3.26}$$

$$c_{5,k} = -\phi_k\bar{c}_{p,PRF96} + \left(7.955\phi_k + \alpha_{i,k+1}\phi_{k-1}\sigma_{k-1} - \Gamma_k\right)\bar{c}_{p,CO2} + \left(\Gamma_k - \alpha_{i,k+1}\phi_{k-1}\sigma_{k-1}\right)\bar{c}_{p,CO} + 8.955\phi_k\bar{c}_{p,H2O} + \left(\frac{\Gamma_k}{2} - \frac{\sigma_{k-1}\phi_{k-1}\alpha_{i,k+1}}{2}\right)\bar{c}_{p,O2} \tag{3.27}$$

$$N_{2,k} = (\phi_{k-1} + 59.1787) + \alpha_{i,k}\left(4.4775\phi_{k-2} + \frac{\sigma_{k-2}\phi_{k-2}}{2} + 59.1787\right) + \alpha_{e,k-1}(\phi_{k-1} + 59.1787) + \alpha_{un,k-1}(\phi_{k-2} + 59.1787) \tag{3.28}$$

$$N_{3,k} = 4.4775\left(\phi_{k-1} + \alpha_{i,k}\phi_{k-2}\right) + 59.1787\left(\alpha_{i,k} + 1\right) + \alpha_{e,k-1}(\phi_{k-1} + 59.1787) + \frac{\Gamma_{k-1}}{2}$$
$$+\alpha_{un,k-1}(\phi_{k-2} + 59.1787) \quad (3.29)$$

The c_3, c_4, and c_5 terms are all terms named for simplification of Equation 3.24. N_2 and N_3 represent the number of moles present in the cylinder prior to and after combustion, respectively. The k subscripts represent which cycle each parameter refers to, with k being the current cycle, k-1 being the previous cycle, and so forth. Additionally, T_{ref} is 298 K, the reference temperature which corresponds to the heat of formation.

The next equation to be discussed is the pressure at the instant of combustion. The pressure is found by applying the ideal gas law to states two and three, before and after combustion.

$$P_{3,k} = \frac{N_{3,k}}{N_{2,k}} P_{2,k} \frac{T_{3,k}}{T_{2,k}} \quad (3.30)$$

There is no volume term present because of the isochoric combustion process. Similarly, the gas constant terms cancel each other out, resulting in the above equation.

In an effort to ensure that Equation 3.30 has no pressure dependence to become one step closer to achieving the state-space control model, the terms in Equation 3.24 can be arranged to form an expression for T_2.

$$T_{2,k} = \frac{\left(c_{2,k-1}\alpha_{i,k} + c_{egr,k-1}\alpha_{e,k-1} + c_{unb,k-1}\alpha_{unb,k-1} + c_{4,k-1} - R_u N_{3,k}\right)T_{3,k} - c_{3,k-1} - c_{5,k-1}T_{ref}}{c_{1,k-1} + c_{2,k-1}\alpha_{i,k} + c_{egr,k-1}\alpha_{e,k-1} + c_{unb,k-1}\alpha_{unb,k-1} - R_u N_{2,k}} \quad (3.31)$$

Equation 3.31 along with Equation 3.16 can be substituted into Equation 3.30 in order to obtain an expression for the peak pressure for the current engine cycle.

$$P_{3,k} = \frac{N_{3,k}}{N_{2,k}}\left(\frac{V_1}{V_{23,k}}\right)^{\gamma} P_{atm}T_{3,k} *$$
$$\frac{c_{1,k-1} + c_{2,k-1}\alpha_{i,k} + c_{egr,k-1}\alpha_{e,k-1} + c_{unb,k-1}\alpha_{unb,k-1} - R_u N_{2,k}}{\left(c_{2,k-1}\alpha_{i,k} + c_{egr,k-1}\alpha_{e,k-1} + c_{unb,k-1}\alpha_{unb,k-1} + c_{4,k-1} - R_u N_{3,k}\right)T_{3,k} - c_{3,k-1} - c_{5,k-1}T_{ref}} \quad (3.32)$$

3.2.5. Isentropic Expansion. After the completion of combustion, the expansion stroke begins with the downward movement of the piston. During this stroke, useful work is produced. Maintaining the assumptions of the ideal model as described in Section 3.1.2, the expansion process is considered to be isentropic, and thus the following relations apply.

$$T_{4,k} = \left(\frac{V_{23,k}}{V_4}\right)^{\gamma-1} T_{3,k} \tag{3.33}$$

$$P_{4,k} = \left(\frac{V_{23,k}}{V_4}\right)^{\gamma} P_{3,k} \tag{3.34}$$

Very similar to Equations 3.15 and 3.16, V is indicative of volume, P of pressure, and T of temperature. The subscript 23 represents the occurrence of combustion, 3 is immediately after combustion but before expansion, and 4 is at the end of expansion prior to the opening of the exhaust valve. The volumes can be determined using the relation shown in Equation 3.17 with the appropriate crank angle degree.

3.2.6. Blowdown and Exhaust. Blowdown refers to the exhaust valve opening slightly before Bottom Dead Center (BDC) so that during the upward exhaust stroke the piston does not have to use work to counteract any remaining pressure in the cylinder. This process is assumed to be isentropic and allows for the exhaust stroke to occur entirely at atmospheric pressure. The following relation shown in Equation 3.35 is thus applicable.

$$T_{5,k} = \left(\frac{P_{atm}}{P_{4,k}}\right)^{\frac{\gamma-1}{\gamma}} T_{4,k} \tag{3.35}$$

State five represents the end of the exhaust stroke right at the point at which the intake valve opens before the induction process begins. Thus the engine cycle is completed and

the equation for the intake temperature of the next cycle can be determined. This update equation will be discussed in §3.8.

3.3. RESIDUAL GAS FRACTION MODEL

3.3.1. Valve Overlap. Residual gas has been shown to be an effective method of providing some control over the start of combustion in HCCI engines [17]. This is accomplished through a combination of temperature and dilution effects. Auto-ignition in HCCI heavily relies on chemical kinetics to occur. Thus, changes in the concentrations of the species from the dilution along with changes in temperature impact combustion timing. Since combustion timing is critical to the stability of the HCCI process, it is important to have an accurate model for predicting the residual gas fraction.

This model is based off of a popular model developed in [25], and the derivation is shown in [26]. The residual gas fraction model is constituted of two main parts, the first of which is the influx of exhaust gases during valve overlap, and the second is gas trapped in the cylinder at exhaust valve closing. The amount of residual due to the latter component can be approximated by only using knowledge about the compression ratio. However, the residual due to the first component is more intricate to estimate. Since the intake port is generally slightly below atmospheric pressure, the exhaust gases tend to flow back into the cylinder when the exhaust valve and intake valves are both open during NVO. The flow dynamics caused by this reversal of flow is complex to model, and thus a correlation for the valve overlap factor (OF) is necessary to properly estimate the amount of residual gas fraction caused by this phenomenon [25].

$$OF = \frac{1.45}{B}(107 + 7.8\Delta\theta_{ov} + \Delta\theta_{ov}^2)\frac{L_{v,max}D_v}{B^2} \tag{3.36}$$

In Equation 3.36, the engine geometry and valve timing are used to develop an approximation for the valve overlap factor (OF). B represents engine bore in mm, $L_{v,max}$ is the averaged maximum value of lift in mm, D_v is the valve inner seat diameter in mm, and $\Delta\theta_{ov}$ is the valve overlap in crank angle degrees. Thus, this expression can be used for engines where the geometry and timing are known.

Equation 3.36 can be used to help determine the total residual gas fraction, the expression for which is shown in Equation 3.37.

$$\alpha_{tot} = 0.401\frac{OF}{N}\left[1 - \exp\left(-4.78\left(1-\frac{P_i}{P_e}\right)^{0.7} - 153.8\left(1-\frac{P_i}{P_e}\right)^{4.5}\right)\right]\frac{P_e}{P_i}\frac{T_i}{T_e} + \frac{1}{r_c}\frac{P_e}{P_i}\frac{T_i}{T_e} \quad (3.37)$$

In the above equation, α_{tot} is the total residual gas fraction, OF is the valve overlap factor, N is the engine speed in revolutions/second, P_i and P_e are the respective intake and exhaust pressures in bar, T_i and T_e are the respective intake and exhaust temperatures in Kelvin, and r_c in the compression ratio. The first term in the correlation represents the contribution of the back-flow of exhaust gas during NVO to the amount of residual gas and the second term is the contribution from the gases trapped by the closing of the exhaust valve.

This model has been shown to maintain accuracy over a wide variety of intake pressures and engine speeds [26]. For most set-points, the residual gas fraction will be a small percentage of the entire in-cylinder mixture. The effect on the combustion timing will be greatest when there is no external EGR present. This is due to the dilution of the mixture and the impact on temperature. However, these effects are mostly unnoticed when external EGR is present. Since the amount of external EGR is much greater than the amount of residual gas, it will provide the dominant changes with the temperature and dilution of the mixture prior to combustion.

3.3.2. Unburned Residual. Since the residual gas fraction has a direct effect on both reactant concentrations and the temperature, it is an important parameter to consider when modeling combustion timing in an HCCI engine. Therefore, the accuracy of this model is imperative to capturing the cyclic effects that are occurring within the cylinder. The method for determining the amount unburned residual uses a linear scaling of the mole fractions of the reactants of the previous cycle between two crank angle limits [3]. These limits are identified as the crank angle where partial burn characteristics start to occur, θ_{PB}, and where complete misfire occurs, θ_{MF}. These limits are pictorially represented in Figure 3.3.

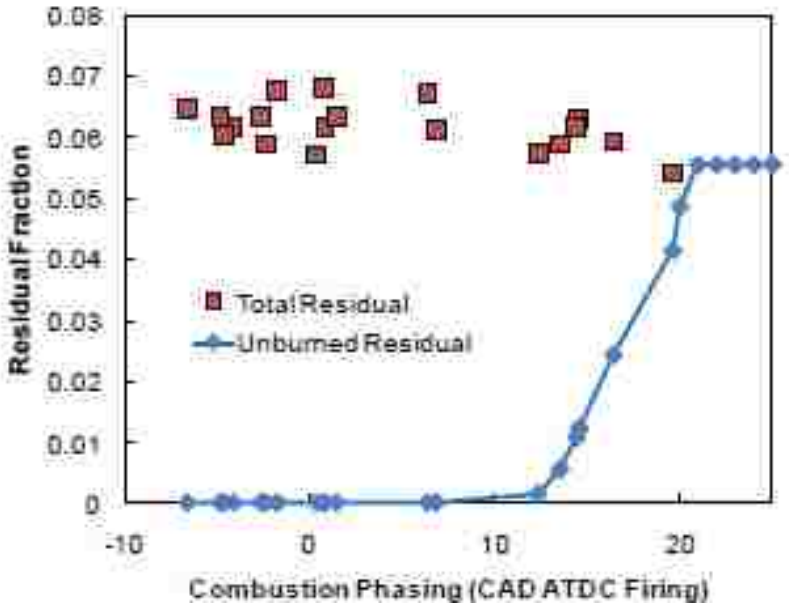

Figure 3.3. Residual Fraction Versus Combustion Phasing from the Model [3]

Created with data from the validated model in [3], the total residual fraction in this figure is represented by the red squares and is computed using the method discussed in the previous section. The blue line and diamonds show the unburned residual fraction. As combustion phases later ATDC, the unburned residual fraction linearly increases starting at the limit of partial burn and ending at the limit of misfire. When combustion occurs around TDC, no unburned residual is present due to complete combustion occurring. Similarly at misfire, the residual is comprised of only unburned residual and internal residual due to NVO since combustion does not occur. It can be seen that the θ_{PB} is at 373 CAD and θ_{MF} is 381 at CAD. These limits are taken directly from [3]. The model that they are taken from was derived for this experimental set-up at Missouri S&T, however, they were found using UTG96 instead of PRF96. Therefore, it is necessary to ascertain whether these limits are still accurate. Figure 3.4 can be used for this purpose.

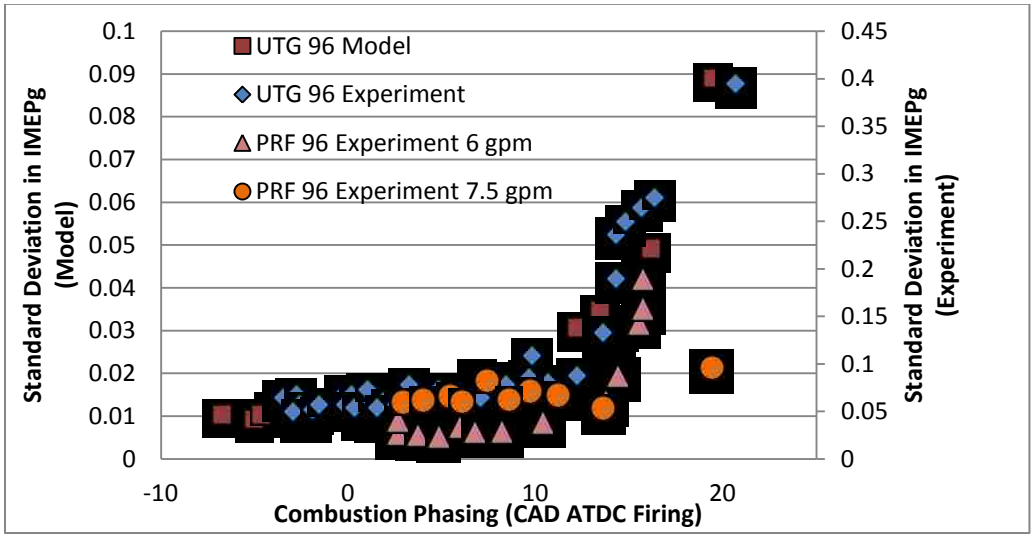

Figure 3.4. Standard Deviation in IMEPg Versus Combustion Phasing

Comparing the experimental data taken from the Hatz 1D50Z engine (represented by the diamond, triangle, and circle data points) shown in this figure, it is noticed that the same trend shown in the UTG96 data is followed for the 6 gpm PRF96 data with the first slight increase in standard deviation of IMEPg occurring around 373 CAD (13 CAD ATDC). Following this slight increase a very steep slope is noticed. The difference occurs in that the point of misfire is distinct in the UTG96 data at a later combustion phasing than the PRF96 at 381 CAD (21 CAD ATDC). On the other hand, the increase in slope doesn't appear to begin taking place in the 7.5 gpm data until closer to 380 CAD. Since limited data are available for the PRF96 fuel in the partial burn range close to the misfire limit, and the trends of the two PRF96 data sets show a delay as to when the increase in slope begins, the assumption is made that the misfire limit is extended beyond 381 to 390 CAD. The sensitivity and impact of this assumption is tested in §5.1.2.

The following equation set describes the linear relationship that governs the unburned residual model.

$$\alpha_{unb,k} = \begin{cases} 0 & \theta_{23} \leq \theta_{PB} \\ \alpha_{tot,k} * \left[1 - \dfrac{\theta_{PB} - \theta_{23}}{\theta_{MF} - \theta_{PB}}\right] & \theta_{PB} < \theta_{23} < \theta_{MF} \\ \alpha_{tot,k} & \theta_{23} \geq \theta_{MF} \end{cases} \tag{3.38}$$

In Equation 3.38, θ_{PB} represents the crank angle at the onset of partial burn, θ_{23} is the crank angle of combustion, θ_{MF} is the crank angle of misfire, α_{tot} is the mass fraction of total residual, and the subscript k denotes the current cycle. Thus, when complete combustion occurs, there is no unburned residual present, and when misfire occurs, all of the residual in the cylinder is unburned. Between these two limits a linear scaling is used which adequately approximates the amount of total residual that is unburned due to the timing of combustion being located within the partial burn regime.

3.3.3. Internal Residual. The term internal residual refers to the portion of the total residual that is comprised of the complete combustion products that are carried to the next cycle and not exhausted. The internal residual is calculated with the same angle limits that are used for unburned residual. For the case of complete combustion, all of the residual is regarded as internal residual. When the angle at which combustion occurs is past the misfire limit, there are no complete combustion products and therefore no internal residual. During the partial burn regime, the internal residual is the amount of residual that is left when all other forms of residual have been determined. These formulas are shown in Equation 3.39.

$$\alpha_{i,k+1} = \begin{cases} \alpha_{tot,k} & \theta_{23} \leq \theta_{PB} \\ \alpha_{tot,k} - \alpha_{unb,k} - \alpha_{e,k} & \theta_{PB} < \theta_{23} < \theta_{MF} \\ 0 & \theta_{23} \geq \theta_{MF} \end{cases} \tag{3.39}$$

In the above equation, α_{tot} , α_i , α_e , and α_{unb} are the total residual, internal EGR, external EGR, and unburned mass fractions respectively, and the θ terms are the angles discussed in §3.3.2.

3.4. DETERMINING MOLAR AMOUNTS AND EQUIVALENCE RATIO

To evaluate the molar amounts of each constituent within the cylinder, the total capacity of the cylinder must be defined. This capacity can be found using the ideal gas law as shown in Equation 3.40.

$$N_T = \frac{P_{in}(V_d + V_c)}{R_u T_{in}} \tag{3.40}$$

This expression captures the density effects by allowing the total number of moles inducted to vary as temperature fluctuates. Now that the capacity has been found, each constituent can be evaluated.

To determine the molar amount of air within the cylinder using partial pressures, the molar amount of residual components within the cylinder will first be determined. Due to valve overlap and engine geometry, a portion of the cylinder contents consists of trapped residual gas from the previous cycle. This amount of residual can be approximated by multiplying the fraction of internal residual by the total number of moles as seen in Equation 3.41.

$$N_{iEGR} = \alpha_i N_T \tag{3.41}$$

Another portion of the total cylinder volume is comprised of external EGR. With the interest of determining the number of moles of EGR inducted into the cylinder, the mole fraction of external EGR must be calculated first by using the expression

$$X_{EGR} = \frac{\alpha_e(\phi + 59.1787)}{(\phi + 59.1787)(1 + \alpha_e) + a_i\left(4.4775\phi + 59.1787 + \frac{\sigma\phi}{2}\right) + a_{unb}(\phi + 59.1787)} \tag{3.42}$$

where α_i, α_e, α_{unb} are the mass fractions of internal EGR, external EGR, and unburned residual respectively; ϕ is the equivalence ratio; and σ is the molar amount of CO carried from the previous cycle, all of which have been defined previously. The mole fraction of external EGR can be used to calculate the number of moles of EGR inducted into the cylinder as seen in the expression in Equation 3.43.

$$N_{EGR} = X_{EGR} N_T \tag{3.43}$$

Unburned residual is also present within the cylinder and this fractional amount is determined using the same method that was used for external EGR. First, the mole fraction needs to be calculated.

$$X_{unb} = \frac{\alpha_{unb}(\phi + 59.1787)}{(\phi + 59.1787)(1 + \alpha_e) + a_i\left(4.4775\phi + 59.1787 + \frac{\sigma\phi}{2}\right) + a_{unb}(\phi + 59.1787)} \tag{3.44}$$

Using the expression in Equation 3.44, the molar amount of unburned residual can be determined as shown below.

$$N_{unb} = X_{unb} N_T \tag{3.45}$$

Now that the various residual species have been accounted for, a main constituent of in-cylinder composition will be found. The molar amount calculated is the moles of fuel inducted per cycle which can be determined by the fueling rate as shown in Equation 3.46.

$$N_F = \frac{2\dot{m}_f}{N * MW_f} \tag{3.46}$$

In this equation, $\dot{m}_f$ is the fueling rate in grams/minute, N is the engine speed in revolutions/minute, and MW_f is the molecular weight of fuel.

Now, the remainder of the cylinder can be filled with fresh air. In favor of continuing to take in account the displacement effect of the residuals, the amount of air inducted should be calculated using partial pressures. When all of the contents of the cylinder are considered, the partial pressure expansion becomes

$$P = X_{EGR}P + X_{iEGR}P + X_{unb}P + X_A P + X_F P \tag{3.47}$$

Rewriting Equation 3.47 in terms of moles rather than mole fractions begets Equation 3.48.

$$P = \frac{N_{EGR}}{N_T}P + \frac{N_{iEGR}}{N_T}P + \frac{N_{unb}}{N_T}P + \frac{N_A}{N_T}P + \frac{N_F}{N_T}P \tag{3.48}$$

Dividing Equation 3.48 through by the pressure and multiplying by the total number of moles results in Equation 3.49.

$$N_A = N_T - N_{EGR} - N_{iEGR} - N_{unb} - N_F \tag{3.49}$$

This expression accounts for the displacement effect by allowing the number of inducted moles of air to vary based on the amount of residual and EGR within the system.

Another important parameter to be found is the amount of fuel required to attain stoichiometric conditions within the cylinder. Equation 3.49 is used in conjunction with the relationship for the stoichiometric F/A ratio to find the stoichiometric moles of fuel in Equation 3.50.

$$N_{Fs} = \frac{N_A MW_a \left({}^{F}/_{A}\right)_{stoic}}{MW_f} \tag{3.50}$$

Equations 3.49 and 3.50 allow the equivalence ratio to adjust slightly as temperature is altered by permitting the amount of air inducted into the cylinder to vary. This fluctuation is consistent with what is observed in the experimental data.

With the stoichiometric moles of fuel now known, the equivalence ratio for this cycle can be determined using Equation 3.51.

$$\phi_k = \frac{N_{F,k}}{N_{Fs,k}} \tag{3.51}$$

The model can now accurately predict the fresh amounts of fuel and air being inducted into the cylinder for each cycle and the equivalence ratio along with different types of residuals and EGR using the equations presented in this section by accounting for the density and displacement effects present within the system.

3.5. MODELING THE ONSET OF COMBUSTION

Since HCCI engines do not have an external combustion trigger unlike conventional spark and compression ignition engines and instead rely on chemical kinetics [2, 14], modeling the onset of combustion accurately is imperative to the model.

To do this, it is important to understand when the combustion process occurs. Auto-ignition occurs when the reactant concentrations and thermodynamic conditions reach adequate levels during compression. Therefore, combustion timing is directly related to the in-cylinder concentrations of the reactants, the temperature, and the pressure [2, 14]. The model predicting combustion timing, then, should take these characteristics into account to be appropriate for this endeavor.

3.5.1. Ignition Timing Model. Bettis [4] compared five different models for predicting the onset of combustion ultimately resulting in using an integrated Arrhenius rate model [27]. The Arrhenius rate model predicts combustion timing in addition to the pressure evolution within the cylinder. The pressure evolution directly correlates to the work output from the engine [4] which is one of the metrics that this model uses as an output. The combustion model was originally calibrated and validated for a lean reaction of air with gasoline-type fuels. Since HCCI uses a fuel lean strategy, the stoichiometric and fuel rich cases need not be evaluated. The verification of the combustion timing model was accomplished by comparing the simulated data to actual engine data from a Hatz 1D50Z HCCI engine. The engine geometry and other parameters can be found in Table 3.1. The experimental set-up is described in further detail in Chapter 4.

Table 3.1. Hatz 1D50Z Engine Parameters

Parameter	Symbol	Value	Units
Equivalence Ratio	Φ	0.38456	--------
Engine Speed	Ω	1800	RPM
Stroke	S	7	cm
Bore	B	9.7	cm
Connecting Rod Length	L_{conrod}	11.042	cm
Compression Ratio	r_c	14.5	--------
Intake Valve Opening	IVO	705	CAD
Intake Valve Closing	IVC	227	CAD
Exhaust Valve Opening	EVO	476	CAD
Exhaust Valve Closing	EVC	18	CAD
Valve Overlap	$\Delta\theta_{ov}$	33	CAD
Valve Diameter	D_v	32	mm
Valve Lift	L_v	8.912	mm

In the experiment, the equivalence ratio was held constant while the intake air temperature was varied in order to effectively change the ignition timing. These same testing conditions could be replicated in the model by setting the equivalence ratio to the desired value and changing the intake temperature value. Data was collected and compared at several different temperatures from the model and the experiment to show that the Arrhenius model was capturing the ignition timing sufficiently. The Arrhenius model uses a single global reaction rate to represent the overall combustion reaction. This is a simplification from reality, because the actual combustion process consists of numerous sub-reactions with hundreds of different steps. These steps are incorporated into the chemical kinetic portion of this model in §3.9 for determining the amount of CO produced cyclically; however, for the ignition timing model including all of these sub-

reactions creates a computational expense that is unnecessary due to the accuracy of this simplified model [4]. The Arrhenius rate is a physics based reaction rate that is typically used for individual reactions in complex models with detailed chemistry [4]. In this case, it relates the combustion reaction to the reactant concentrations and temperature within the cylinder. Due to these parameters having a dominant effect on HCCI combustion, the Arrhenius reaction rate has potential to estimate the ignition timing with high reliability. In mathematical terms, the model involves integrating a single Arrhenius reaction rate equation [27] from the crank angle degree of intake valve closing to the crank angle degree where combustion occurs. These integration limits are chosen because all appreciable reactions start when compression begins and end at the onset of combustion, since combustion is assumed to be instantaneous. This expression can be seen in Equation 3.52.

$$F_{des} = \int_{IVC}^{SOC} \left(\frac{A \exp\left(-E_a/R_u T\right) [fuel]^m [O_2]^n}{\omega} \right) d\theta \tag{3.52}$$

Equation 3.52 includes concentration terms for the fuel and oxygen in the reactants, $[fuel]$ and $[O_2]$ respectively. The concentrations can be determined by using the representative balanced chemical equation for PRF96 shown in Equation 3.4. ω represents the engine speed in rad/sec and T is temperature at the beginning of compression [4]. The remaining constants A, E_a/R_u, m, and n are empirical parameters [4] that are determined from combustion kinetics experiments [28] for various types of fuels. This study focuses on PRF96 as a fuel since gasoline-type fuels eliminate the

complexities associated with low temperature heat release and because the chemical kinetic mechanism described later in §3.9 requires the use of a primary reference fuel.

With the focus of this current study being to identify the influence of the amount of CO on the cyclic dynamics of the engine, the Arrhenius rate model selected by Bettis was modified so that the CO would have a direct effect on the ignition timing model. Thus, Equation 3.53 was used.

$$CO_{2,cr} = \int_{IVC}^{EOC} \left(\frac{A \exp\left({}^{-E_a}/_{R_u T} \right) [CO_2]}{\omega} \right) d\theta \tag{3.53}$$

Equation 3.53 includes concentration terms for the carbon dioxide in the products, $[CO_2]$. This concentration can be determined by using the representative balanced chemical equation for PRF96 shown in Equation 3.18. ω represents the engine speed in rad/sec and T is temperature at the beginning of compression [4]. The remaining constants A, E_a, and R_u are empirical parameters [4] that are determined from combustion kinetics experiments [28] for various types of fuels.

The Arrhenius rate parameters corresponding with PRF96 are seen in Table 3.2. Since PRF96 is 96% iso-octane, C_8H_{18}, and 4% n-heptane, C_7H_{16}, by volume, the Arrhenius rate parameters for the former are used. Between the two, the only value that varies is the pre-exponential Arrhenius factor, A, and it differs by about ten percent. The sensitivity of the model to this factor will be tested later in §5.1. The combustion parameters in Table 3.2 below can be substituted into the model to estimate the onset of combustion.

Table 3.2. Combustion Parameters for Integrated Arrhenius Rate [28]

Parameter	Symbol	Value	Units
Integrated Arrhenius Rate Parameters	A	4.6×10^{11}	$(mol/cm^3)^{1-m-n}/s$
	E_a/R_u	15,098	K

In essence, this Modified Arrhenius rate expression uses all of the same components that the original Arrhenius rate equation does, except that it substitutes the molar amount of CO_2 instead of the molar amount of fuel and O_2 and the upper limit of integration was changed to be the End of the Cycle (EOC), 720 CAD, so that the integration could be stopped whenever the desired amount of carbon dioxide was created as further described with the next two equations. Therefore, instead of ignition occurring when the necessary amount of fuel has been destroyed, the model is now based on the amount of CO_2 created. This distinction is important, because the molar amount of CO_2 is dependent upon the amount of CO produced, as shown in Equation 3.54.

$$CO_{2,cr} = \int_{IVC}^{EOC} \left(\frac{A \exp\left(-E_a/R_u T\right)\left[7.955\left(\phi_k + \alpha_{i,k+1}\phi_{k-1}\right) - \Gamma_k\right]}{\omega} \right) d\theta \qquad (3.54)$$

The expression in the square brackets is reduced by the quantity of CO produced in that cycle, as indicated by the term representing the molar amount of CO, Γ. Now that the ignition timing model has been defined, it is important to align the results of the model with the experimental data.

In order for the Arrhenius rate expression to be able predict the ignition timing at various inlet conditions, it needs to be initialized at an experimental data point. To enhance the focus on the partial burn/misfire regime, the point at which this expression is initialized was selected to be the most retarded of the data points collected from the Hatz 1D50Z engine operating on PRF96, thus closest to the partial burn regime. This point is at an intake temperature of 467.1809 K at a fueling rate of 9 gpm. This yields a start of combustion at 365.2 CAD. The threshold value, which represents the point at which combustion begins was then adjusted in the code until the start of combustion angle matched the experimental data for the inlet conditions. The threshold value, denoted by K_{th}, that coincides with these conditions can be seen in Equation 3.55 below.

$$K_{th} = 0.00334 \tag{3.55}$$

With the threshold established, the model can be used to approximate the start of combustion angles for the other inlet conditions tested experimentally. This is accomplished by evaluating the Modified Arrhenius rate expression by trapezoidal integration and comparing the integrated value at each step with the threshold value to determine the start of combustion. The resulting start of combustion values can be recorded to determine correlation between the model and experimental data. These results are shown in Figure 3.5.

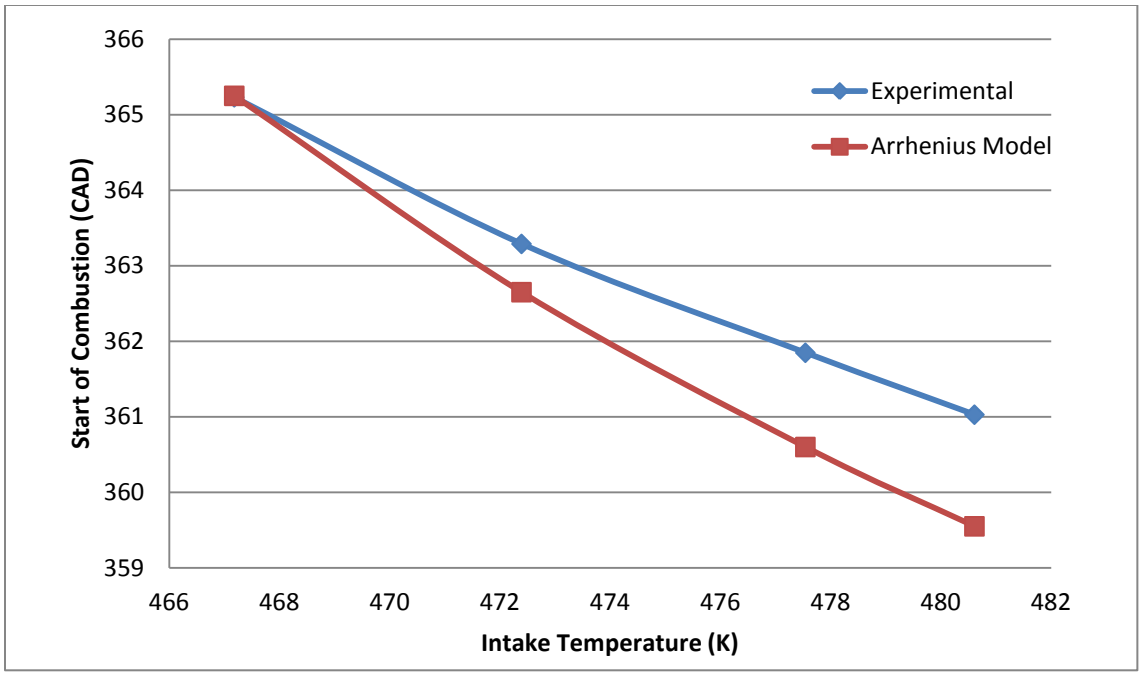

Figure 3.5. Integrated Modified Arrhenius Rate Combustion Tracking (9 gpm)

Figure 3.5 shows that the Modified Arrhenius Rate model does an adequate job of predicting when the start of combustion occurs. The correct trend is produced from the model, and the magnitudes are within 1.5 CAD over a nearly 14 degree Kelvin increase in the intake temperature. Since the partial burn/ misfire regime occurs within a few crank angle degrees and because the model was initialized at the most retarded ignition timing, the start of combustion will be closely approximated for the conditions of partial burn. Additionally, the robustness of the model, evidenced by the availability of combustion parameters, makes it easily able to approximate other fuels. The sensitivity of the Modified Arrhenius Rate model will be tested in §5.1.

3.6. VARIABLE Δθ CORRELATION

Although HCCI combustion occurs quickly, it is not perfectly instantaneous. Therefore, a finite amount of time for combustion must be accounted for within the model. The model as it currently stands is discrete in nature and assumes a constant volume combustion process. To address this phenomenon, the point of instantaneous combustion has been shifted in the model from SOC to a point of very high energy release based on experimental heat release data by a variable Δθ correlation. This Δθ represents the crank angle degrees between SOC and experimental CA50, which is the crank angle where 50 percent of the total heat release has occurred as shown in §4.2.5. Previously, HCCI models have included a similar term accounting for the finite nature of combustion [27] that was held constant for each engine set point. However, more recently it has been shown that experimental data suggests that the term varies with engine set point [4]. The development of a multivariable correlation was based on a model that related Δθ to chemical kinetics through SOC, the temperature at SOC, and reactant concentrations. All three of these variables were deemed necessary to maintain the highest accuracy in the prediction of the Δθ value as compared to experimental data obtained from the Hatz. This conclusion is illustrated in Figures 3.6 and 3.7.

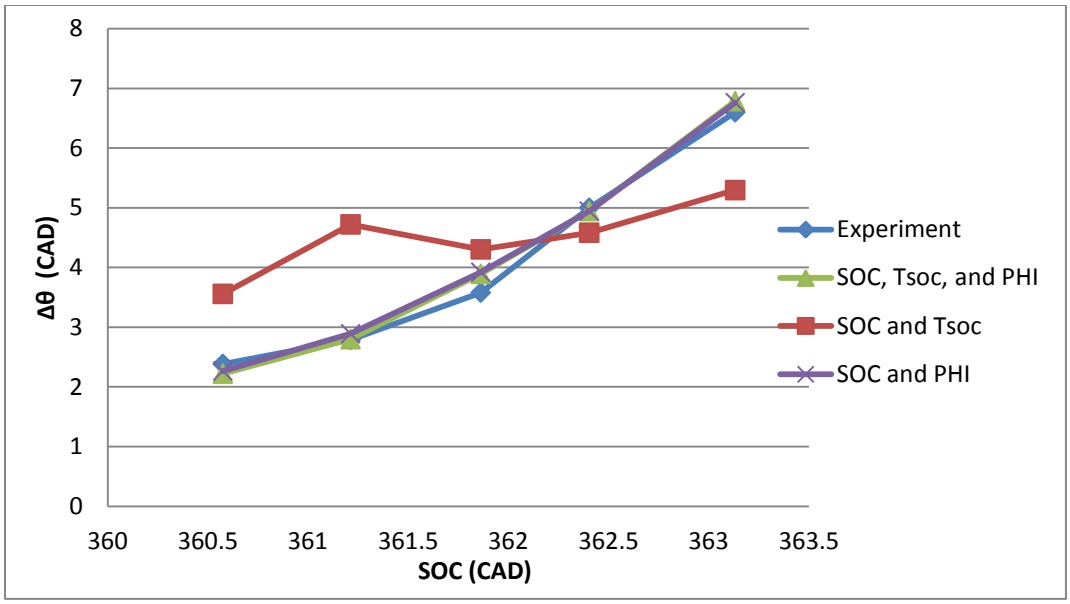

Figure 3.6. Comparison of Δθ Between Experiment and Correlation Variants using PRF96 at 7.5 gpm

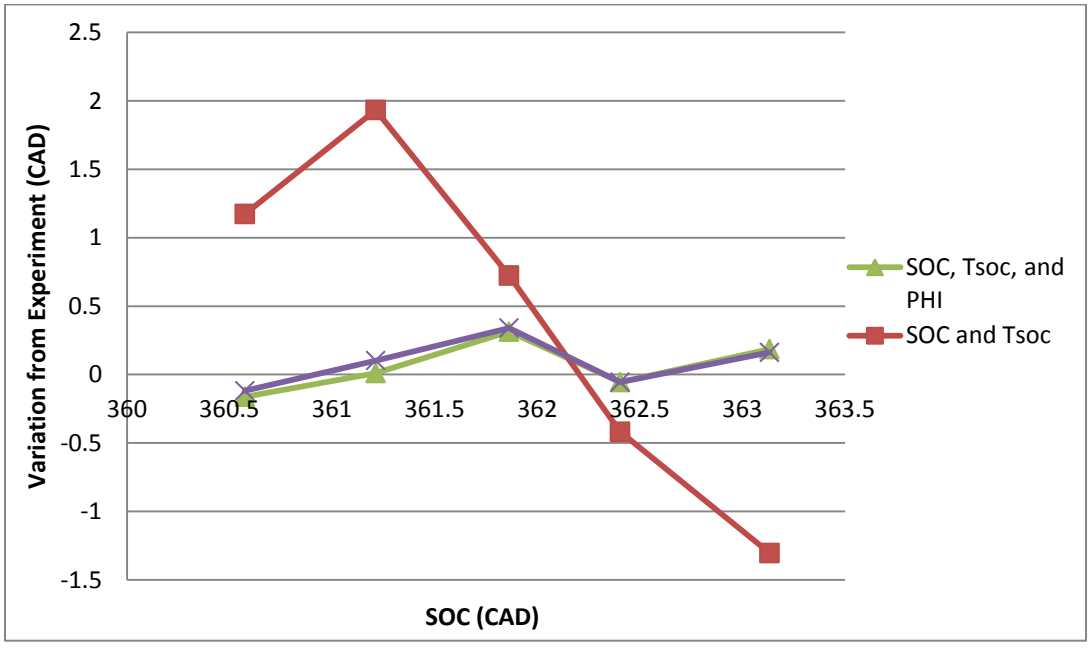

Figure 3.7. Comparison of Variation of Predicted Value from Experimental Data with Correlation Variants using PRF96 at 7.5 gpm

Figure 3.6 shows the three different correlations as compared to the experimental data at a flow rate of 7.5 grams/minute (gpm). It can be quickly observed that the correlation the only uses SOC and T_{SOC} is much less accurate than the other two. The difference from the experimental data with these variables can be further observed in Figure 3.7 which shows the difference of the predicted $\Delta\theta$ value from the experiment. The other two correlations much more accurately predict the experimentally obtained $\Delta\theta$ value, with a slight favor towards the three variable correlation. Additionally, since the three variable method of $\Delta\theta$ correlation was used in [4] which is the basis for this model and the accuracy differences are minute, this is the one that was selected. Using the experimentally obtained data, Equation 3.56 was developed using the variable parameters of SOC, T_{SOC}, and PHI.

$$\Delta\theta_{k+1} = \left[3.38 \times 10^{-55}(0.0001665)^{\phi_k}(0.99844781)^{(V_1/V_{soc,k+1})^{\gamma-1}T_{1,k+1}}(1.43866189)^{\theta_{soc,k+1}}\right] \quad (3.56)$$

Further testing of the accuracy of this correlation, by substitution of experimental values into the expression in Equation 3.56 yields the results in Figure 3.8.

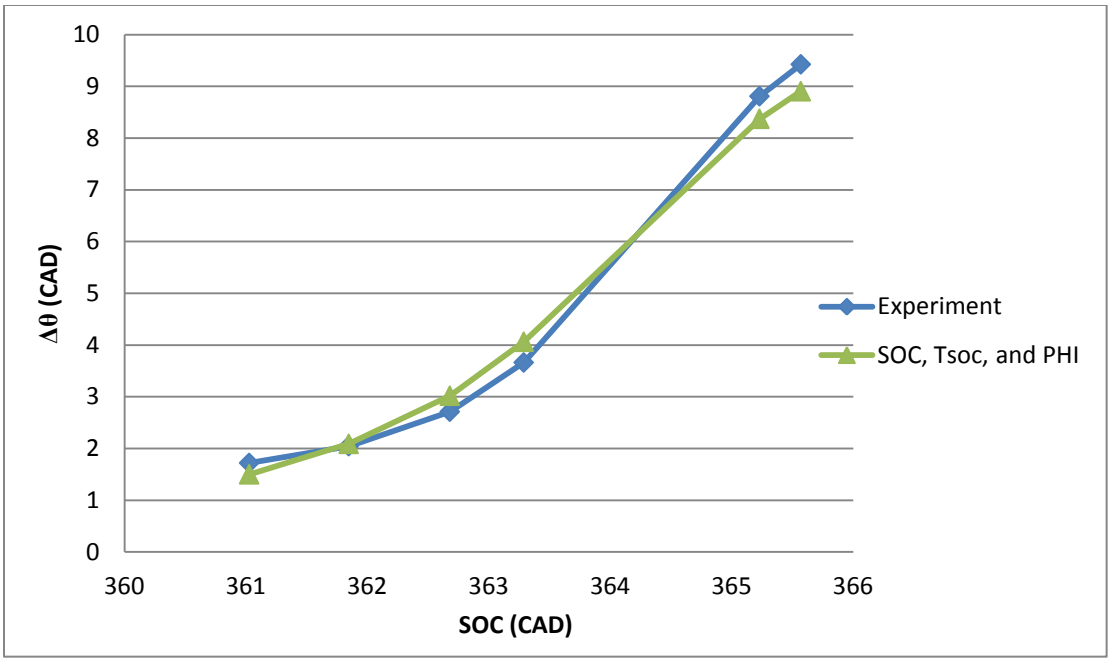

Figure 3.8. Comparison of Δθ Between Experiment and Correlation using PRF96 at 9 gpm

Figure 3.8 demonstrates that the multivariable correlation in Equation 3.56 respectably predicts Δθ as the intake temperature and fueling rate vary. Thus this expression is important to include in the model so that the peak pressure and CA50, which are dependent upon combustion timing and duration, can be more accurately predicted. Further demonstration that the variable correlation is better than a constant Δθ value is shown in [4].

3.7. CONTROL MODEL OUTPUTS

3.7.1. Angle of Constant Volume Combustion – θ_{23}. The determination of the location of combustion is one of the most critical pieces to the HCCI engine cycle, and thus the majority of the assumptions made revolve around this factor. The combustion timing model selected was the Modified Arrhenius Rate as previously mentioned. Modified to determine the amount of carbon dioxide created instead of the amount of fuel destroyed, the expression shown in Equation 3.57 is the culmination of these assumptions. Thus, the start of combustion occurs when a predetermined amount of carbon dioxide has been created as defined by the threshold value used to benchmark this expression to the experimental data as described in §3.5.1.

$$CO_{2,cr} = \int_{IVC}^{EOC} \left(\frac{A \exp\left({}^{-E_a}/_{R_u T} \right) \left[7.955\left(\phi_k + \alpha_{i,k+1} \phi_{k-1} \right) - \Gamma_k \right]}{\omega} \right) d\theta \qquad (3.57)$$

Equation 3.57 is evaluated by the trapezoidal method of integration over the crank angle degrees from IVC to EOC at half angle intervals. The total is summed until the threshold is reached. The model then records the index of this angle as the location of the start of combustion. Joining this with the information that was presented in §3.6 that the point of instantaneous combustion has been shifted in the model from SOC to a point of very high energy release based on experimental heat release data by a variable Δθ correlation, Equation 3.58 displays the output equation for determining the angle where constant volume combustion occurs.

$$\theta_{23,k} = \theta_{SOC,k} + \Delta\theta_k \qquad (3.58)$$

3.7.2. Peak Pressure. Keeping with the control model from which this model is derived from, peak pressure needs to be defined using only the inputs and state variables within the system. To accomplish this, Equations 3.15 and 3.24 were substituted into Equation 3.32 to create a nonlinear dynamic expression for the in-cylinder peak pressure.

$$P_{3,k} = \frac{N_{3,k}}{N_{2,k}} P_{atm} \left(\frac{V_1}{V_{23,k}}\right) * \frac{c_{3,k-1} + \left(c_{1,k-1} + c_{2,k-1}\alpha_{i,k} + c_{egr,k-1}\alpha_{e,k-1} + c_{unb,k-1}\alpha_{unb,k-1} - R_u N_{2,k}\right)\left(\frac{V_1}{V_{23,k}}\right)^{\gamma-1} T_{1,k} + c_{5,k-1}T_{ref}}{\left(c_{2,k-1}\alpha_{i,k} + c_{egr,k-1}\alpha_{e,k-1} + c_{unb,k-1}\alpha_{unb,k-1} + c_{4,k-1} - R_u N_{3,k}\right)T_{1,k}} \quad (3.59)$$

Equation 3.59 relates the peak pressure, P_3, to the state variables and inputs resulting in this output formula. It can be seen that the peak pressure is dependent on combustion timing through the volume at which combustion occurs, V_{23}.

3.7.3. Pressure Rise Rate. If ignition timing becomes too advanced, there is a risk of large amounts of energy being released due to the nearly instantaneous ignition of a homogeneous mixture in HCCI combustion. This energy is released during the compression stroke, where the piston is traveling upwards, opposing the downward force. This can generate high levels of combustion noise which over time could cause damage to the engine [2, 16]. Therefore, a threshold for the pressure rise rate is typically established to prevent the engine noise, known as ringing, from becoming excessive. This limit is generally accepted to be 10 bar/CAD [4]. Using the peak pressure, P_3, along with the combustion duration, $\Delta\theta$, a basic correlation was created to include this limiting factor within the model as shown in Equation 3.60.

$$PRR_k = \frac{\left(P_{3,k} - P_{SOC,k}\right)}{\Delta\theta_k} \quad (3.60)$$

This expression defines the pressure rise rate as the pressure change from the beginning of combustion to the peak pressure, divided by the length of the combustion event. Utilizing Equations 3.56 and 3.59 in conjunction with Equation 3.60 yields:

$$PRR_k = \frac{N_{3,k}}{N_{2,k}} P_{atm} \left(\frac{V_1}{V_{23,k}}\right) * \frac{c_{3,k-1} + \left(c_{1,k-1} + c_{2,k-1}\alpha_{i,k} + c_{egr,k-1}\alpha_{e,k-1} + c_{unb,k-1}\alpha_{unb,k-1} - R_u N_{2,k}\right)\left(\frac{V_1}{V_{23,k}}\right)^{\gamma-1} T_{1,k} + c_{5,k-1}T_{ref}}{\left(c_{2,k-1}\alpha_{i,k} + c_{egr,k-1}\alpha_{e,k-1} + c_{unb,k-1}\alpha_{unb,k-1} + c_{4,k-1} - R_u N_{3,k}\right)T_{1,k}} - P_{SOC,k}}{\left[3.38 \times 10^{-55}(0.0001665)^{\phi_k}(0.99844781)^{(V_1/V_{SOC,k+1})^{\gamma-1}T_{1,k+1}}(1.43866189)^{\theta_{SOC,k+1}}\right]} \quad (3.61)$$

Equation 3.61 defines the pressure rise rate in terms of inputs and state variables, resulting in another output equation for this control model.

3.7.4. Gross Indicated Work. Although peak pressure can give a semblance of the engine output, a more precise performance indicator is the work that is output from the engine. Engines are needed to meet power requirements in order to match the customer's desires, and this necessitates a certain amount of work output from the engine. Thus, work was selected to be an output from the model.

To keep the expression simple, gross indicated work was chosen to depict the overall work output from the engine. This assumption is feasible since it considers the work done in both the compression and expansion strokes, which accounts for the majority of the work done in any given cycle. The P-V diagram shown below displays the compression, expansion, and gross indicated work for a generic cycle.

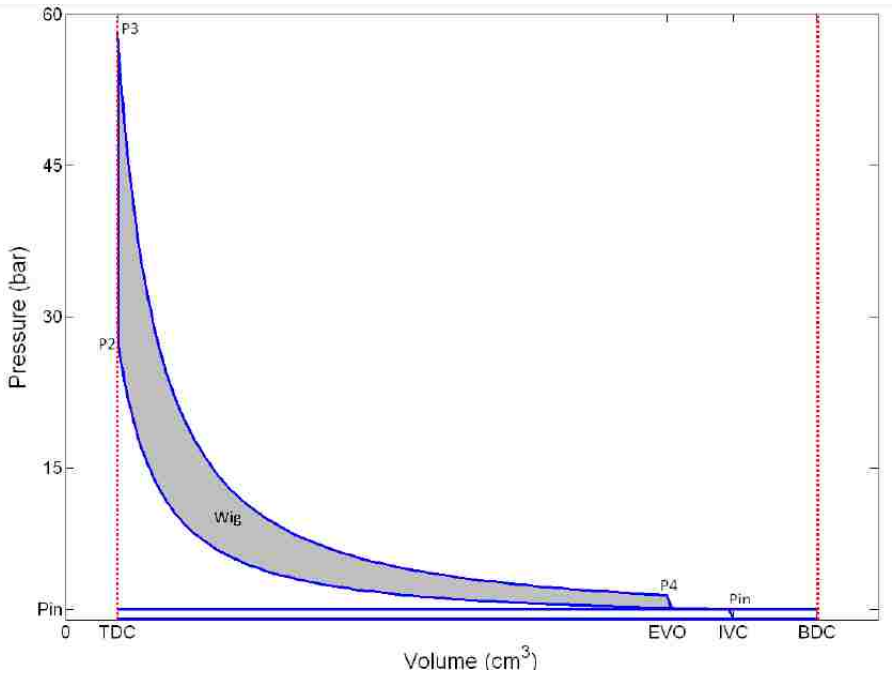

Figure 3.9. Pressure-Volume Diagram for an HCCI Engine Cycle

Figure 3.9 shows a pressure-volume trace for a generic HCCI engine cycle generated by the Hatz 1D50Z engine. Equation 3.62 below approximates the work for this engine cycle.

$$W = \int_{V_1}^{V_2} PdV \tag{3.62}$$

To calculate the gross indicated work, it was assumed that the compression and expansion processes were polytropic, which allows for the following simplification to be made:

$$PV^n = \text{Constant} \tag{3.63}$$

Applying a previous assumption, that the intake charge occurs at atmospheric pressure, and a new assumption, that the polytropic exponent is equal to the ratio of specific heats, i.e. $n = \gamma$, Equation 3.63 can be substituted into Equation 3.62 to result in the compression work when integrated from V_4 to V_{23}.

$$W_{comp,k} = \frac{P_2 V_{23} - 0.01157 V_4}{1 - \gamma} \tag{3.64}$$

Figure 3.9 showed that there is an additional small amount of compression work that occurs between IVC and EVO due to the valve timing. Again, assuming that the intake pressure is atmospheric, Equation 3.63 can again be substituted in to Equation 3.62 and integrated to determine this new amount of work.

$$W_{comp2,k} = \frac{0.01157 V_4 - P_{in} V_1 + P_{in}(1 - \gamma)(V_1 - V_4)}{1 - \gamma} \tag{3.65}$$

For the expansion process, Equation 3.63 was again utilized with Equation 3.62 with the assumption that the blowdown process ends at atmospheric pressure. Integrating from V_{23} to V_4 results in Equation 3.66.

$$W_{exp,k} = \frac{P_4 V_4 - P_3 V_{23}}{1 - \gamma} \tag{3.66}$$

Totaling the three components of the indicated gross work shown in Equations 3.64-3.66 produces the following expression.

$$W_{ig,k} = \frac{P_4 V_4 - P_3 V_{23} + P_2 V_{23} - 0.01157 V_4}{1 - \gamma} + \frac{0.01157 V_4 - P_{in} V_1 + P_{in}(1 - \gamma)(V_1 - V_4)}{1 - \gamma} \tag{3.67}$$

Substituting Equations 3.15, 3.16, 3.24, 3.32, and 3.34 into Equation 3.67 yields the expression for the control model output of gross indicated work written entirely in terms of inputs and state variables.

$$W_{ig,k} = \frac{\left[V_4\left(\frac{V_{23,k}}{V_4}\right)^{\gamma} - V_{23,k}\right]\left[\left(\frac{N_{3,k}}{N_{2,k}}\right)dP_{in}\left(\frac{V_1}{V_{23,k}}\right)\right]}{\left[\left(c_{2,k-1}\alpha_{i,k} + c_{egr,k-1}\alpha_{e,k} + c_{unb,k-1}\alpha_{unb,k} + c_{4,k-1} - R_u N_{3,k}\right)T_{1,k}\right](1-\gamma)} +$$

$$\frac{P_{in}\left[\left(\frac{V_1}{V_{23,k}}\right)^{\gamma} V_{23,k} - V_1 + (1-\gamma)(V_1 - V_4)\right]\left[\left(c_{2,k-1}\alpha_{i,k} + c_{egr,k-1}\alpha_{e,k} + c_{unb,k-1}\alpha_{unb,k} + c_{4,k-1} - R_u N_{3,k}\right)T_{1,k}\right]}{\left[\left(c_{2,k-1}\alpha_{i,k} + c_{egr,k-1}\alpha_{e,k} + c_{unb,k-1}\alpha_{unb,k} + c_{4,k-1} - R_u N_{3,k}\right)T_{1,k}\right](1-\gamma)}$$

where

$$d = c_{3,k-1} + \left(c_{1,k-1} + c_{2,k-1}\alpha_{i,k} + c_{egr,k-1}\alpha_{e,k-1} + c_{unb,k-1}\alpha_{unb,k-1} - R_u N_{2,k}\right)\left(\frac{V_1}{V_{23,k}}\right)^{\gamma-1} T_{1,k} + c_{5,k-1}T_{ref}$$

(3.68)

3.7.5. Efficiency. Once the amount of work output has been calculated, it is simple to find the efficiency of how the engine was operating at a given set-point. The efficiency term shown in Equation 3.69 is determined using the amount of work output normalized by the amount of fuel energy input.

$$\eta = \frac{W_{ig,k}}{N_{f,k} LHV_f} \tag{3.69}$$

To achieve the output expression in terms of system inputs and state variables, Equation 3.68 was substituted into Equation 3.69 to produce:

$$\eta_k = \frac{\left[V_4\left(\frac{V_{23,k}}{V_4}\right)^{\gamma} - V_{23,k}\right]\left[\left(\frac{N_{3,k}}{N_{2,k}}\right)dP_{in}\left(\frac{V_1}{V_{23,k}}\right)\right]}{\left[\left(c_{2,k-1}\alpha_{i,k} + c_{egr,k-1}\alpha_{e,k} + c_{unb,k-1}\alpha_{unb,k} + c_{4,k-1} - R_u N_{3,k}\right)T_{1,k}\right](1-\gamma)(100)\left(N_{f,k} + \alpha_{unb,k}N_{f,k-1}\right)LHV_{PRF96}} +$$

$$\frac{P_{in}\left[\left(\frac{V_1}{V_{23,k}}\right)^{\gamma} V_{23,k} - V_1 + (1-\gamma)(V_1 - V_4)\right]\left[\left(c_{2,k-1}\alpha_{i,k} + c_{egr,k-1}\alpha_{e,k} + c_{unb,k-1}\alpha_{unb,k} + c_{4,k-1} - R_u N_{3,k}\right)T_{1,k}\right]}{\left[\left(c_{2,k-1}\alpha_{i,k} + c_{egr,k-1}\alpha_{e,k} + c_{unb,k-1}\alpha_{unb,k} + c_{4,k-1} - R_u N_{3,k}\right)T_{1,k}\right](1-\gamma)(100)\left(N_{f,k} + \alpha_{unb,k}N_{f,k-1}\right)LHV_{PRF96}}$$

where

$$d = c_{3,k-1} + \left(c_{1,k-1} + c_{2,k-1}\alpha_{i,k} + c_{egr,k-1}\alpha_{e,k-1} + c_{unb,k-1}\alpha_{unb,k-1} - R_u N_{2,k}\right)\left(\frac{V_1}{V_{23,k}}\right)^{\gamma-1} T_{1,k} + c_{5,k-1}T_{ref}$$

(3.70)

3.8. STATE UPDATE EQUATIONS

Since this model, updated with the PRF96 fuel, is based off of a state-space method of control, it was necessary to ensure that all of the output equations and state

variables of the system are completely dependent upon the inputs and state variables from the previous cycle. These state update equations are used to allow the model to estimate what will occur in the next cycle, and allows the controller to select an appropriate control input for those conditions. These state update equations have already been derived as shown in Equations 3.14, 3.37, and 3.58. However, they are formulated with the five state thermodynamic cycle, and have yet to be updated so that they are only functions of the inputs and state variables.

The first state update expression to be reformulated is α_{tot}, which is the amount of trapped residual that is cyclically carried forward. In order to ensure that this equation is written entirely in terms of inputs and state variables, Equation 3.37 needs to be redeveloped. By substituting in the appropriate values for Hatz 1D50Z engine geometry used in this study as shown in Table 3.1, the expression can be simplified. In addition to the geometry terms, there are pressure terms that the formula is dependent upon. By averaging experimental data for the intake and exhaust pressure, the accuracy of the residual calculation is preserved. Using these conditions in conjunction with Equations 3.15, 3.24, and 3.32-3.35 can be sequentially substituted into Equation 3.37 to achieve the state update equation for the residual. The result is shown in Equation 3.71.

$$\alpha_{tot,k+1} = .1010700925T_{in,k}/$$

$$\left[\frac{\left(c_{2,k-1}\alpha_{i,k} + c_{egr,k-1}\alpha_{e,k-1} + c_{unb,k-1}\alpha_{unb,k-1} + c_{4,k-1} - R_u N_{3,k}\right)T_{1,k}}{\frac{N_{3,k}}{N_{2,k}} d\left(\frac{V_1}{V_{23,k}}\right)}\right]^{(\gamma-1)/\gamma} \left[\frac{d}{c_{2,k-1}\alpha_{i,k} + c_{egr,k-1}\alpha_{e,k-1} + c_{unb,k-1}\alpha_{unb,k-1} + c_{4,k} - R_u N_{3,k}}\right]$$

$$\text{where } d = c_{3,k-1} + \left(c_{1,k-1} + c_{2,k-1}\alpha_{i,k} + c_{egr,k-1}\alpha_{e,k-1} + c_{unb,k-1}\alpha_{unb,k-1} - R_u N_{2,k}\right)\left(\frac{V_1}{V_{23,k}}\right)^{\gamma-1} T_{1,k} + c_{5,k-1}T_{ref} \tag{3.71}$$

The next state update variable considered is the temperature at the beginning of compression, T_1. In order to reformulate this expression in terms of only inputs and state

variables, it is necessary to substitute Equations 3.15, 3.24, and 3.32-3.35 into the previously developed expression for this variable, Equation 3.14. The result is shown below in Equation 3.72, where $\alpha_{tot,k+1}$ is replaced with the new state update expression in Equation 3.71.

$$T_{1,k+1} = \frac{c_{1,k}T_{in,k} + c_{egr,k}\alpha_{e,k}T_{egr} + \chi\left(c_{2,k}\alpha_{tot,k+1} + c_{unb,k}\alpha_{unb,k}\right)\left[\frac{\left(c_{2,k-1}\alpha_{i,k} + c_{egr,k-1}\alpha_{e,k-1} + c_{unb,k-1}\alpha_{unb,k-1} + c_{4,k-1} - R_u N_{3,k}\right)T_{1,k}}{\frac{N_{3,k}}{N_{2,k}}d\left(\frac{V_1}{V_{23,k}}\right)}\right]^{(\gamma-1)/\gamma}}{c_{1,k} + c_{2,k}\alpha_{tot,k+1} + c_{egr,k}\alpha_{e,k} + c_{unb,k}\alpha_{unb,k}} * \left[\frac{d}{c_{2,k-1}\alpha_{i,k} + c_{egr,k-1}\alpha_{e,k-1} + c_{unb,k-1}\alpha_{unb,k-1} + c_{4,k-1} - R_u N_{3,k}}\right] \tag{3.71}$$

The final state variable is θ_{23} which represents the angle where peak pressure and thus combustion occurs within the cycle. The output expression in Equation 3.58 is used to produce the state update equation for this parameter.

$$\theta_{23,k+1} = \theta_{SOC,k+1} + \Delta\theta_{k+1} \tag{3.72}$$

In order to remain true to the original form of the nonlinear state-space control model that this study is based on, the output and state space equations have been derived to be entirely dependent upon the input and state variables defined within this model. The nonlinear aspect of this formulation is desired to prevent important trends being lost in the simplification required of a linear model. Thus, the operating range of the non-linear model is not as limited as the linear model would be.

3.9. CHEMICAL KINETIC MODEL

With all of the equations from the Bettis/Attebery model rederived for the PRF96 fuel, attention can be turned to the method of determining the amount of CO that will be fed into the next cycle to evaluate its effect on combustion.

3.9.1. Chemical Mechanism. The chemical kinetic mechanism selected for use in this study is the skeletal mechanism of Tsurushima [8]. This mechanism was selected for use because through its 33 species and 38 reactions, it accurately describes the chemical reaction without a heavy computational load so that it can be paired with the thermodynamic model to evaluate the cyclic effect of residual gases on the start of combustion. Tsurushima designed this mechanism to be applicable with any Primary Reference Fuel (PRF), and as mentioned in §3.2.1, PRF96 was selected for use in this study due to having a similar octane index to fuels that had been successfully run on the Hatz 1D50Z.

CHEMKIN was selected to be used for the chemical kinetics simulations. It is a Fortran-based program originally developed by Sandia National Laboratory for the analysis of gas-phase chemical and plasma kinetics [7, 29]. Within CHEMKIN, a constant volume, zero-dimensional, adiabatic system was chosen to be the basic conditions. This system adequately depicts the near constant volume combustion that is inherent in HCCI while eliminating the complexities introduced by adding extraneous variables. Additionally, the simulated charge is assumed to be perfectly premixed allowing for temperature and compositional gradients across the cylinder to be removed from consideration.

For a simulation to begin, inputs required from the user for the chemical kinetic mechanism are equivalence ratio, temperature at the end of isentropic compression prior to combustion, and pressure at IVC. The presence of species in addition to fuel and air may also be specified in mass amounts within the premixed initial charge. In this way, effects of internally trapped residual species can be evaluated. The partial burn regime

can be investigated by reviewing the results of the simulation prior to 100% of the energy being released.

3.9.2. CO Determination during Partial Burn. In order to calculate the amount of CO produced during each cycle, the pressure at IVC, the temperature at the second thermodynamic state, and the equivalence ratio are needed to initiate the CHEMKIN code. Since the five-state thermodynamic model is a MATLAB code and the chemical kinetic model is Fortran, it was necessary to ensure that the computational expense was minimized when coupling the two models. Therefore, rather than feeding the updated cyclic variables calculated in MATLAB into Fortran each iteration, it was decided to try to determine if any simplifications were possible. If any simplifications could be made to generate chemical kinetic results under a few selected sets of conditions and have the five-state thermodynamic model retrieve information from those data sets without jeopardizing accuracy, then the computational expense would be greatly reduced.

To determine the appropriate simplifications, CHEMKIN results were generated for a large range of input conditions, all representative of the conditions that replicate those seen during partial burn. Experimental data was collected at three different fueling rates, 6, 7.5, and 9 grams per minute (gpm), so therefore the input conditions had to include data for the partial burn regime at all three fueling rates [7]. The intake temperatures that induce partial burn were carefully collected experimentally by slowly lowering the intake temperature of the engine from stable combustion conditions one degree Kelvin at a time and allowing the engine to stabilize at each point until misfire occurred. In addition to generating data for different fueling rates and temperatures, the CHEMKIN model was run with varying amounts of residual CO added into the inlet

conditions. Once all of this data was collected, comparisons could be made to determine the acceptable simplifications.

For each fueling rate, it was observed that for the entire range of temperatures that exhibit partial burn characteristics, the amount of CO produced at different stages along the combustion process varied minimally. This is shown in Figures 3.10 and 3.11 for the 6 gpm fueling rate.

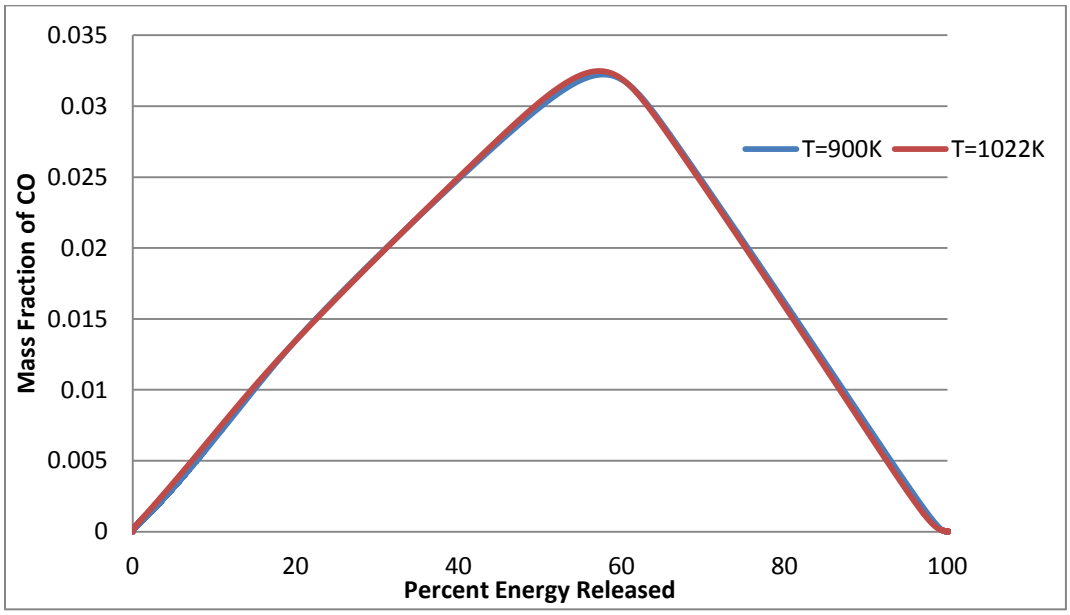

Figure 3.10. Mass Fraction of CO Versus Percent Energy Released for 6 gpm from CHEMKIN

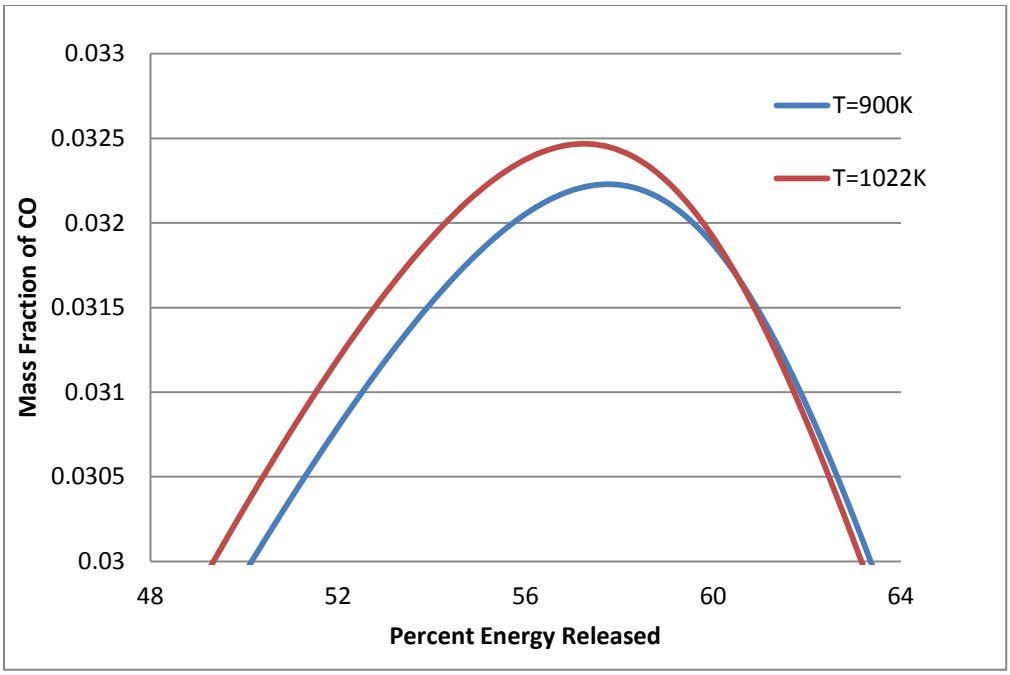

Figure 3.11. Exploded View of the Top of Figure 3.10.

Figure 3.10 displays the mass fraction of CO produced during the evolution of the combustion process from 0 to 100% energy released as determined by CHEMKIN. The temperatures of 900K and 1022K are the lower and upper limits of the range where partial burn characteristics are exhibited for all three fueling rates; the extremes of the partial burn regime were included to emphasize that the temperature immediately prior to combustion and by extension the intake temperature plays a very small role in the amount of CO produced. Also, since the partial burn zone for each distinct fueling rate is encompassed within a few degrees Kelvin, the temperature range was expanded to encompass all of partial burn for every fueling rate used in this study. The traces shown are thus for this expanded temperature range, covering all three fueling rate partial burn

zones. The results for the 6 gpm fueling rate are displayed. It can be observed that there is less than a 0.6 percent difference in the mass fraction of CO. This can be more easily seen when regarding Figure 3.11 which is an exploded view of the top portion of Figure 3.10. Similar trends were noticed for the other fueling rates of 7.5 and 9 gpm. Therefore, there only needs to be one temperature from state two evaluated in CHEMKIN for each flow rate. The selected temperatures for each flow rate were halfway between the point of misfire and partial burn so that the maximum potential percent difference for each case was less than 0.3.

However, this is not the case with the internal CO amounts. There is a wide range of how much CO is within the engine cylinder depending on the completeness of combustion. This can be observed via mass fraction in Figure 3.12.

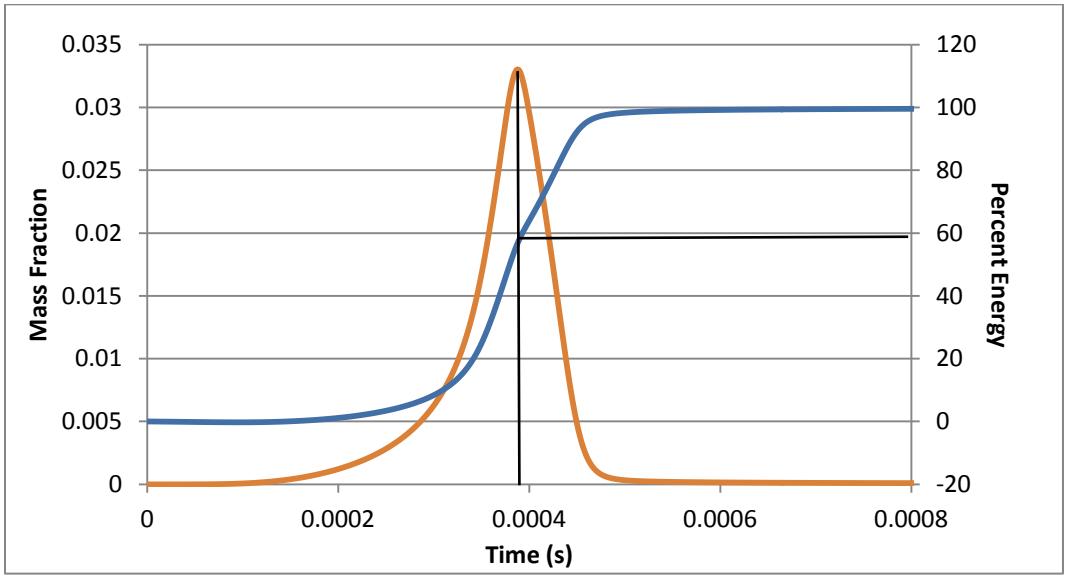

Figure 3.12. Mass Fraction of CO Versus Time for 6 gpm and T_2=1105K

Figure 3.12 was attained with the CHEMKIN code and shows that the mass fraction of CO that is present within the cylinder varies substantially during combustion on the primary axis. The secondary axis shows percent energy that has been released, displaying the completeness of combustion. It can readily observed that the maximum CO production occurs when 56% of the energy has been released during the combustion process, and that there is a rapid increase and decrease in the mass fraction of CO around that point. Since the focus of this study is on the effect that the residual CO has on ignition, it is necessary to include several partitions to determine this effect with a reduced computational expense. Therefore, to accurately predict the amount of CO produced at different stages of combustion, more than one mass fraction value will need to be considered in order to capture the effect of the residual. To accommodate this, the data was studied to determine if there were any natural breakpoints that could be utilized. The results of this assessment can be seen in Figure 3.13.

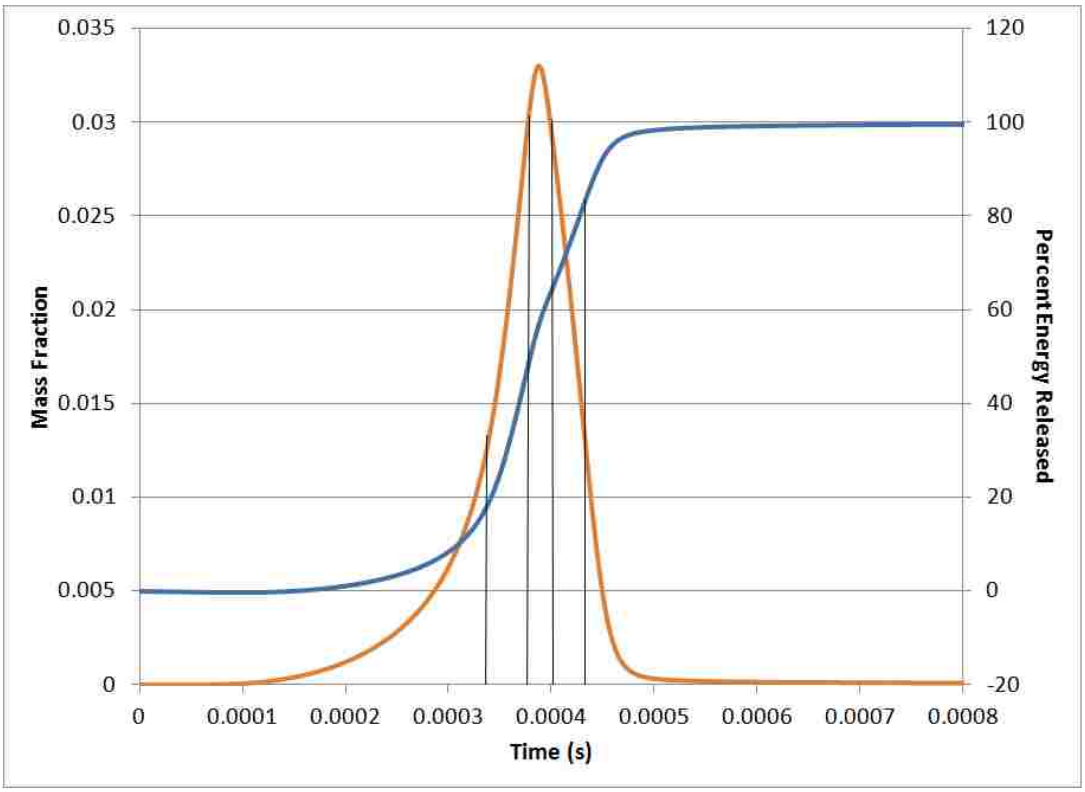

Figure 3.13. Mass Fraction of CO and Percent Energy Versus Time with Partitions for 6 gpm and T_2=1105K

Figure 3.13 contains a plethora of information. It was generated using the CHEMKIN model with the input of 6 gpm, a temperature of 1105K, and atmospheric pressure. On the primary vertical axis it shows the mass fraction of CO produced versus time, as shown by the orange line, same as Figure 3.12. The secondary axis shows the percent energy released during combustion over time as depicted by the blue line, also shown in Figure 3.12. Since the mass fraction of CO produced versus percent energy release stays consistent over the full range of state two temperatures that generate partial burn characteristics (as shown in Figures 3.10 and 3.11), it seemed plausible to determine the appropriate breakpoints using these two traits.

The first breakpoints determined were immediately surrounding the maximum amount of CO. A range was desired that would capture this extremum, and that had a minimal percent difference. Thus, the values bounding the maximum CO were chosen to be at 50% energy released, and at 65% energy released. The mass fractions of CO at these two bounds are similar for all of the data sets generated from CHEMKIN, and they have less than a 10% difference from the maximum value. These breakpoints are indicated by the two central black vertical lines in Figure 3.13. The other two breakpoints displayed are at 20% and 85% energy released. They were selected in a similar manner as above, by looking at the data generated from CHEMKIN and observing where an appropriate cut-off would be to preserve the integrity of the data by considering small areas where the mass fraction of CO did not change too substantially while also not causing heavy computational expense requirements. The mass fraction of CO at the values of 20% and 85% are also similar. Thus, the breakpoints chosen resulted in five distinct zones for consideration in the feed-forward model for the residual CO, from 0-20%, 20-50%, 50-65%, 65-85%, and 85-100%.

Due to the parabolic nature of the CO production, a simplification can be made to reduce the amount of data sets required to be available within the MATLAB code. This helps to reduce computational expense and can be observed in Figure 3.14.

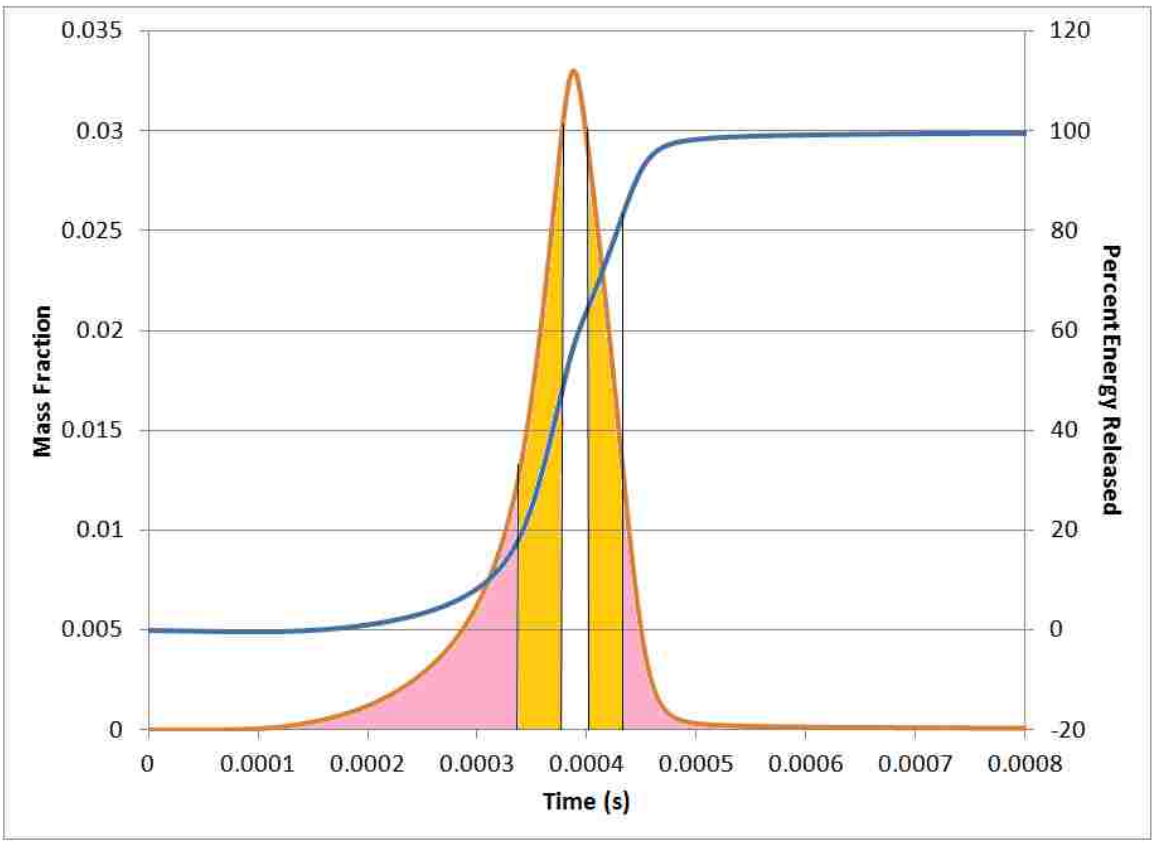

Figure 3.14. Mass Fraction of CO and Percent Energy Versus Time with Shaded Partitions for 6 gpm and T_2=1105K

Since the breakpoints are spaced along the parabola at positions where the mass fraction of CO is similar and they are centered around the maximum value of CO produced, the mirrored sections have similar properties. This is displayed by the shading of the partitions with orange and pink. Thus, the CO mass fractions in the 0-20% energy released area are reflected in the 85-100% energy released area. This pattern is also present for the 20-50% and 65-85% areas, shaded in orange. This reduces the amount of data sets that need to be accessed by the model to capture the residual effect of CO to a total of twelve. There are four data sets for each of the three fueling rates evaluated, 6,

7.5, and 9 gpm and only one temperature evaluated at each of these fueling rates, consistent with the onset of partial burn. Three of these four data sets are distinguished by the different color shadings in the partitions of Figure 3.14, pink, orange, and white, by allotting the amount of residual that remains from the previous cycle. Thus, if the previous cycle had a percent energy that was associated with a value in the pink shaded zone, the current cycle would add the maximum mass fraction of CO from that zone to the initial charge. The last of these four data sets is the case when zero CO residual is included in the initial charge in the CHEMKIN data. This set is used for the case of 100% energy released, which is equivalent to complete combustion.

3.10. CHEMICAL KINETIC AND THERMODYNAMIC MODEL COUPLING

In order for the feed-forward portion of this model to be applicable to this experimental set-up, the CHEMKIN generated data had to be accessible by the MATLAB model. Instead of trying to take the variables generated by the five-state thermodynamic model, feed them into the Fortran CHEMKIN model as inputs, generate the data and then export the CO data back to MATLAB for each iteration, it was decided to generate the CHEMKIN data as readable spreadsheet files to reduce computational expense. The twelve data sets generated with the CHEMKIN model for the determination of the effect of residual CO are therefore referenced in a series of nested loops within the MATLAB model as can be seen in Appendix B. The order of these operations are pictorially explained using the flowchart in Figure 3.15.

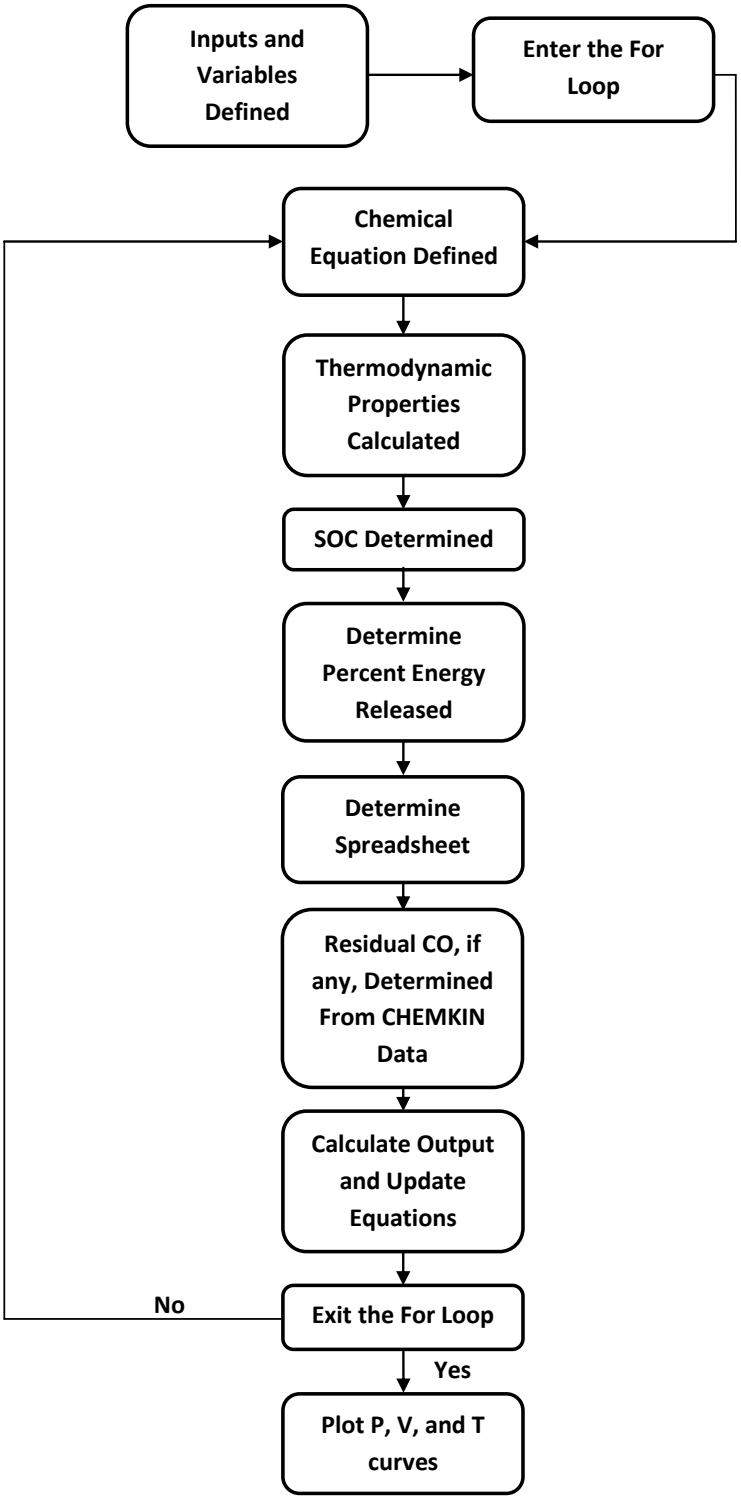

Figure 3.15. Code Coupling Flowchart

The process begins, as depicted in Figure 3.15, with the declaration of the inputs for the coupled feed-forward model. These inputs are the same as those for the five-state thermodynamic model, and are the fuel flow rate, the intake temperature, and mass fraction of external EGR. The amount of iterations can be altered by changing the number of cycles to run. After these values are defined, the program can start. The chemistry is defined and the thermodynamic states are calculated, as well as the molar amounts and equivalence ratio. The next step in the flow chart is to determine the percent energy released.

3.10.1. Percent Energy Released. The CHEMKIN model outputs the temperature, the pressure, the heat released in kJ, the percent energy released, and the molar and mass fractions of many of the chemical compounds that occur during the combustion process during each time step of 0.000001 second. In order to be able to access the amount of CO produced during each cycle where partial burn occurs, the variable of percent energy released was chosen to be calculated within the MATLAB model to relay information between the five-state model and the data sets generated. The percent energy release was determined in the five-state model as Equation 3.73 shows.

$$ER = \begin{cases} 99.0 & \theta_{23} \leq \theta_{PB} \\ 100 * \left[\dfrac{\theta_{PB} - \theta_{23}}{\theta_{MF} - \theta_{PB}}\right] & \theta_{PB} < \theta_{23} < \theta_{MF} \\ 0.0 & \theta_{23} \geq \theta_{MF} \end{cases} \tag{3.73}$$

A linear relationship similar to the one utilized for the mass fraction of internal and unburned residual is the basis of the percent energy release calculation. For the case of complete combustion, the percent energy released is set equal to 99.0%. The maximum amount of energy released determined by the CHEMKIN model for the generated data sets never quite reaches 100%, so 99.0% is used in its place. For the case of complete

misfire, 0% energy is released. A linear relationship is assumed to exist in between these two points to determine the amount of energy released for cycles that fall within the partial burn regime.

3.10.2. Accessing Spreadsheet Data. This method of determining the percent energy released allows for the mass fraction of CO to be accessed from the data spreadsheets by calculating the value of the percent energy released, finding the row location of that value in the selected spreadsheet, then selecting the mass fraction of CO associated with that row.

In order to select the appropriate spreadsheet, there are two factors that are important. The first factor is the fuel flow rate. As an input value, it remains the same throughout all of the iterations for each case that is run. The other important factor is the percent energy released from the previous cycle. This is valuable because it tells how much residual is carried over into the current cycle. The percent energy of the previous cycle is compared to the ranges decided when the partitions were set with the shaded areas in §3.9.2 in Figure 3.14. This selects the spreadsheet with the appropriate amount of CO added into the initial charge calculated from the chemical kinetic model. The mass fraction of CO is found using the percent energy released from the current cycle.

3.10.3. Scaling the Mass Fraction Of CO. Once this mass fraction of CO is obtained, it is necessary to obtain the molar amount of CO for use in the Modified Arrhenius Integration equation. This is a simple calculation accomplished using Equation 3.74.

$$[X] = \omega_X * \frac{m_{tot}}{MW_X} \tag{3.74}$$

Equation 3.74 displays that the molar amount of a compound, X, is the mass fraction of that compound, ω_X, multiplied by the total mass of the mixture, m_{tot}, divided by the molecular weight, MW_X. The total mass of the mixture is found in the chemical kinetic model, and the molecular weight is easily identifiable for a basic compound such as CO. Once the molar amount is determined, it is necessary to ascertain that it is of the same scale that the chemical equation in the five-state thermodynamic model is using. This is done using a ratio with the assistance of another basic compound, O_2. The molar amount of this compound is read from the spreadsheet using the same methodology that is used to obtain CO, and the molar amount is calculated using the chemical balance equation from the five-state thermodynamic model's chemistry shown in §3.2.4 Equation 3.18. With these values, Equation 3.75 can be used to determine the scaled value of CO that is ready for use within the Arrhenius equation.

$$[CO]_{5s} = [CO]_{CHEM} * \frac{[O_2]_{5s}}{[O_2]_{CHEM}} \tag{3.75}$$

The subscript $CHEM$ indicates the amount taken from the CHEMKIN data, and the $5s$ denotes that it originates from the five-state thermodynamic model. With all of these values now known, the output and update equations can be determined for that iteration, and once all of the cycles are complete, it will exit the program and plot the necessary data. The entire code can be seen in Appendix B.

4. EXPERIMENTAL SETUP

4.1. MISSOURI S&T HCCI ENGINE

4.1.1. Engine Setup and Control. The engine used to obtain data for the validation of this model is a modified 1D50Z Hatz engine that is located in the Internal Combustion Engine and Spray Dynamic Research Laboratory at Missouri S&T. The engine setup is displayed in Figure 4.1.

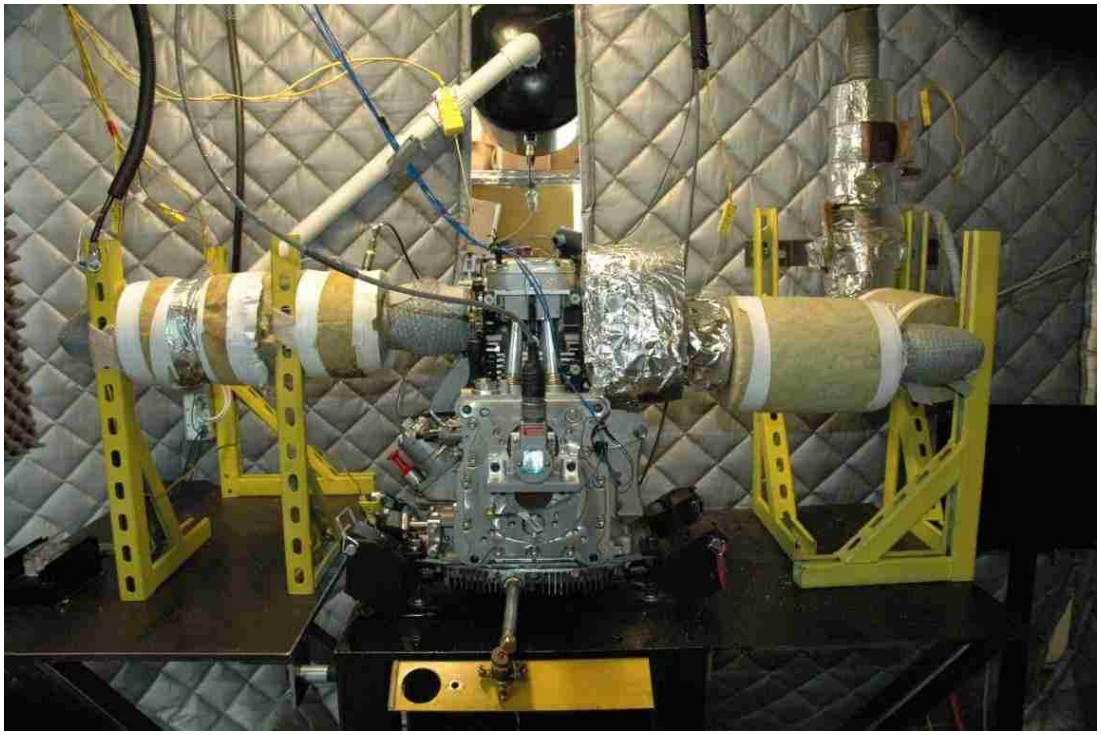

Figure 4.1. Hatz 1D50Z Experimental Setup

This single-cylinder air cooled diesel engine has a modified piston to reduce the compression ratio from 20.5 to 14.5 in order to operate in the HCCI combustion mode. The modification of the piston was carefully considered in order to maintain necessary mixing in the cylinder and the representative equation of the new piston head profile is discussed in detail in [20]. Furthermore, the experimental set-up was modeled after the engine present at Oak Ridge National Lab (ORNL) and its single-cylinder geometry allows for simplification in the predictive modeling of the dynamic cyclic behavior. The geometry and timing parameters for this engine are catalogued in Table 4.1.

Table 4.1. Modified Hatz Engine Specifications

Engine	Hatz 1D50Z (modified)
Number of Cylinders	1
Number of Strokes	4
Bore (mm)	97
Stroke (mm)	70
Compression Ratio	14.5
Displacement Volume (L)	0.517
Cooling	Air
Intake Valve Opening* (ATDC)	345
Intake Valve Close* (BTDC)	133
Exhaust Valve Open* (ATDC)	116
Exhaust Valve Close* (BTDC)	342
Intake/Exhaust Valve Overlap (CAD)	33

*Valve events referenced at TDC of the power stroke and defined at the point of 0.15 mm lift

4.1.2. Engine Instrumentation. HCCI combustion requires a homogeneous mixture to be inducted into the engine cylinder from the intake air manifold. The mixture consists of pre-heated air and vaporized fuel. A Sylvania 6 kW air heater maintains the desired temperature by being coupled with an Omega process controller. Cyclic variations are removed from the heater temperature by using a variable transformer with a constant low level of voltage. The amount of air is monitored by a laminar flow element. The custom atomizer used in congruence with the Hatz engine can be seen in Figure 4.2.

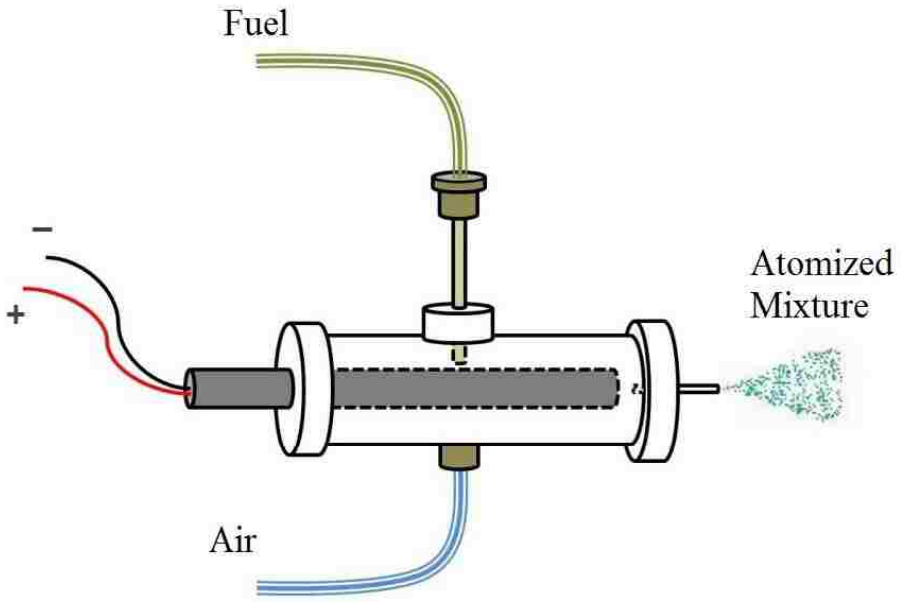

Figure 4.2. Diagram of Atomizer

The cartridge heater, where the temperature is precisely set at a point above the boiling point of the fuel, but below the auto-ignition temperature, vaporizes the fuel. The fuel drip nipple is located just above the heater surface in order to prevent fuel droplets from forming. This prevents variation in cyclic fuel flow as caused by droplet formation. A low flow, high speed FMI metering pump precisely controls the fuel so that there is a constant flow onto the heater. The atomized fuel is brought into the intake manifold by a small amount of airflow of 5.5 liters per minute. The fuel flow is metered with a rotameter calibrated to the testing fuel. More specific details regarding the basis of this atomizer can be found in [3, 30].

The engine speed is regulated with a 22.371 kilowatt Baldor eddy current dynamometer that is connected to the output shaft of the engine. Additionally, there is a BEI Precision shaft encoder that enables the data retrieved from the engine to be viewed in $1/5^{th}$ Crank Angle Degree (CAD) increments over each 720 CAD cycle. The shaft assembly also includes a Lebow 1604 series torque transducer.

The pressure that occurs within the cylinder is monitored with a Kistler 6045A pressure transducer that is mounted flush inside the cylinder head. The flush mounting allows for the cylinder volume to be unaffected. Flush mounting at the center of the cylinder is commonly used to investigate the auto-ignition event of knock in SI engines [3]. Therefore, since the combustion process is initiated by an auto-ignition event, this type of installation was deemed appropriate. The Kistler 6045A pressure transducer requires a charge amplifier due to it being a charge type transducer. Therefore, a Kistler Dual Mode Amp Type 5010 amplifier is also included among the instrumentation on this engine system. The amplifier setting used is 10 MU(bar)/Volt, and it converts the

transducer charge into a voltage recognized by the data acquisition system. Figure 4.3 displays the instrumentation mentioned above.

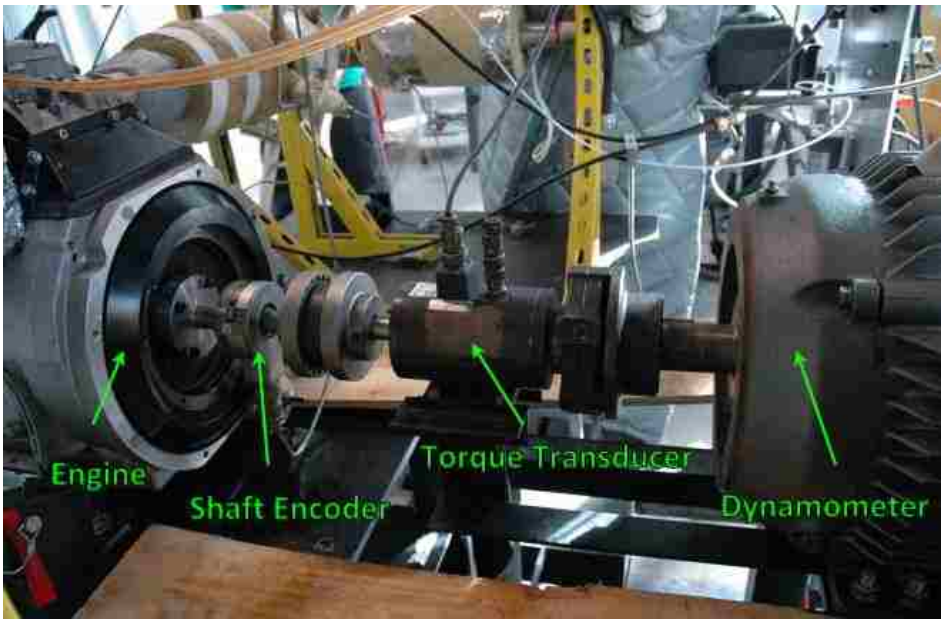

Figure 4.3. Experimental Shaft Assembly

Two important parameters to measure are the fuel and air flow, since the fueling rate has a significant effect on the in-cylinder temperature required to achieve stable combustion. The intake air flow is measured with a Merriam laminar flow element that is coupled to both GE Druck and Omega pressure transducers. The fuel flow is metered with the atomizer and thus the experimental fuel to air ratio (F/A) can be determined. In addition to this, there are pressure transducers and thermocouples installed

in the engine to provide more data to monitor further parameters. Additional detailed information can be found in [3].

4.1.3. Exhaust Instrumentation. In order to determine the cyclic impact of the exhaust gases on the next cycle, it is important to record exhaust temperature and pressure cyclically. The temperature is measured using a fast response thermocouple developed by Engine and Control Monitoring (ECM) called the FastTEMP Kit. This can measure the exhaust gas temperature with a resolution of 0.2 CAD, as determined by the shaft encoder mentioned in §4.1.2. The thermocouple has a response time of 0.004 seconds and is a six inch long 1/16" Type-K TC. To maintain the best accuracy in the sensitive data collection system, the temperature gradient across the thermocouple sensor cable is minimized. Also, in order to decrease strain in the thermocouple wires that could result in noisy data and reduced sensor life, the thermocouple was hard mounted in the exhaust manifold close to the exhaust valve. Additional information about the thermocouple and how to correct for non-linearity caused by Type-K thermocouples can be found in [3]. The exhaust pressure in the manifold was measured with a water cooled Kistler 4049A high temperature gas pressure transducer couple with a PR-Amplifier Type 4622A. This instrumentation has a response time of 0.1 milliseconds and is located in the exhaust manifold close to the thermocouple.

4.1.4. Data Acquisition. The multiple rate/ resolution data acquisition (DAQ) system used to read the output from the instrumentation is capable of capturing both crank angle resolved and temporally resolved data at the same time with sampling rates up to 200 kHz. Crank angle and time stamps are applied to all data collected via internal counters. The interface selected to use was LabVIEW, in which a combustion diagnostic

code has been developed to monitor the combustion behavior in real-time to assess the data integrity during engine operation.

4.1.5. Residual Gas Injector. In order to investigate the effects of specific residual gas species on combustion timing, a custom Residual Gas Injector (RGI) is installed in the port where the original diesel fuel injector was. Thus, the chemical kinetic effect of individual species can be evaluated by cyclically injecting predetermined amounts during the intake stroke to achieve the necessary homogeneous in-cylinder conditions. The components of the RGI are an injector body made from high-grade steel, and a Lee Company single coil solenoid valve. The injector body of the Residual Gas Injector was designed with the same outer dimensions of the OEM fuel injector for the Hatz 1D50Z so that modifications to the engine are minimal. The RGI can be seen in Figure 4.4.

Figure 4.4. Custom Residual Gas Injector

The single-coil solenoid valve has a response time of 0.015 seconds and allows gas injection of a maximum of 7% by mass of the inlet charge to be mixed with the fresh charge in-cylinder. The solenoid valve is accompanied by a multi-seal, also from the Lee Company. The multi-seal allows for the solenoid valve to withstand pressures of 4000 psi. This RGI was engineered by Attebery and supplementary figures and information can be found in [3] and [7] and in Appendix A.

LabVIEW and Drivven support cards allow the RGI to maintain comparable operation with a fuel injector. The Port Fuel Injector Module Kit includes a CompactRIO (cRIO) module for driving low and high impedance Port Fuel Injectors (PFI) and general purpose automotive solenoid valves. Each driver channel on the PFI support card is controlled by a LabVIEW FPGA VI. Each individual channel is operated in real time and controlled for timing and duration. The basis of the system is a NI-cRIO 9022 Real Time Controller that communicates with the LabVIEW top level programs. Additional cards installed into this driver system were a NI-9411 and ESTTL card, and a NI-9215 card. The former of these allows for engine position tracking, while the latter monitors the engine pressure as an analog input. Finally, the RGI is driven by the aforementioned PFI driver support card. This setup, in conjunction with the DAQ system mentioned in Section 4.1.4 allows for gas species to be directly added into the cylinder prior to Intake Valve Close (IVC). This system can be seen in Figure 4.5.

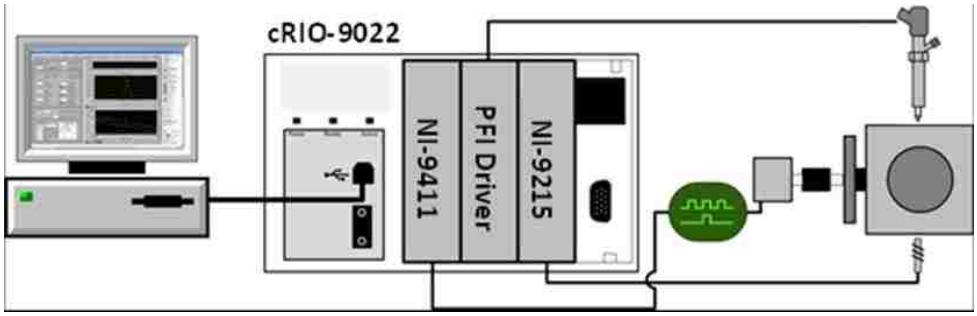

Figure 4.5. RGI Driver System Diagram

4.2. DATA PROCESSING AND ANALYSIS PROGRAM

The majority of the data post-processing is completed through MatLAB so that each parameter in every cycle can be independently viewed, as well as a running average over the entire set point for each parameter of interest. This program was created by Massey, and is explained in more detail in [30]. This allows for engine behavior to be quantified for comparison. The program employs a zero-dimensional single-zone heat release analysis to investigate the combustion energy release process. Many variables are required for these computations and they are discussed in the following subsections.

4.2.1. Cylinder Volume. For the heat release computation, the first variable to consider is the instantaneous cylinder volume, V_θ. This parameter can be calculated using Equations 4.1 and 4.2 from Heywood [9].

$$V_\theta = V_C + \frac{\pi B^2}{4}(l + a - s) \tag{4.1}$$

In Equation 4.1, V_C represents the engine cylinder clearance volume, B is the cylinder bore diameter, l is the connecting rod length, and a is the crankshaft radius. The crank

angle is represented by θ. The distance between the crankshaft axis and the piston pin axis is s. The variable s from Equation 4.1 is defined as

$$s = a\cos(\theta) + \sqrt{(l^2 - a^2\sin^2(\theta))} \tag{4.2}$$

A pictorial representation of the geometry described mathematically in Equations 4.1 and 4.2 is shown in Figure 4.6.

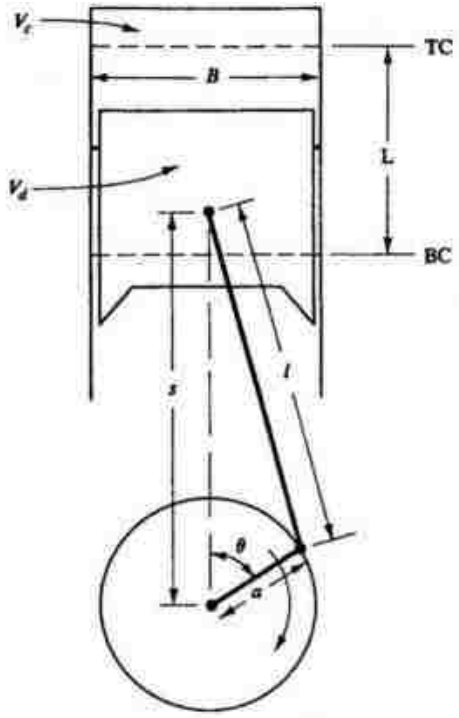

Figure 4.6. Slider-Crank Cylinder Geometry [31]

An additional volume parameter that is required for the heat release analysis is the cylinder volume derivative with respect to crank angle as seen in Equation 4.3.

$$\frac{dV_\theta}{d\theta} = \frac{d}{d\theta}\left[V_C + \frac{\pi B^2}{4}(l + a - s)\right] \tag{4.3}$$

It is important to note that in the previous equation, V_C, B, l, and a are all constants and thus Equation 4.3 can be simplified as shown in Equation 4.4.

$$\frac{dV_\theta}{d\theta} = -\frac{\pi B^2}{4}\frac{ds}{d\theta} \tag{4.4}$$

In order to further reduce Equation 4.4, the next step is to take the derivative of Equation 4.2 with respect to θ.

$$\frac{ds}{d\theta} = -a\sin(\theta)\left[1 + \frac{a\cos(\theta)}{\sqrt{(l^2 - a^2\sin^2(\theta))}}\right] \tag{4.5}$$

Finally, Equation 4.5 can be substituted into Equation 4.4 resulting in a formula for the instantaneous volume derivative based on crank angle.

$$\frac{dV_\theta}{d\theta} = \frac{\pi B^2}{4}a\sin(\theta)\left[1 + \frac{a\cos(\theta)}{\sqrt{(l^2 - a^2\sin^2(\theta))}}\right] \tag{4.6}$$

4.2.2. Cylinder Pressure. For the purpose of removing error from the pressure data, the cylinder pressure should be smoothed to remove the high frequency pressure waves caused by cavity resonances. The cylinder pressure of the Hatz 1D50Z was filtered through a cosine-low pass filter. The method behind the data filtration begins with performing a Fourier transform on the raw cylinder pressure data, and is followed by multiplying the cylinder pressure spectrum by the cosine filter. Then an inverse Fourier transform is used to convert the filtered pressure back into the time domain. Additional information on pressure smoothing can be found in [30].

Furthermore, the derivative of the cylinder pressure with respect to crank angle is desired to be found. This instantaneous cylinder pressure derivative is more commonly known as the Pressure Rise Rate (PRR), and can be used to determine if the engine is in a

stable operating regime. Using the central difference method of numerical differentiation [32], Equation 4.7 is formed.

$$PRR = \frac{dP_\theta}{d\theta} = \frac{P_{\theta+h} - P_{\theta-h}}{2h} \tag{4.7}$$

The crank angle resolution of the shaft encoder is represented by the variable h, which in this study is equivalent to 0.2 crank angle degrees.

4.2.3. In-Cylinder Temperature. The instantaneous gas ratio of specific heats, γ, is calculated for the heat release analysis by using the instantaneous in-cylinder temperature. The equation for the temperature is formed assuming that the fuel-air mixture maintains constant properties, and subsequently that this mixture behaves as an ideal gas. Furthermore, if the computation is performed between Intake Valve Close (IVC) and Exhaust Valve Open (EVO), then the engine cylinder can be approximated as a closed thermodynamic system. Thus, the instantaneous in-cylinder temperature, T_θ, is calculated as follows in Equation 4.8.

$$T_\theta = \frac{T_{IVC} P_\theta V_\theta}{P_{IVC} V_{IVC}} \tag{4.8}$$

In this equation, T_{IVC}, P_{IVC}, and V_{IVC} respectively represent the cylinder temperature, pressure, and volume at IVC.

4.2.4. Heat Release. Following the derivation of all of the parameters included in Equation 4.9, the Heat Release Rate (HRR) equation can now be displayed.

$$HRR = \frac{dQ}{d\theta} = \frac{\gamma}{\gamma - 1} P_{\boldsymbol{\theta}} \frac{dV_{\boldsymbol{\theta}}}{d\theta} + \frac{\gamma}{\gamma - 1} V_{\boldsymbol{\theta}} \frac{dP_{\boldsymbol{\theta}}}{d\theta} \tag{4.9}$$

In Equation 4.9, Q represents heat release, and all other variable are described in prior sections. With the interest of finding the heat release, the above equation can by numerically integrated with the composite trapezoidal rule in MatLAB.

4.2.5. Engine Performance Metrics. With the intent of quantifying the engine output, Net Indicated Mean Effective Pressure, henceforth referred to as IMEPn, is often used. Otherwise known as the net work per engine cycle normalized by the cylinder displacement volume, IMEPn is defined in Equation 4.10.

$$IMEPn = \frac{1}{V_d}\int_{V_0}^{V_{720}} P_\theta dV \tag{4.10}$$

In this equation, V_d represents the displacement volume, and the integration limits V_0 and V_{720} are the initial and final volumes of a complete cycle. The subscripts are the crank angle degree values of their respective number. This is representative of integration, and thus IMEPn, over all four strokes of the engine cycle. Using the smoothed pressure data in addition to the composite trapezoidal rule, IMEPn can be expressed using Equation 4.11.

$$IMEPn = \frac{1}{2V_d}\sum_{j=1}^{\frac{720}{h}} \left[P_{\theta_j+h} + P_{\theta_j}\right]\left[V_{\theta_j+h} + V_{\theta_j}\right] \tag{4.11}$$

The crank angle resolution of the shaft encoder is represented by h, as it was in Equation 4.7, and θ_j is the crank angle at index j.

A second important performance metric is the volumetric efficiency, η_v, which measures the effectiveness of the induction process of an engine.

$$\eta_v = \frac{2\dot{m}_a}{\rho_{a,i} V_d N} \tag{4.12}$$

In Equation 4.12 $\dot{m}_a$ represents the measured mass air flow, $\rho_{a,i}$ is the density of the air at intake, and N is the engine speed in revolutions/second.

Other critical metrics include CA10, CA50, and CA90 when experimentally analyzing HCCI performance. These variables represent the crank angle degree where the

respective percentage heat release occurs. Thus, CA10 is the crank angle degree where 10 percent of the total heat release has occurred. From this, it can similarly be seen that CA50 and CA90 refer to the crank angle degree where 50 percent and 90 percent of the total heat release has occurred. These crank angle values are demonstrated in Figure 4.7 which was generated using sample data from the CHEMKIN code.

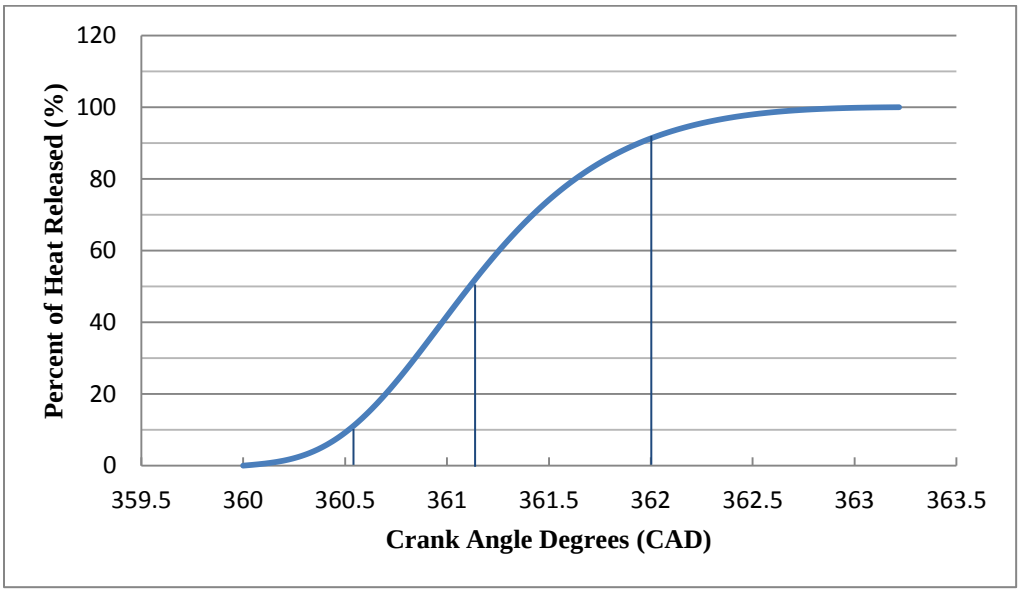

Figure 4.7. Percent of Heat Released Versus Crank Angle Degrees (CAD)

In the above figure, the CA10, CA50, and CA90 values are denoted with vertical lines, and their respective values are approximately 360.55 CAD, 361.2 CAD, and 362 CAD.

After the heat release analysis described in Section 4.2.4 has been completed, the percentages of heat release, and subsequently the crank angle locations of those values

can be determined. In HCCI, it is common to use CA10 as a marker for the SOC, since there is not an external combustion trigger present. Thus, the SOC in Figure 4.6 is estimated as 360.55 CAD.

In this study, the location of CA50 is used to determine the crank angle degree where the event of combustion occurs, represented by the output variable θ_{23} which in this instance is equivalent to 361.2 CAD. This is demonstrated in §3.6 by finding $\Delta\theta$, shifting the point of instantaneous combustion from SOC (CA10) to θ_{23} (CA50).

The final metric for this study that can be determined using these crank angle markers is the Burn Duration which defines the length of combustion in crank angle degrees. The mathematical representation of this parameter is shown in Equation 4.14.

$$Burn\ Duration = CA90 - CA10 \tag{4.14}$$

An example calculation using Equation 4.14 in conjunction with Figure 4.6 shows that the Burn Duration is 1.45 CAD for this cycle.

5. MODEL VALIDATION

Now that the theories and assumptions behind the model have been defined, as well as the methods and equipment for conducting the experiment, it is necessary to demonstrate that the model can accurately predict the trends that occur in the experimental data.

5.1. SENSITIVITY TESTING

5.1.1. Arrhenius Rate. One of the most important parameters within this model is the combustion timing. The Modified Arrhenius Rate model that is used for determining the location of the start of combustion needs to be further investigated. The Arrhenius rate parameters corresponding with PRF96 were determined by using the quantities defined for iso-octane which is the major component of this fuel mixture. Of the two parameters that are used, A and E_a/R_u, only the former needs to be evaluated for sensitivity. This is due to the latter term being the same for iso-octane and n-heptane. In order to examine the sensitivity of the combustion timing to the pre-exponential Arrhenius factor, A, the integral was initialized at the same experimental point as in §3.5.1 by altering the threshold value K_{th} for every new value of A. This allows a direct comparison of the effect of A on the combustion timing. These results can be seen in Figure 5.1.

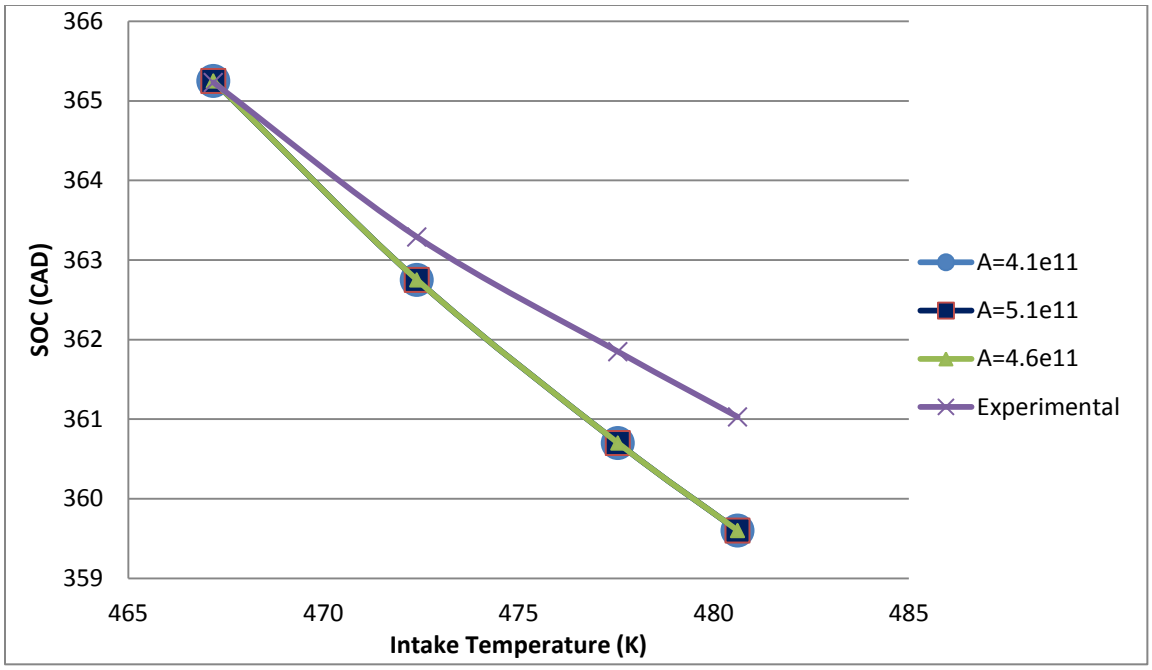

Figure 5.1. Modified Integrated Arrhenius Rate Sensitivity to A for 9 gpm

Figure 5.1 clearly shows that the combustion timing is not sensitive to a change in the pre-exponential factor. There were three different A values tested. The green line represents the value that is used in the model for PRF96. The dark blue is the pre-exponential factor for n-heptane, and the value where A is equivalent to 4.1e11 was an equidistant step in the opposite direction. The predicted values of the angle of the start of combustion did not vary at all once the model was re-benchmarked to the new value of A. Thus, this study will use the value of A that was originally determined, 4.6e11.

Further sensitivity testing for the Integrated Arrhenius Rate model for the variables of α, χ, and E_a can be seen in [4].

5.1.2. Sensitivity of the Percent Energy Released and α_{unb} Angle Cutoff

Limits. These crank angle limits are identified as the crank angles where partial burn characteristics start to occur, θ_{PB}, and where complete misfire occurs, θ_{MF} as discussed in §3.3.2. In order to adequately model PRF96, the limits were chosen to be 373 and 390 respectively. It is necessary to examine the sensitivity of the model to these partial burn and misfire angle limits. First, the effect of these limits on the Percent Energy Released will be discussed. Figure 5.2 is presented for this purpose.

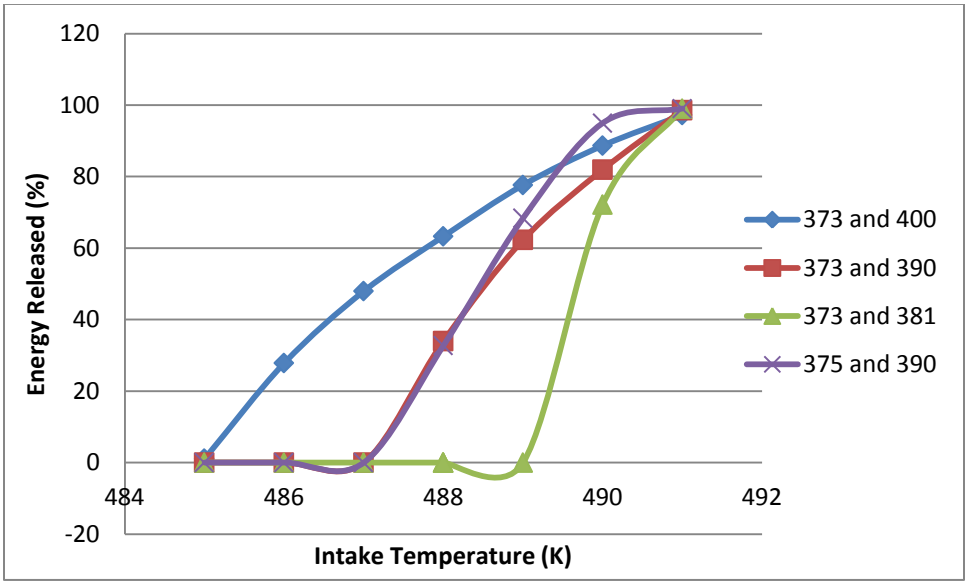

Figure 5.2. Sensitivity Analysis of Angle Cutoff Limits on Percent Energy Released

It can be observed in Figure 5.2 that as the combustion gets less stable, as evidenced by a lower percent energy released, the angular limits have a larger impact. This is logical

since the cutoff limits refer to when partial burn and misfire occur. Therefore, all of the data points during the point of complete combustion at T=491 K for a fuel flow rate of 6 gpm align. Then as partial burn starts to occur by a gradual reduction of the intake temperature by one degree at a time, the cutoffs start to have a greater impact as to how quickly combustion fades to misfire. For the limits of 373 and 381, the smallest range of partial burn, the slope is the steepest with complete misfire for a temperature of 489 K and complete combustion at 491 K. The widest range of 373 and 400 shows a gradual slope with complete misfire not occurring until a temperature of 485 K. However, this range is not representative of the onset of partial burn being only a few degrees away from misfire. The range chosen for this model can be seen in between these two extremes as indicated by the red markers with limits of 373 and 390, closely imitated by the purple line with limits of 375 and 390. The difference between these two is that the purple sustains complete combustion a little longer and thus has two data points close to the 100% energy released line. This graph demonstrates that the percent energy released is fairly sensitive to the angle cutoff limits.

Subsequently, the effect of these angular limits on the molar amount of CO can be evaluated. Since the amount of CO, as represented by Γ, is directly dependent upon the percent energy released in this model, it can be expected that it is also fairly sensitive to the angle cutoff limits. These results can be seen in Figure 5.3.

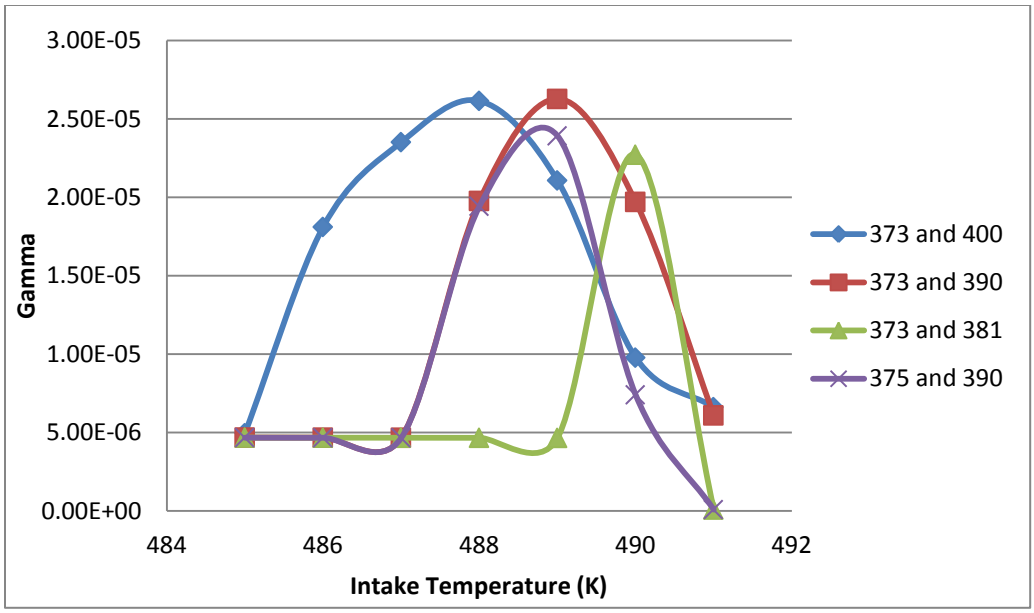

Figure 5.3. Sensitivity of Gamma to the Angle Cutoff Limits

Figure 5.3 displays that when complete misfire occurs for each of the limits, the amount of CO is the same. As the combustion shifts from misfire to partial burn, the amount of CO produced behaves in a parabolic manner as is consistent with Figure 3.2 with the maximum amount being produced at 56% of the energy released, or roughly halfway through the partial burn zone. Then as complete combustion is neared, the amount of CO produced drops back off to a minimum amount to be considered. The breadth of these parabolas is impacted by the angle cutoff values. Thus, the amount of CO produced in that cycle to be fed forward into the next cycle is sensitive to the angle cutoff values.

The final variable to be considered in the sensitivity analysis of the angle cutoff values is the start of combustion. The results of this investigation are shown in Figure 5.4.

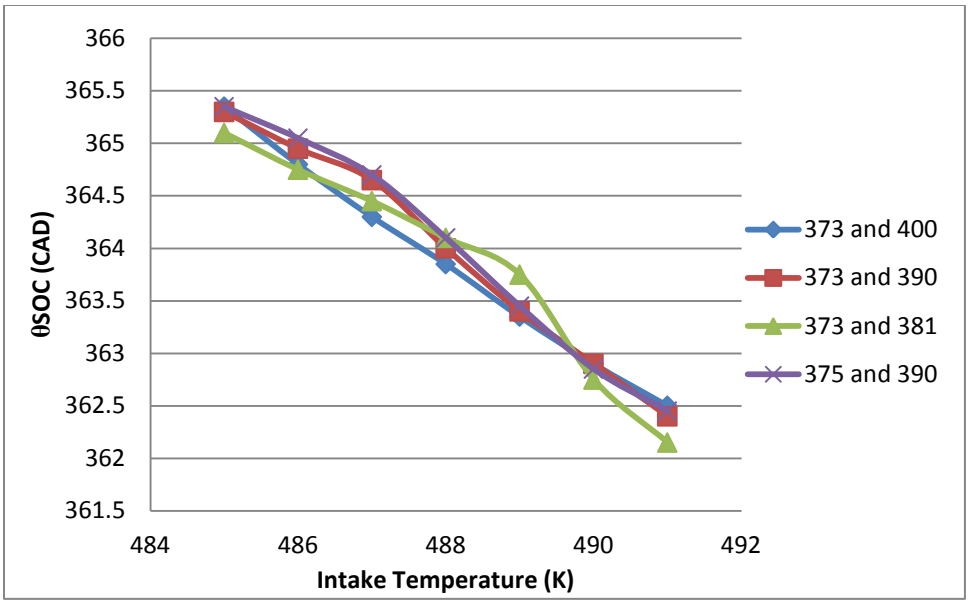

Figure 5.4. Sensitivity of Start of Combustion to the Angle Cutoff Limits

In this figure, it can be observed that there is some variation in the angle location of the start of combustion due to the differences of the angle cutoff limits. It appears at first that it is mainly a linear trend, but upon closer inspection, it seems like there are slight increases in the estimated start of combustion when the inlet temperature is towards the center of the partial burn regime. Overall, the location of the start of combustion does not change by a large amount due to the different angle cutoff limits for misfire and partial burn, but there is a small effect that is present. The variation of the start of combustion will be further examined in the discussion of results in Chapter 6.

5.2. EXPERIMENTAL VERSUS MODEL GENERATED OUTPUT VARIABLES

Now that the assumptions behind the model have been tested, it is important to demonstrate the fidelity of the model by comparing the experimentally gathered data to the results from the model. The variables to be examined are those of the model outputs of peak pressure, P_3, the crank angle degree where combustion/peak pressure occurs, θ_{23}, and the pressure rise rate, PRR. Additionally, the exhaust temperature T_5 will be tested to ensure that the five-state thermodynamic assumptions are valid. If the model outputs can predict the trends that appear in the experimental data, then it can be assumed that the model can preserve the integrity of the capabilities and limitations of the experimental results while investigating the partial burn regime. The approximate onset of the partial burn regime will be indicated by a black segmented vertical line in the following figures.

5.2.1. Peak Pressure. The output of peak pressure was chosen due to providing a basis for the work output from each engine cycle in addition to its location coinciding with the occurrence of combustion. In order to examine the accuracy of the model, the intake temperature was varied in accordance with the experimental values to compare the trends produced. The results for the fuel flow rate of 9 gpm are shown in Figure 5.5.

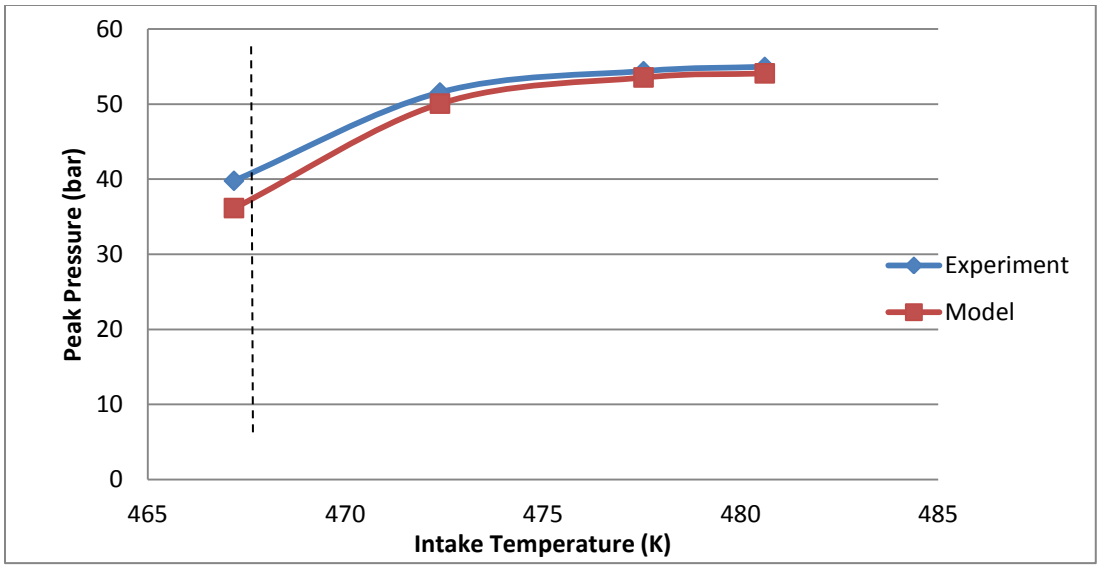

Figure 5.5. Comparison of Experimental and Model Peak Pressure Data (9 gpm)

Figure 5.5 demonstrates that the model predicts the peak pressure very accurately, in magnitude as well as trend. It can be observed that for the lower intake temperatures that the model has a slightly steeper slope than the experimental data. The slope of both lines gets steeper as the intake temperatures get lower due to the approach of the partial burn regime. The onset of partial burn is approximated by the segmented line for clarity. Thus, it is logical that the peak pressure is lower when combustion is not stable. Overall, the model predicts the behavior of the peak pressure accurately as compared to the experimental data. This can be further validated by comparing the peak pressures at a different set point.

Further confirmation of the tracking of the peak pressures by the model can be examined by using a different fueling rate. These results are shown in Figure 5.6.

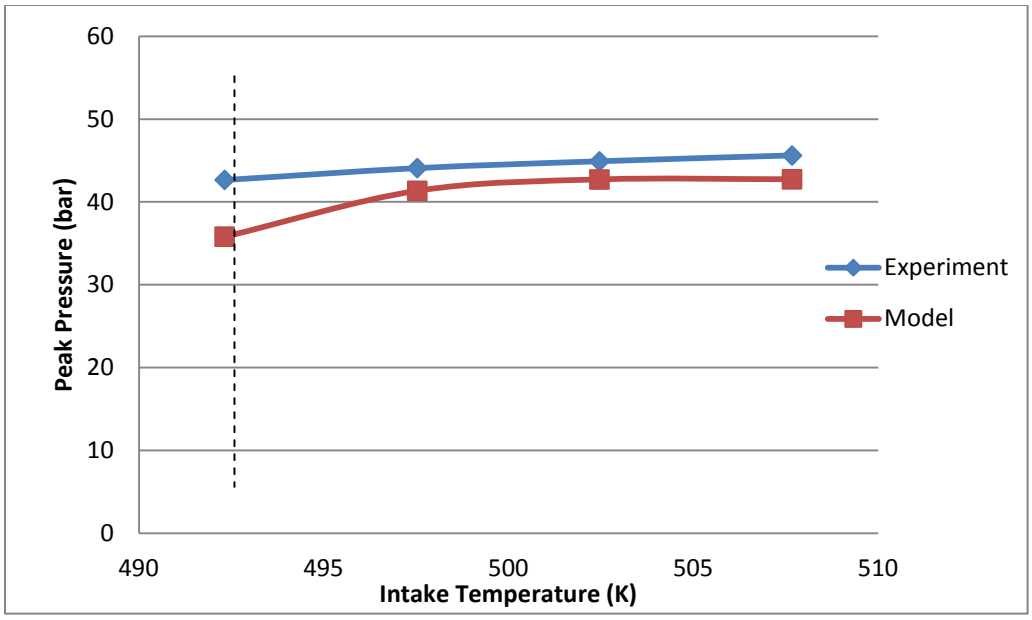

Figure 5.6. Comparison of Experimental and Model Peak Pressure Data (6 gpm)

This figure further enunciates that the slope of the model is steeper than the experiment at the onset of partial burn. Yet, the overall trend is still accurate that there is only a slight slope during stable combustion and then a more pronounced slope in the lower temperature ranges. The peak pressure is lower when it is entering the partial burn regime. Thus, the model has a suitable performance when predicting how the peak pressure will behave across temperature and fueling rate set points.

5.2.2. Crank Angle Location of Combustion. The second output parameter considered for the validation of this model is the crank angle location of combustion. This parameter is also closely related with the start of combustion through the combustion duration term, $\Delta\theta$, which is described in §3.6. This parameter was tested by

leaving all variables the same except for varying the intake temperature as it was done in the experiment. The results for this can be seen in Figure 5.7.

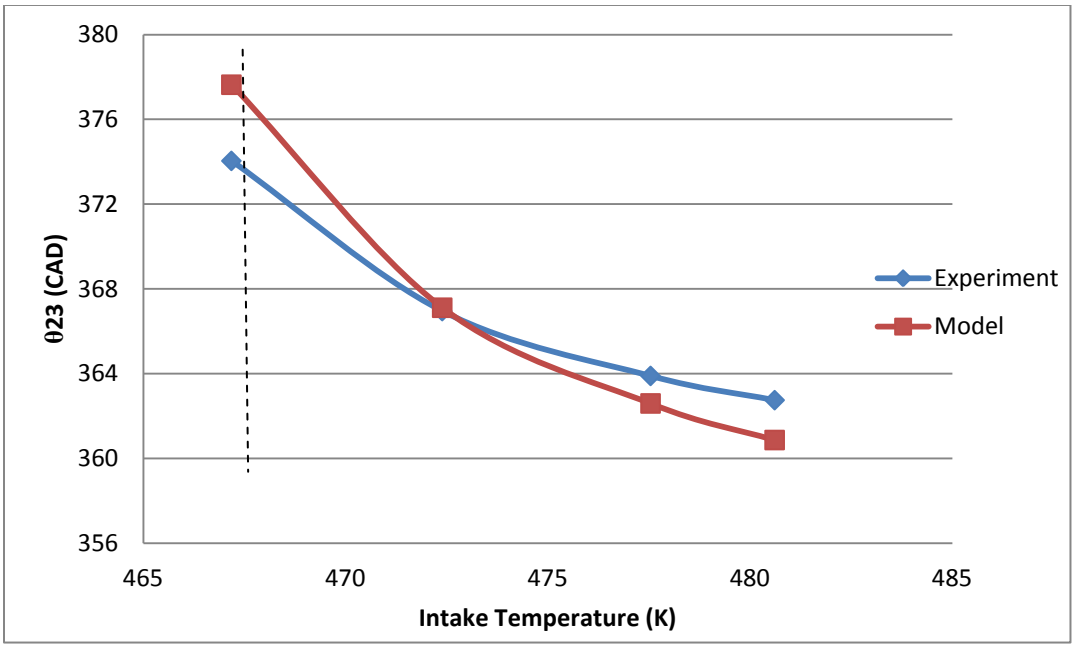

Figure 5.7. Comparison of Experimental and Model Location of Combustion (9 gpm)

Figure 5.7 shows that the model does a reasonable job of predicting the location of combustion as represented by θ_{23}. The general magnitudes predicted by the model are a little off, and the slopes of the lines are slightly different, but the overall trend appears to be captured by the simulation. This is very good because the θ_{23} isn't directly calibrated in this model. It is based off of the calibration of the start of combustion in addition to the multi-variable combustion duration correlation represented by $\Delta\theta$. The model was

benchmarked to the start of combustion at the 9 gpm flow rate as shown in §3.5.1, and thus it would be expected that this flow rate would elicit results closer to the model when compared to the other fueling rates. Thus it is important to also analyze the quality of the simulations at a different fueling rate. These results can be seen in Figure 5.8.

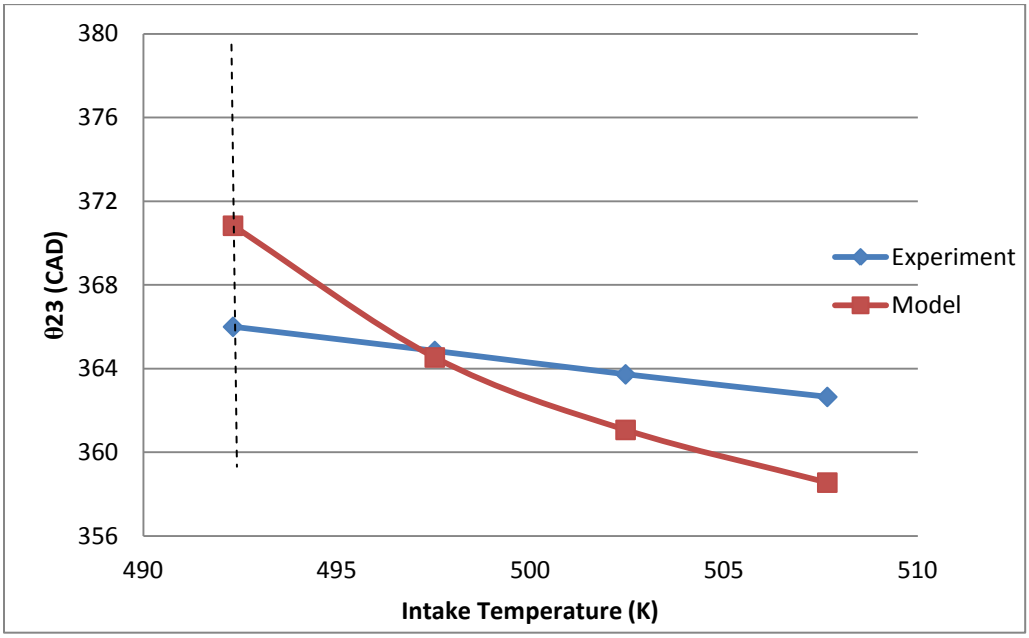

Figure 5.8. Comparison of Experimental and Model Location of Combustion (6 gpm)

In order to observe the largest discrepancy between the model and the simulation, the furthest fueling rate of the three rates tested in this study from the benchmarked rate of 9 gpm is shown in Figure 5.8. For this fueling rate of 6 gpm the general trend of the location of combustion parameter is still present, with an increase in θ_{23} as the intake

temperature gets closer to the onset of partial burn. The experimental data suggests that in actuality partial burn occurs a few degrees Kelvin lower than in the model, but the general effect of temperature on θ_{23} is captured. The disparity in this trend is a direct result of the location of the start of combustion not being benchmarked at this flow rate. The model had much higher accuracy predicting this parameter at the flow rate for which it was benchmarked. A direct correlation can be seen between the tracking of θ_{23} in Figure 5.8 and the trend displayed in its matching start of combustion trace in Figure 5.9.

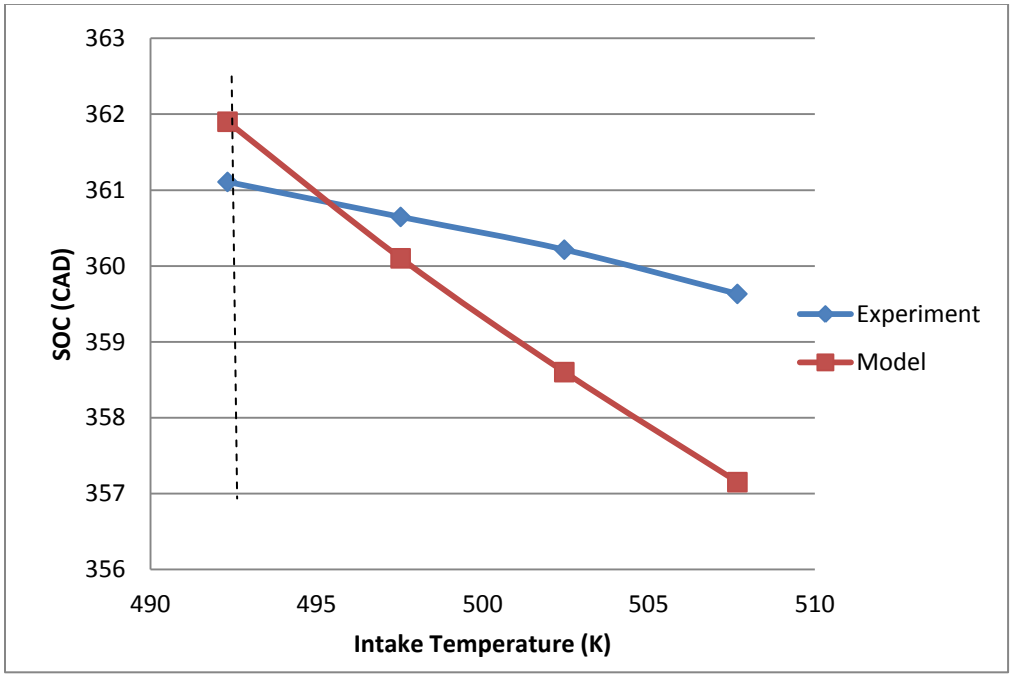

Figure 5.9. Comparison of Experimental and Model Start of Combustion (6 gpm)

The steeper slope of the experimental data is again apparent in Figure 5.9 comparing the start of combustion to the intake temperature for 6 gpm. This explains the difference in the very close tracking of θ_{23} at 9 gpm as opposed to a looser approximation at 6 gpm. Start of combustion is coupled with θ_{23} through the combustion duration term $\Delta\theta$ which was shown in §3.6 to have a very close correlation between experimental and model data. However, although the trend is less accurate for this flow rate than for the one at which it is benchmarked, it still passably estimates the effect of temperature within a few crank angle degrees on the combustion variables needed for this study.

5.2.3. Pressure Rise Rate. The last model output to be evaluated for the validation of the model is the pressure rise rate. This is an important variable due to it having the ability to depict the acceptable operating range of the HCCI combustion mode. This parameter was tested by varying the intake temperature as it was done in the experiment. The results for this can be seen in Figure 5.7.

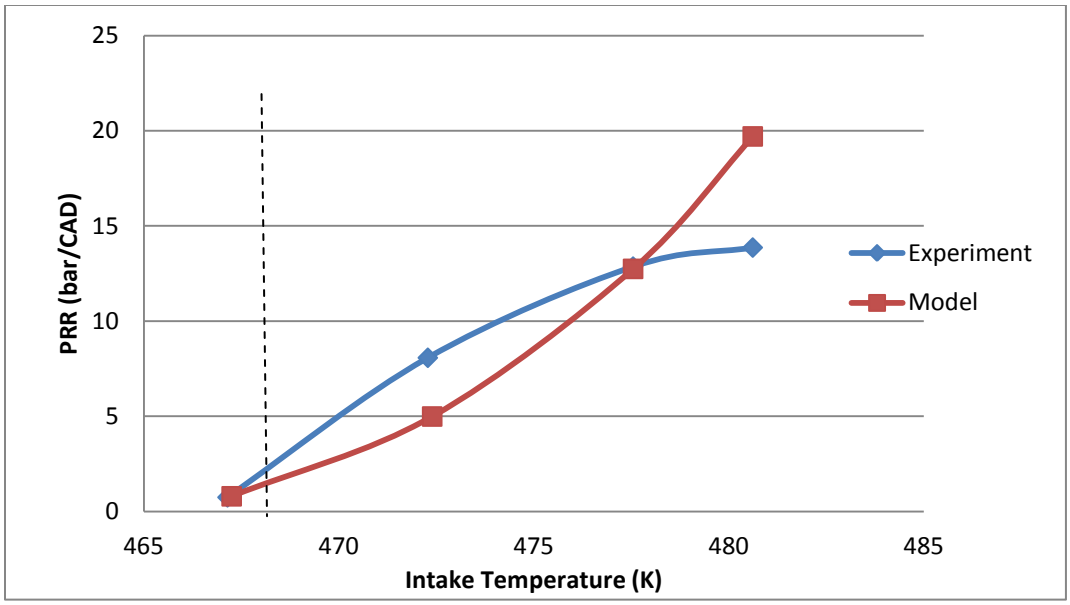

Figure 5.10. Comparison of Experimental and Model PRR (9 gpm)

Figure 5.10 shows the results of the model and the experimental data for the pressure rise rate at a flow rate of 9 gpm. It can be observed that the model seems to have a positive slope whereas the experimental data suggests that the PRR behaves with a negative slope. However, the magnitudes of the predicted values at the extremities of the accepted HCCI operating range are approximated fairly accurately. The upper limit of the operating range is bounded by high pressure rise rates (> 10 bar/CAD) due to excess engine noise, and the lower limit is evidenced by the onset of partial burn. Above the upper limit, it seems that the model overestimates the value for the pressure rise rate, but since this is not within the acceptable range, it doesn't affect the model's behavior where it is important.

To further ensure that the model can adequately capture the trend of the PRR, another flow rate was evaluated. These results can be viewed in Figure 5.11.

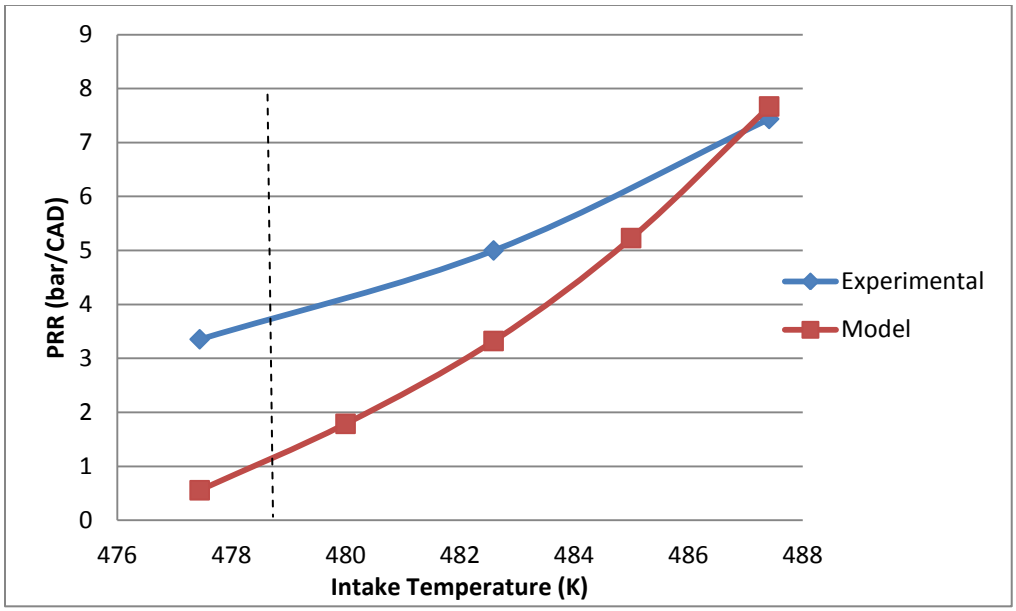

Figure 5.11. Comparison of Experimental and Model PRR (7.5 gpm)

In Figure 5.11 it can be noticed that for this flow rate, both of the trends show increasing slopes. The model was used to generate some additional points to ensure that the data followed the trend line suggested by the three experimental data points. Using the experimental data available, for these flow rate it appears that the model predicts the magnitude of the PRR at the upper limit of the operating range well, and that it underestimates the magnitude of the PRR at the onset of partial burn. Thus, the model

approximates that partial burn will occur a few degrees Kelvin higher than the experimental data shows. This is still acceptable, because the model doesn't need to be capable of exactly predicting the temperature degree of the onset of partial burn as long as it can estimate the behavior that occurs when partial burn is occurring.

5.2.4. Exhaust Temperature. The exhaust temperature is the final variable validated from the five-state thermodynamic portion of the model. This parameter is important through the direct impact on the subsequent cycle's temperature through the residual species. The ability of the model to predict this variable is shown below for a flow rate of 9 gpm.

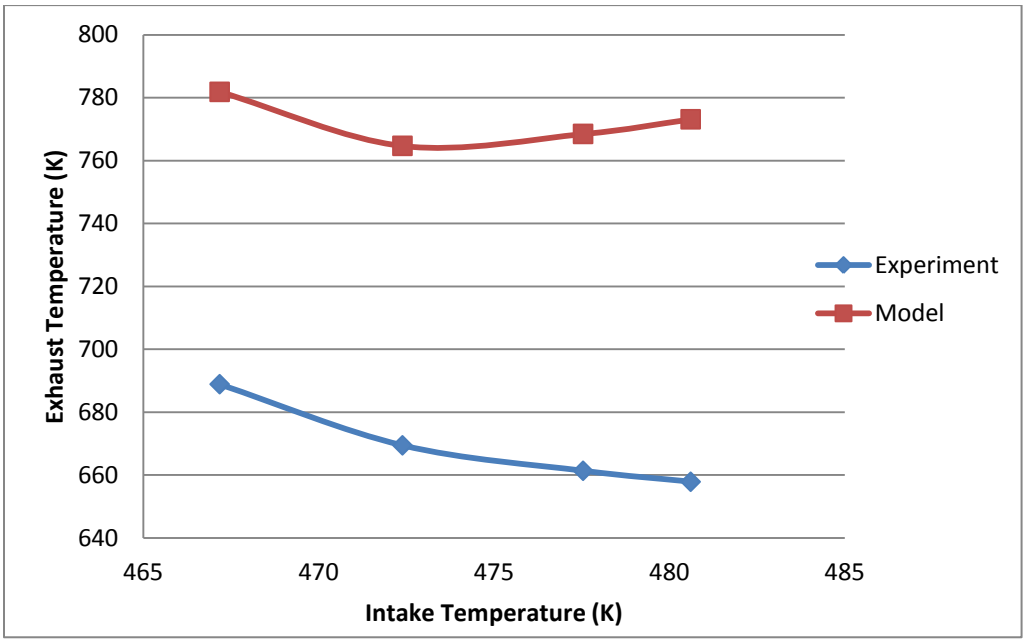

Figure 5.12. Comparison of Experimental and Model Exhaust Temperature (9 gpm)

For the comparison of the trends shown in Figure 5.12, this study refers to [4] which is the basis for the five-state thermodynamic portion of this model. The trends displayed in this figure are very similar to those shown in Figure 3.14 of [4] as shown in Figure 5.13.

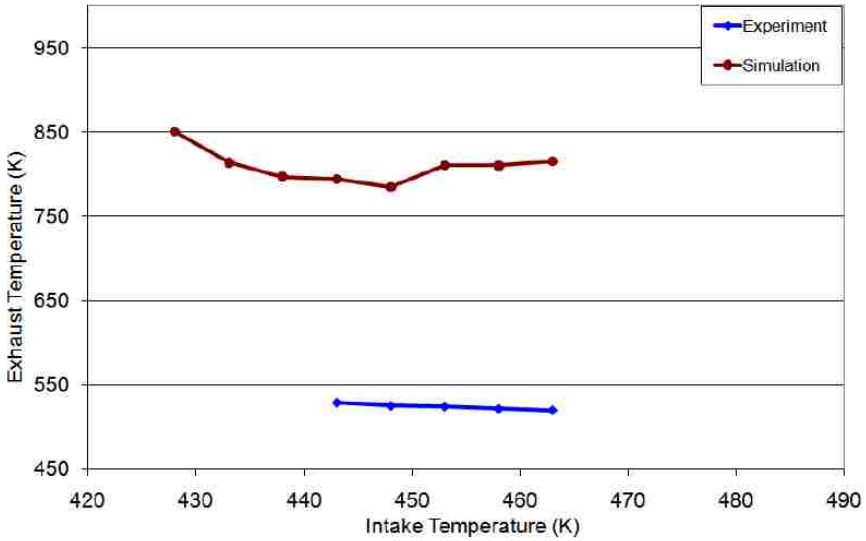

Figure 5.13. Comparison of Experimental and Model Exhaust Temperature (9 gpm) from Figure 3.14 of [4]

The model first decreases in the exhaust temperature and then begins to increase exactly as seen in the results of Bettis [4]. This can be easily observed by comparing the trends of the model and the simulation in Figure 5.12 and 5.13. Additionally, the model over-predicts the temperature seen in the experiment due to the idealized model not capturing the inefficiencies and heat loss associated with the Hatz engine. The experimental

exhaust temperature has a slight decrease with the increase of the intake temperature due to the ignition timing being further past TDC. All of these patterns, which are also captured by that original validated model, further help to solidify the validation of the updated model with the new chemistry for PRF96.

In order to show that these trends carry across set points, the model was used to calculate the exhaust temperatures for a fueling rate of 6 gpm and these results were compared to the experimental data as shown in Figure 5.14.

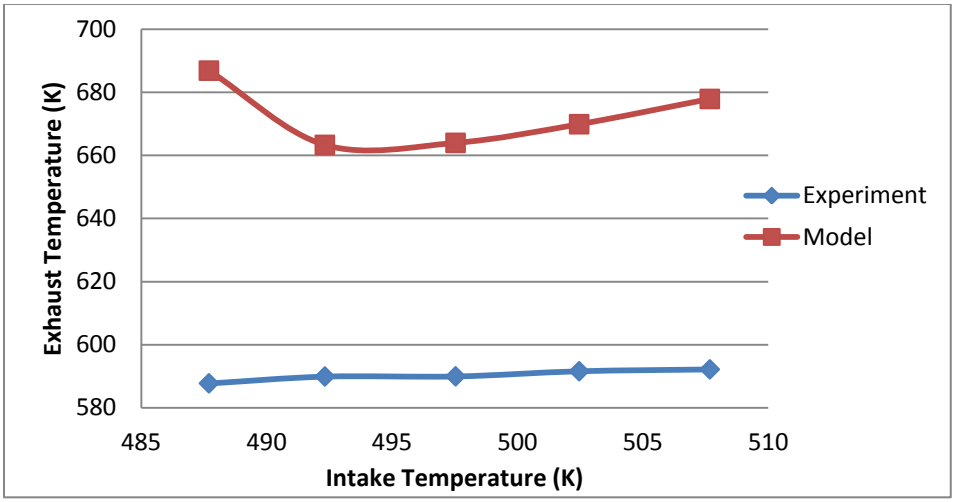

Figure 5.14. Comparison of Experimental and Model Exhaust Temperature (6 gpm)

Both the model and experimental results again display the same correlations when compared to the results of Bettis for the same fueling rate as shown in Figure 5.15.

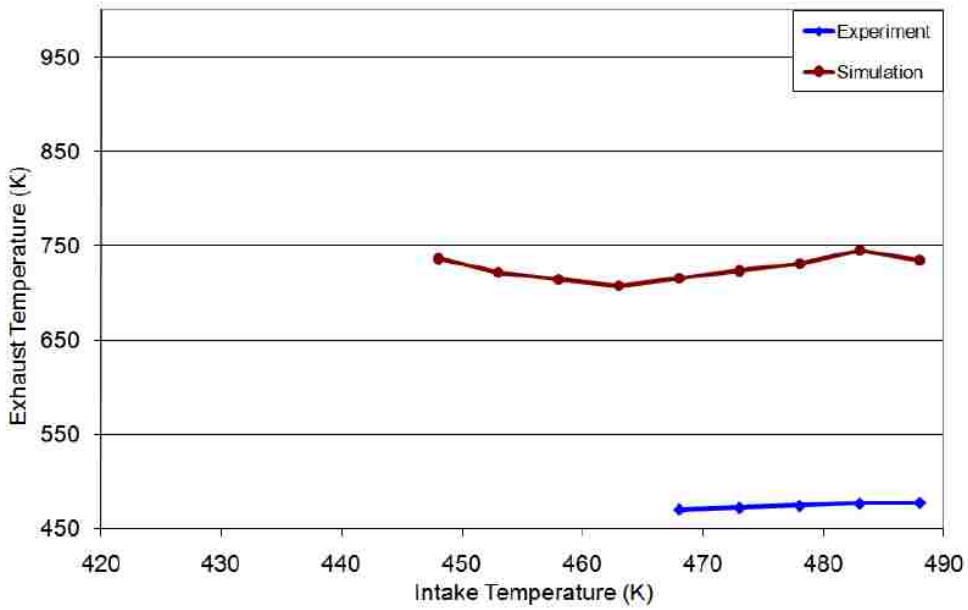

Figure 5.15. Comparison of Experimental and Model Exhaust Temperature (6 gpm) from Figure 3.23 of [4]

In these figures, it can be seen that the experimental exhaust temperature is increasing as the intake temperature is, and that again the model overestimates the temperature. The slight decline in the model temperature is present in both Figures 5.14 and 5.15 followed by a steady increase. The confirmation of these trends for this second fueling rate affirms the validation of the updated model for the PRF96 chemistry.

Further validation of many other variables calculated by the five-state thermodynamic portion of the model can be seen in [4] demonstrating the ability of the model to predict the behavior of the pressure and temperature at each different state of the cycle.

5.3. CHEMICAL KINETIC MODEL VALIDATION

The chemical kinetic portion of this model is used to simulate the amounts of carbon monoxide that are produced during each cycle. In the interest of using the chemical kinetic model to its greatest extent, it is important that the amounts of carbon monoxide estimated are indicative of the quantities that are naturally produced within the engine. This will allow for the best analysis of the cyclic dynamic effects that are produced. If the carbon monoxide is shown to have an effect at the levels produced naturally, then it could potentially be used as a control mechanism for ignition. However, before any results can be discussed, it must be shown that the chemical kinetic model does indeed produce reliable species concentrations.

Correspondence with Ernst [7] describes that the chemical kinetic simulation accomplished with CHEMKIN can be used to determine that the mass concentrations of critical species, in this specific case CO, evaluated under different states of incomplete combustion and carried into the subsequent engine cycles. The CHEMKIN program was compiled with Intel Visual Fortran XE 2011. Using this simulation, the user inputs initial conditions of equivalence ratio, temperature after compression immediately prior to combustion, pressure at IVC, and an optional presence of additional species as a mass amount within the premixed initial charge. The constant volume combustion process is simulated and returns the amounts of each chemical species that is created within combustion at each desired time step along with the percent energy that is released. The results from the skeletal mechanism of Tsurushima used in the CHEMKIN simulation were compared with a detailed PRF mechanism developed at the Lawrence Livermore National Laboratory [33]. This detailed mechanism consists of 1,034 species and 4,238

reactions as opposed to the Tsurushima mechanism's [8] use of 33 species and 38 reactions. The mole fractions estimated by the two separate mechanisms are seen in Figure 5.16.

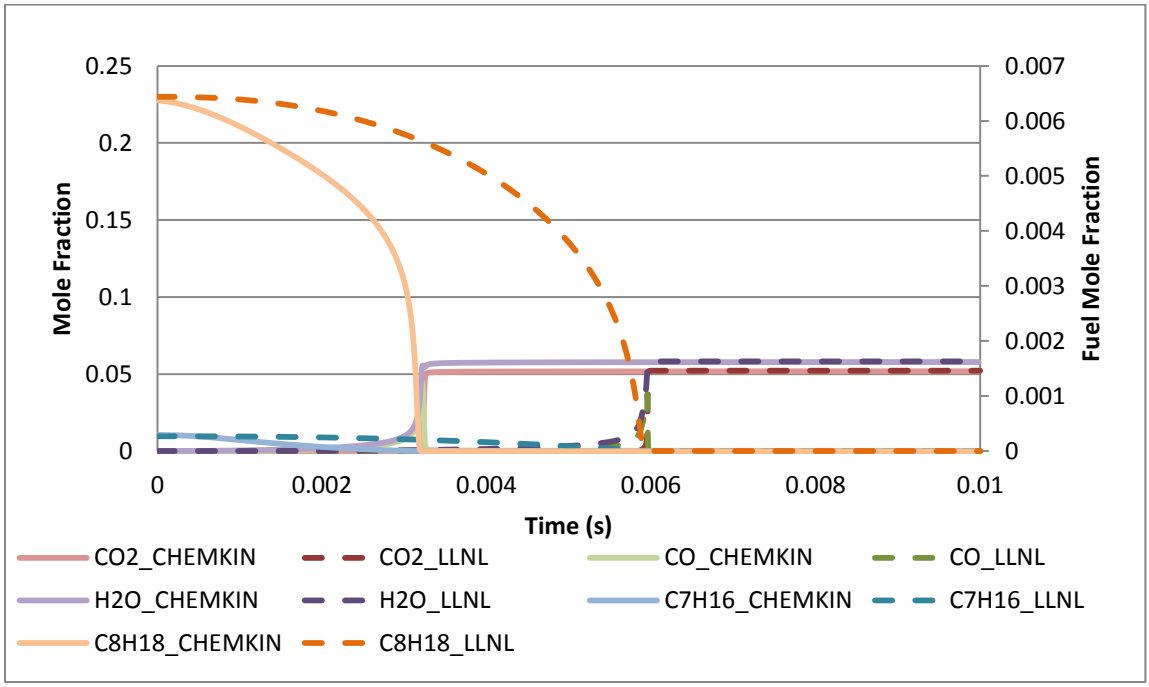

Figure 5.16. Species Validation for $\varphi = 0.40$, $T_o = 950\ K$, $P_o = 28\ atm$ [7]

The mole fractions for all species except the two fuel components are on the primary vertical axis in Figure 5.16. The fuel component quantities are seen on the secondary axis. It can be noticed that the species were calculated using time as the increment. The dashed lines represent the values of the species as determined using the LLNL detailed

kinetic mechanism while the solid lines represent the skeletal Tsurushima mechanism. It is observed that the steady state value of each species is identical between the two distinct mechanisms. The difference noticed between the use of the detailed and skeletal mechanisms is the time at which the steady state value is attained. The reduced mechanism predicts that the oxidation process occurs at an earlier time. However, the time at which these values are attained is not the basis for determining the measure of the completeness of combustion in the CHEMKIN model. Instead it was based on the amount of total fuel energy released during the simulations [7]. Therefore as long as the species evolution follows the same trends between the two mechanisms, the output is deemed acceptable [7]. Thus, the skeletal Tsurushima chemical kinetic mechanism used in this model is validated in its results when compared to the highly detailed kinetic model created by Lawrence Livermore National Labs for the evaluation of how PRF reacts during combustion at inlet conditions that are viable for the experimental set-up of the Hatz 1D50Z.

5.4. OPERATING RANGE.

HCCI is known for having a limited range where stable combustion is viable. Data gathered from the Hatz 1D50Z experimental set-up at Missouri S&T shows that there is a narrow window where the combustion timing produces stable operation. Bounded by the partial burn regime that ultimately results in misfire on the one end of the spectrum, and unacceptable noise output produced by high pressure rise rates on the other, it becomes pertinent to determine the full range of acceptable operation that is applicable to the Hatz while operating in HCCI mode. This range was determined by

incrementing the temperature from 300 to 800 K in conjunction with incrementing the fuel flow rate from 1 to 25 gpm to cover the entire spectrum of combustion for this model.

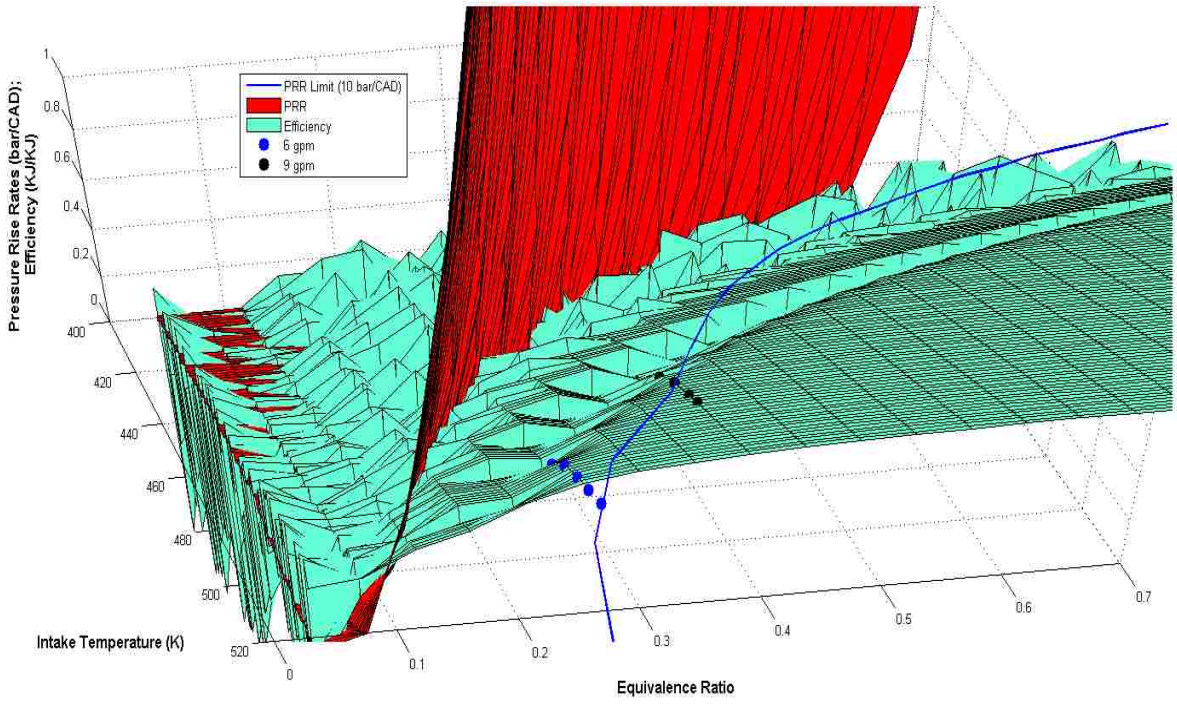

Figure 5.17. HCCI Efficiency and PRR "Waterfall" Plot

A snippet of these modeling results, showing the operating window where the ignition timing produces sustainable combustion, is shown in Figure 5.17. The red surface shows that the Pressure Rise Rate (PRR) rapidly increases from near zero to large values. The upper PRR limit is demarcated by the blue line. This line is reflected down from the PRR surface to indicate where the red surface crosses the 10 bar/CAD threshold. The teal

surface is indicative of the efficiency (work out/fuel energy in). The efficiency serves as a rough indicator of when stable combustion is occurring. It is from this surface that the plot is likened to a waterfall. During higher equivalence ratios from 0.28 and greater, and intake temperatures from 440 K and greater, where advanced combustion timing is present, the surface is smooth and fairly constant. As the equivalence ratios and intake temperatures decrease, the surface becomes more ragged until it falls down into the partial burn/ misfire regime where retarded combustion timing occurs. Partial burn is clearly indicated by the jagged "waves" showing unstable combustion. The bounds of the stable operating window are the red PRR surface on the left, and the blue line on the right. This is a fairly limited area, demonstrating the narrow zone of stable combustion that HCCI mode is known for. In order to display the accuracy of the model, experimental data is also shown on the chart for fueling rates of 6 and 9 gpm. It can be noticed that the lower edges of the data sets are right on the cusp of the "waterfall" and the upper edges are at the noise limit of a pressure rise rate of 10 bar/CAD. This shows that the model is predicting a reasonable operating window for HCCI combustion.

If Figure 5.17 is compared to the resulting waterfall plot from Bettis, on which this model is based, a few differences are noticed. This can be seen in Figure 5.18.

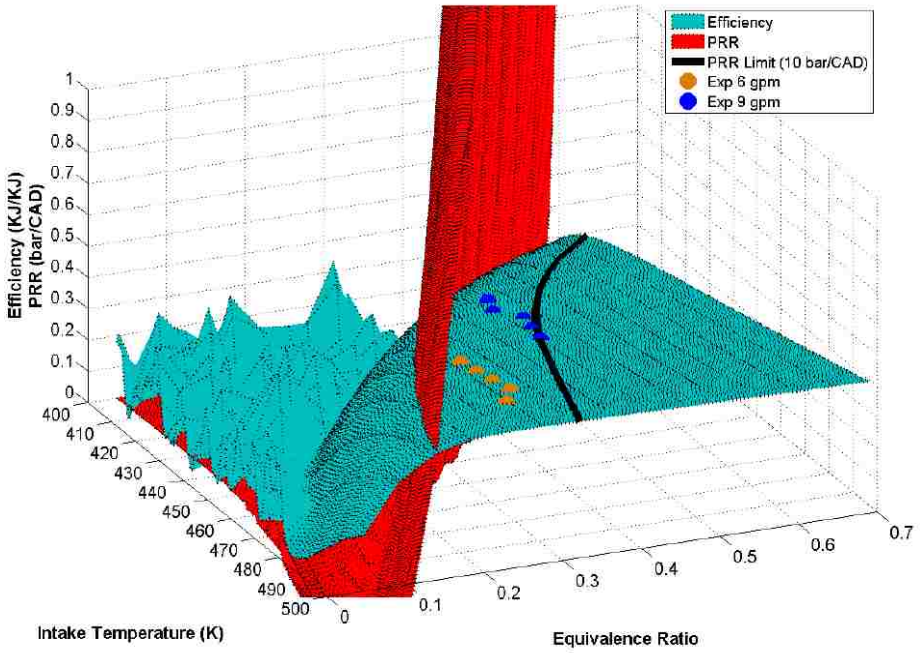

Figure 5.18. Bettis' Waterfall Plot [4]

Figure 5.18 was generated by Bettis with the same methodology used in this study. The differences in the models are the fuels used and the addition of the chemical kinetic model. A comparison between Figure 5.17 and 5.18 shows that the efficiency surface for the new model is slightly jagged before it reaches the red PRR surface whereas the efficiency surface in Figure 5.18 is completely smooth. Since the fuel composition used in Bettis' model is iso-octane, which comprises 90% of the fuel used in this study, PRF 96, compositional differences through the five-state model seems to not be the factor causing the surface to be rough. Thus, it is assumed that the surface is affected by the chemical kinetic model. The precise effects of the chemical kinetic model will be discussed in Chapter 6.

6. SIMULATION RESULTS AND DISCUSSION

To fully evaluate the effects of carbon monoxide on the pertinent parameters within this model, many different cases need to be considered. First the effect caused by the amount of carbon monoxide naturally produced will be examined followed by the effects caused by an artificially elevated amount. Then the return maps created by perturbing selected factors will be discussed to examine the correlation between the cycles. These will be created for both partial burn and complete combustion cases to observe the differences therein.

6.1. NATURALLY PRODUCED CARBON MONOXIDE

Since the primary focus of this study is on the effects of carbon monoxide on the different parameters calculated in the model, the naturally produced amount of carbon monoxide as predicted by the model was varied first to identify the results. Since the model, for any given set point, converges to a steady state value, it is necessary to include perturbations caused by a Gaussian random number generator to capture the stochastic variations typically seen in experiments. This Gaussian random number generator was added to the molar amount of naturally produced quantities of carbon monoxide, as denoted by Γ in the model, within the engine with a mean of zero and a magnitude that represents typical variations experienced in experimentation. The results depicted in Figure 6.1 below were observed.

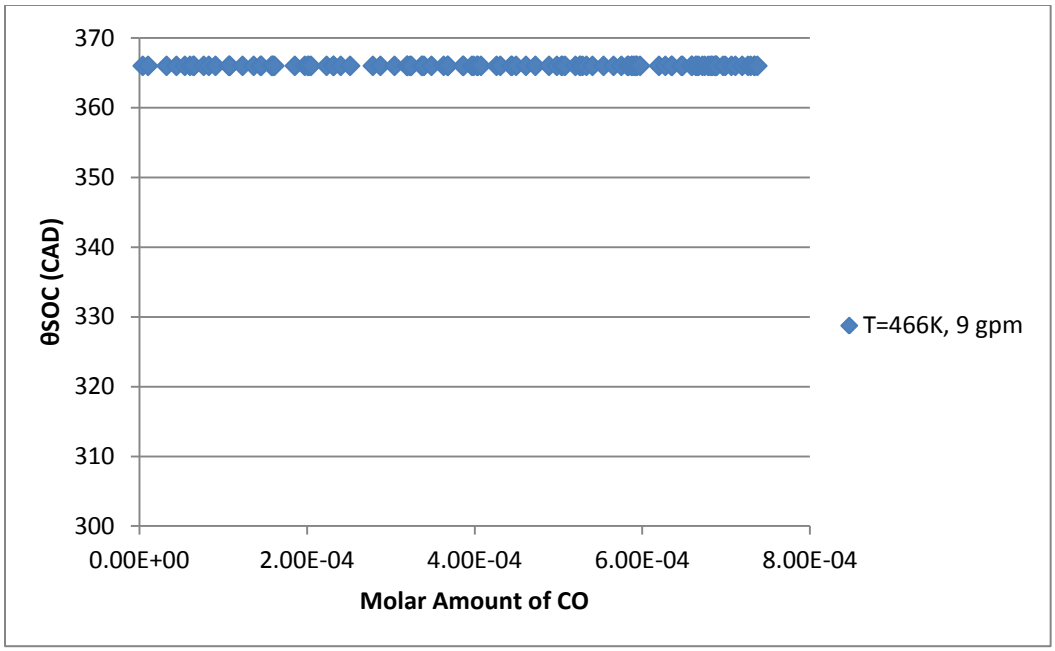

Figure 6.1. θ_{SOC} Versus Molar Amount of CO for T_{in}=466 K and 9 gpm

Figure 6.1 demonstrates that when slightly varied, the naturally produced amount of carbon monoxide at this set point of an inlet temperature of 466 K and a fueling rate of 9 gpm does not have an effect on the angle of the start of combustion. This set point was chosen because it was in the partial burn regime close to the misfire limit. The location of this set point in partial burn is more clearly seen in Figure 6.2.

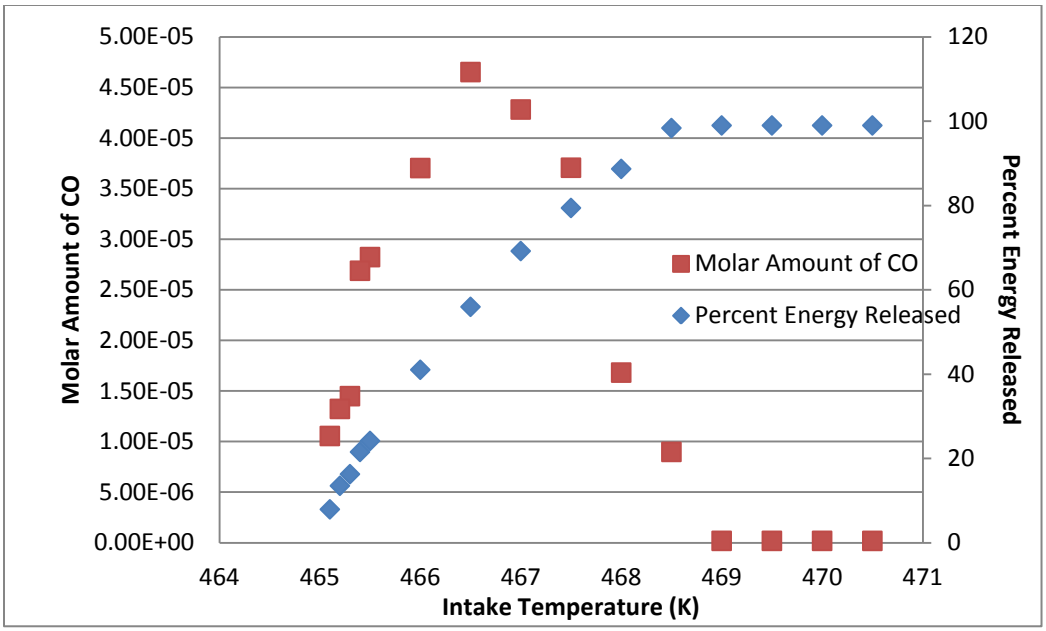

Figure 6.2. Molar Amount of CO and Percent Energy Released Versus Intake Temperature for 9 gpm

Figure 6.2 demonstrates that for a fueling rate of 9 gpm the model predicts that the onset of partial burn will occur at 468 K and complete misfire will occur at 465 K. Thus, the set point used to create Figure 6.1 is close to the point of misfire in the partial burn regime.

Even though no effect was produced on the location of start of combustion as shown in Figure 6.1, it does not conclusively imply that carbon monoxide has no effect at all. But, it does suggest that the amount of carbon monoxide that is found in the engine cylinder as determined by this model is insufficient to impact SOC. Therefore, it is instructive to increase the amount of carbon monoxide artificially to determine if it has any potential to be used as a control mechanism.

6.2. ARTIFICIALLY INCREASED CARBON MONOXIDE

In order to investigate the effect of an artificially increased amount of carbon monoxide, a multiplier was applied to the molar amount of CO and the model was allowed to converge to the steady state. This multiplier was varied over several magnitudes to observe the effect on the start of combustion. These results can be seen in Figure 6.3 with the multipliers being listed in the legend of the graph.

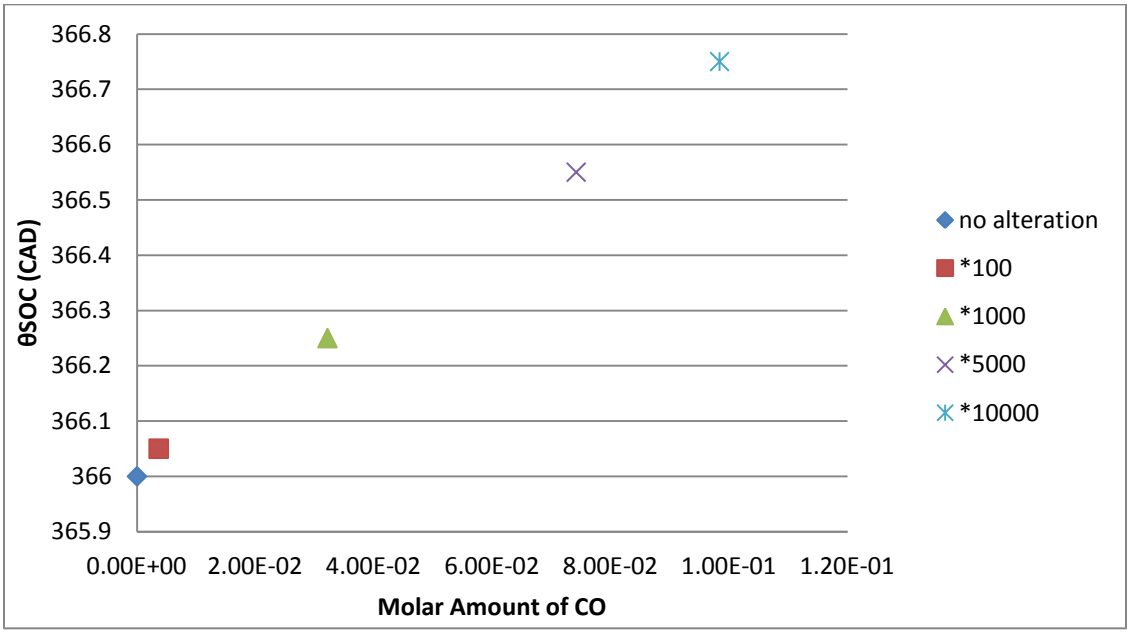

Figure 6.3. θ_{SOC} When Multipliers are Applied to CO Amount at T_{in}=466K and 9 gpm

Figure 6.3 clearly shows that increasing the molar amount of CO from the naturally produced quantity to several orders of magnitude larger (from 10^{-5} to 10^{-1} moles, or mole

fractions from 10^{-7} to 10^{-3}) provides an impact on the location of the angle of the start of combustion by three quarters of a crank angle degree. This is a noticeable, but not outstanding, amount of fluctuation that could help to provide control over the location of combustion during partial burn, even though it requires the addition of CO to the system to elicit this behavior. To further examine this behavior and considering that these results were obtained by using a simple multiplier on the molar amount of CO, the Gaussian random number generator was added back onto the CO amount in addition to the multiplier to induce the model to fluctuate around this greater amount of CO production instead of allowing the model to converge on a single value to observe the resulting behavior.

In order to verify that the coupling of the five-state thermodynamic model and the chemical kinetic model is behaving as intended for this increased quantity of CO, the relationship between the molar amount of carbon monoxide and the percent energy released can be compared. This is shown in Figure 6.4.

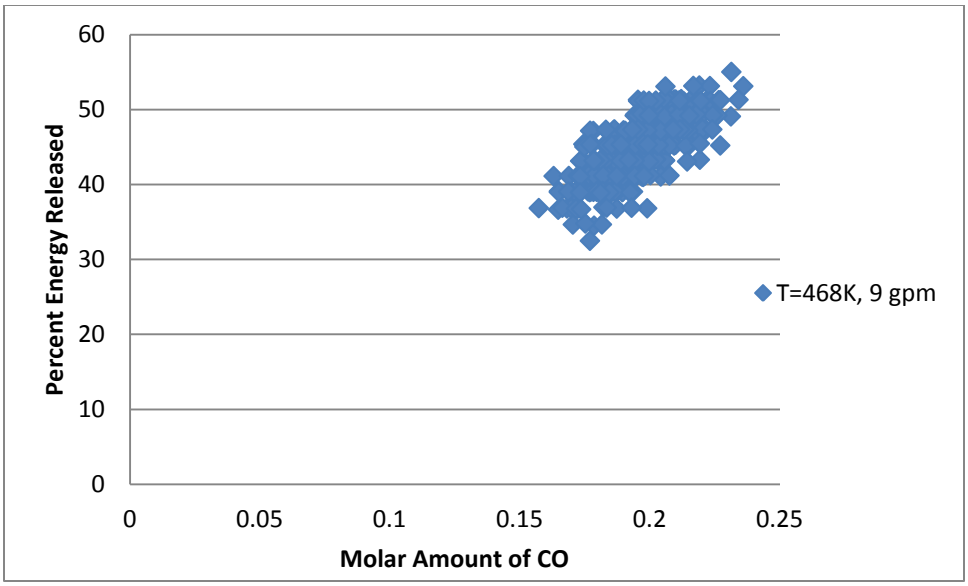

Figure 6.4. Percent Energy Released Versus Molar Amount of CO*5,000 for T_{in}=468K and 9 gpm

Figure 6.4 is generated using the multiplier and the Gaussian generator on the molar amount of CO for a set point that has a two degree higher intake temperature and is therefore closer to complete combustion than misfire as will be explained later in Figures 6.7 and 6.8. The graph shows the anticipated relationship between the percent energy released and the molar amount of CO suggesting that the code coupling is functioning properly. As discussed in §3.9.2, the maximum amount of carbon monoxide produced within the engine occurs when 56% of the energy is released and that the maximum feed forward window assumed for this model occurs between 50 and 65%. Thus the behavior displayed in this figure is as expected, with a positive trend for the slope. Since the maximum value of feed forward is not yet reached for this data set, only one half of the parabola is shown accounting for the positive slope.

With the proper function of the model established the effect of carbon monoxide on the location of the start of combustion can be examined.

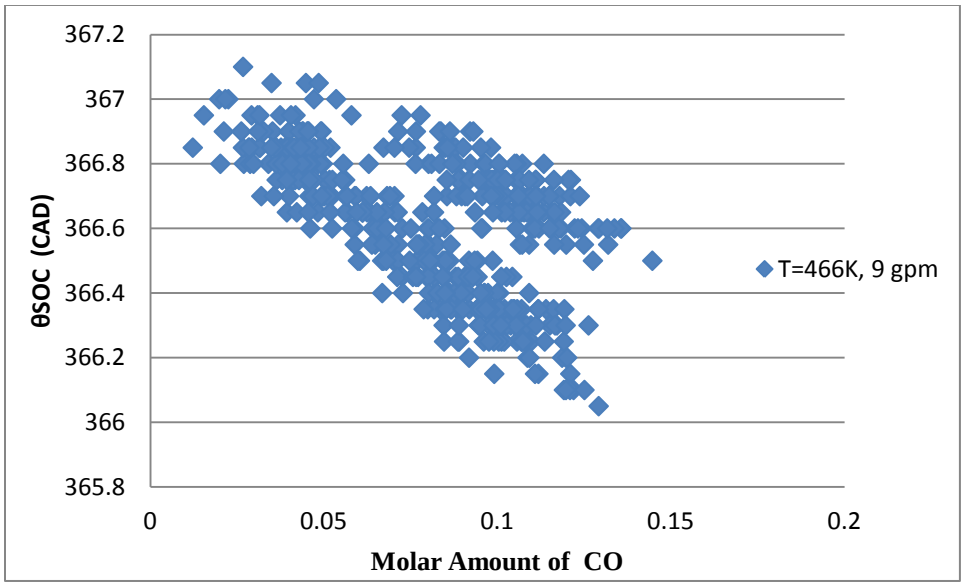

Figure 6.5. θ_{SOC} Versus Molar Amount of CO*5,000 for T_{in}=466K and 9 gpm

The same set point and Gaussian random number generator conditions were used to generate Figure 6.5 as Figure 6.1 while also including a multiplier of 5,000 on the molar amount of CO determined by the model. Now, instead of results indicating that the crank angle degree of the start of combustion remains the same, a trend emerges. As the molar amount of CO increases, the combustion timing advances. It is also noticed that there seem to be two separate sets of data. This is due to the carbon monoxide amounts being generated from the chemical kinetic model for two different amounts of residual fed from

the previous cycle. These different quantities were explained by the partitioning of the residual feed forward amounts in Figure 3.14. The smaller set of data located more to the upper right of the figure is the result of a higher concentration of CO within the cylinder even though the molar amounts are the same causing the timing to be more advanced than for the lower concentration of CO. Neither data set should be considered to have a higher amount of accuracy due to the differences in concentration. If the data is sorted such that only one partition of the feed forward amounts from the spreadsheets is considered, then this separation issue is resolved as seen in Figure 6.6.

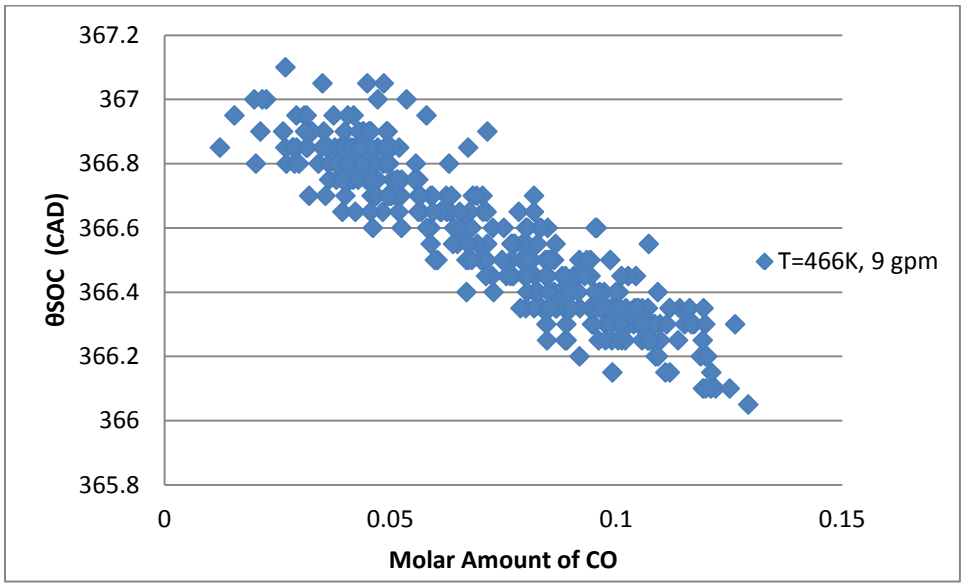

Figure 6.6. θ_{SOC} Versus Sorted Molar Amount of CO*5,000 for T_{in}=466K and 9 gpm

Figure 6.6 confirms the assumption that the separation of data was caused by the molar amount of CO being determined from different spreadsheets. The graph also shows that the model predicts that the location of the start of combustion varies by a full crank angle degree. In order to investigate the full range of the partial burn zone it was deemed necessary to examine how much of the partial burn range was covered by this set point as shown in Figure 6.7.

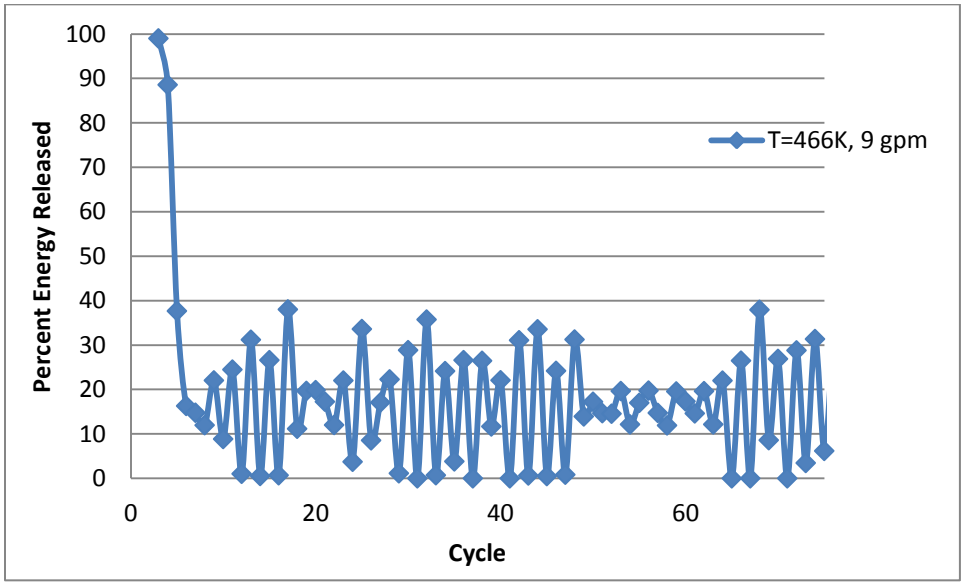

Figure 6.7. Percent Energy Released Versus Cycle for T_{in}=466K and 9 gpm

Figure 6.7 was created using the same technique as the previous two figures, with a multiplier of 5,000 being applied to the molar amount of CO along with a Gaussian random number generator. The model was run for 500 cycles; Figure 6.7 only shows the

first 75 for clarity. It can be seen that the percent energy released behaves in an oscillatory manner from cycle to cycle, where a state of lower energy is succeeded by a state of higher energy. This suggests that there are cyclic dynamics present that are created by the carbon monoxide. This figure also shows that the current set point reflects the end of the partial burn zone as it approaches misfire. As discussed previously, this model assumes that the completeness of combustion is directly correlated with the percent energy released. Thus zero percent energy released equates to misfire. Except for the first few cycles where the model is being initialized, this set point causes a maximum energy release of 40% with oscillation in between this maximum value and misfire.

Since this set point is on the lower end of partial burn, it would be prudent to examine a similar set point that can account for another portion of the partial burn regime closer to complete combustion to see if the trends noticed for this section of the regime are duplicated when combustion is closer to complete. Thus, to investigate this upper realm of partial burn, the intake temperature was increased by two degrees and all other inputs remained the same, including the Gaussian number generator and the multiplier of 5,000 applied to the molar amount of CO determined by the model.

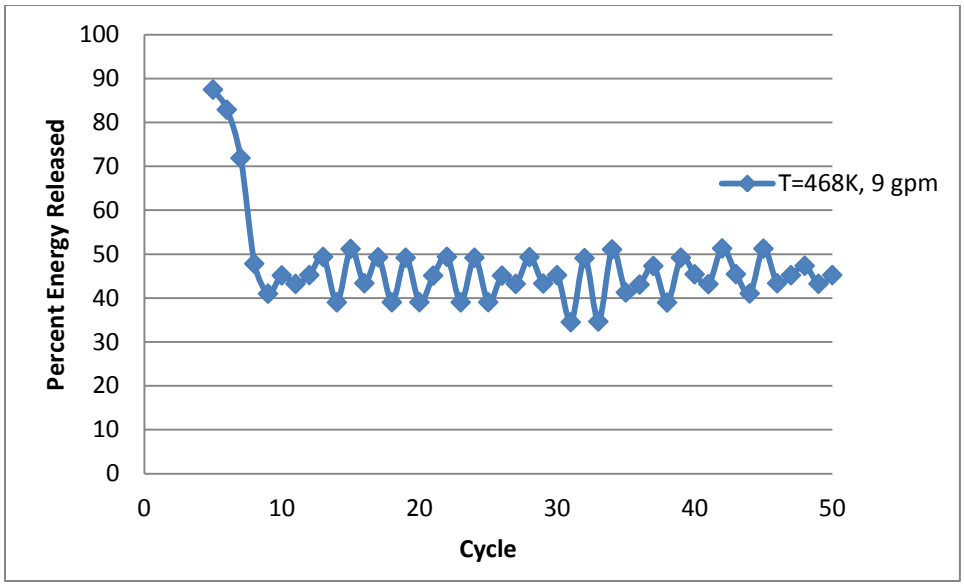

Figure 6.8. Percent Energy Released Versus Cycle for T_{in}=468K and 9 gpm

As Figure 6.8 shows, the two degree temperature increase resulted in shifting the percent energy release up closer towards complete combustion. The model predicted that the first few cycles would be nearer to complete combustion finally converging around the area of the percent energy released that has a greater amount of residual to be fed forward. The oscillatory trend with the percent energy is still present for this set point. Thus, the addition of carbon monoxide causes a higher energy cycle to be followed by a lower energy cycle. In addition to the relation between the percent energy released and the cycle number, the last set point also examined the relation between θ_{SOC} and the molar amount of CO. To identify if a similar trend is replicated for this set point as for the previous one, Figure 6.9 is taken into consideration.

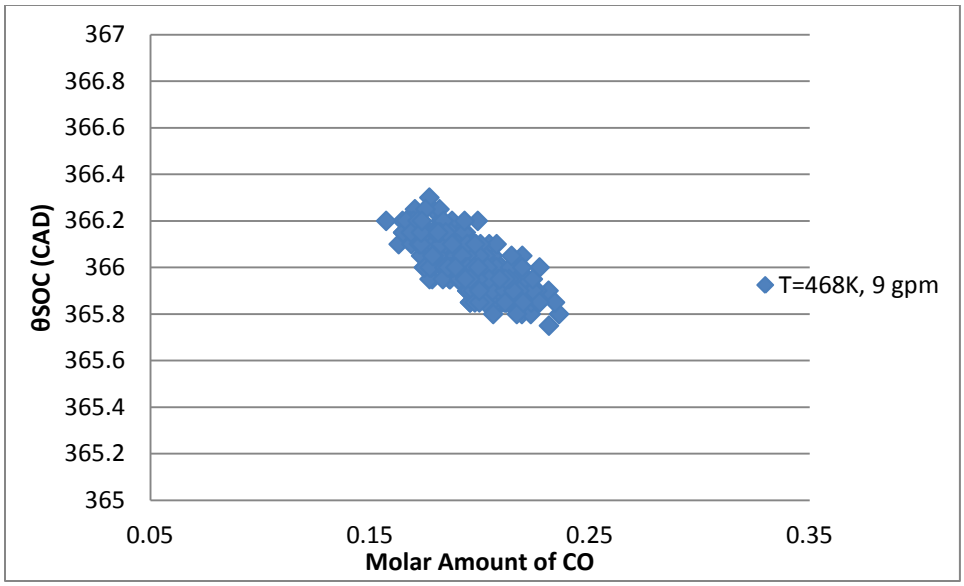

Figure 6.9. θ_{SOC} Versus Molar Amount of CO*5,000 for T_{in}=468K and 9 gpm

Figure 6.9 displays that a similar trend indeed occurs. The molar amount of carbon monoxide considered for this case is still altered by a multiplier and a small perturbation by the Gaussian random number generator. This trend suggests that the combustion timing is advanced by a higher molar amount of carbon monoxide while within the partial burn regime. This set point also displays that the location of the start of combustion varies by three quarters of a crank angle degree. This amount of variation could be of aid in the control of an engine operating in HCCI mode during partial burn.

Since it has now been determined that CO can have an effect on the location of the start of combustion if levels higher than those naturally produced in the engine are present, return maps can be examined to determine the cyclic impact.

6.3. RETURN MAPS

Return maps are a powerful tool that are used to determine interactions between cyclic events. They show, without averaging, correlation between every individual pair of consecutive events. They are created by plotting each value of the desired parameter against the value of the same parameter in the next cycle. If a pattern emerges, then the values affect each other between cycles and it is termed as deterministic. If, however, a small unstructured circular data set emerges representing a Gaussian random distribution, then there are no prior cyclic effects which suggests that the variations seen are stochastic. Furthermore, it is important that the graphs use the same limits for both axes so that the shape of the trend stays true and is not skewed. These maps will primarily be used to examine cyclic dynamics during partial burn to determine the effect of carbon monoxide on many different parameters.

6.3.1. Variation of Artificially Increased Carbon Monoxide during Partial Burn.

To analyze the full cyclic effect that carbon monoxide addition has, the return maps of the location of the start of combustion (θ_{SOC}), the output parameter of work and by extension the efficiency and Indicated Mean Effective Pressure (IMEP), and the exhaust temperature (T_5) will be presented. For the sake of continuity, the set point was selected to create the return maps is the same as was used for generating the trends in the previous section with an intake temperature of 468 K, a flow rate of 9 gpm, a multiplier of 5,000 and the Gaussian random number generator with a mean of zero on the calculated molar amount of carbon monoxide. The cyclic effect of the first parameter to be considered, the location of the start of combustion, is shown in Figure 6.10 below.

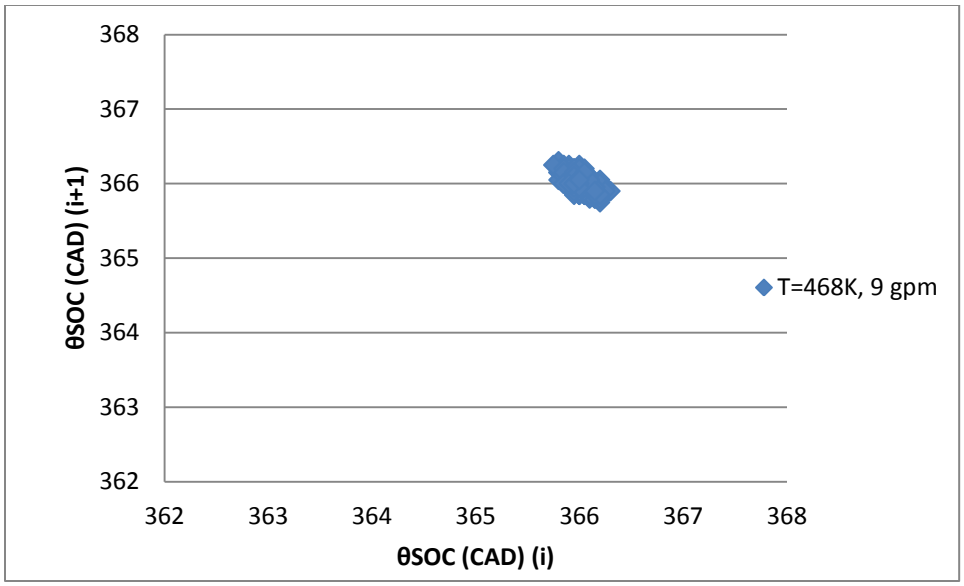

Figure 6.10. Return Map of θ_{SOC} for T_{in}=468 K and 9 gpm

The deterministic shape of the data, an elliptical shape as opposed to a circular form, in Figure 6.10 suggests that there is a negative cyclic correlation when the molar amount of carbon monoxide within the engine cylinder is varied for this set point. This adds weight to the claim that carbon monoxide could be used as a control during partial burn. It is important to consider these effects across different set points to see if the potential for control is realistic. Thus, a similar point is considered for the lowest fueling rate of 6 gpm (an equivalence ratio of 0.28 compared to 0.44). The intake temperature was raised to 489 K to bring the combustion into the partial burn regime for this lower fueling rate, and the multiplier of 5,000 and the Gaussian random number generator remain as they were. With these small alterations, Figure 6.11 was created.

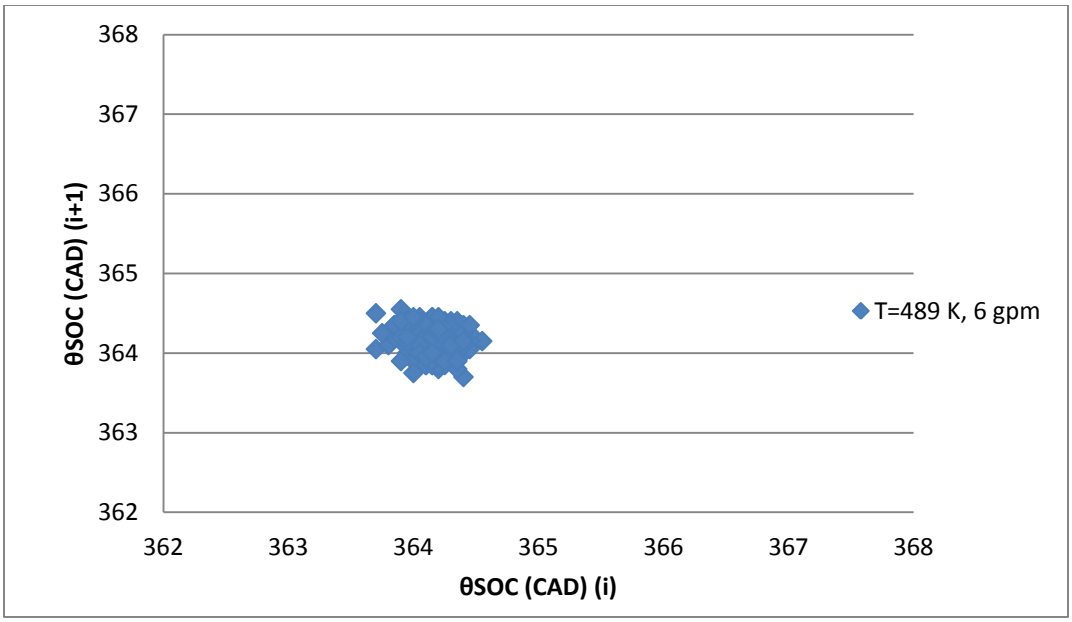

Figure 6.11. Return Map of θ_{SOC} for T_{in}=489 K and 6 gpm

It can be observed in Figure 6.11 that the determinism displayed for the higher fueling rate is still present, although the trend is a little weaker. This is consistent with the experimental results that Attebery shows in [3] in that more determinism is present at higher fueling rates. Even though the experiments in [3] were run with indolene as opposed to the PRF96 used in this study, they were generated using the engine described in this work with the same methodologies, and the fuel has the same octane number. A few of Attebery's results can be seen in the figure below.

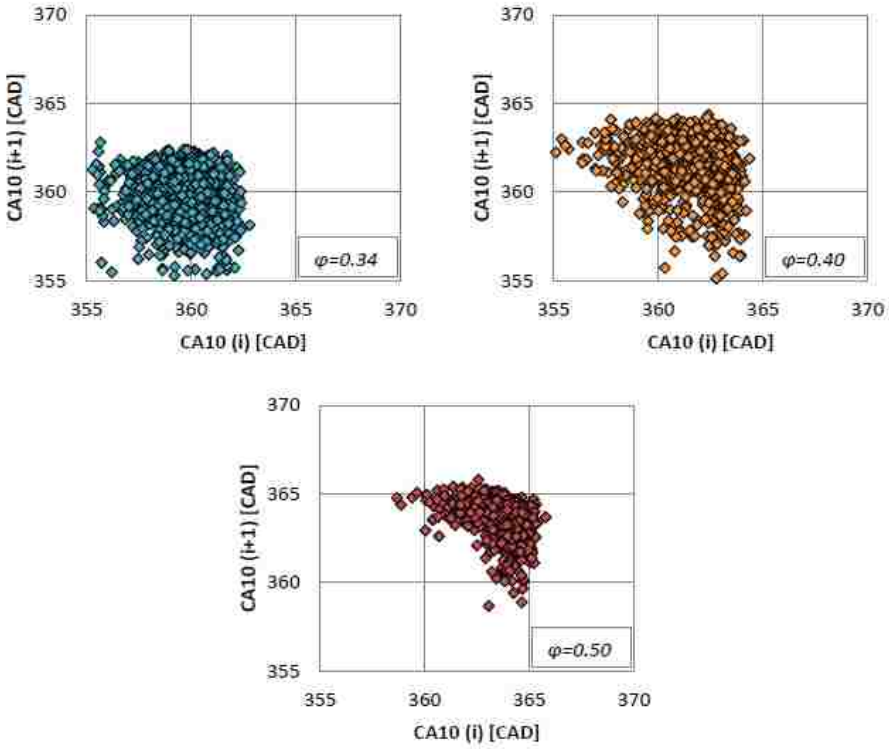

Figure 6.12. Attebery Return Maps for CA10 (θ_{SOC})

Figure 6.12 displays the experimental results that Attebery obtained from the 1D50Z Hatz engine running indolene. Another difference of note is that these were created using increased internally trapped residual gas instead of pure carbon monoxide. As was explained in §4.2.5, CA10 is synonymous with the crank angle degree where combustion starts, θ_{SOC}. The lower fueling rate of 6 gpm is equal to an equivalence ratio of 0.28, which is slightly lower than the data in the top left return map. The higher fueling rate of 9 gpm, equivalence ratio of 0.44, falls in between the other two return maps. The determinism can be seen to increase with load as it does with the predicted data from the simulation. The type of determinism, as shown by the shape, is slightly different between

the model and the experimental data with the experimental data having a boomerang-shaped appearance and the simulated data being more elliptical in nature. This suggests that in the elliptical shaped return maps a high quantity is followed by a low quantity in the next cycle, whereas in the boomerang some cycles display very little variance.

Overall, the simulated data shows that the deterministic traits of the location of the start of combustion get more prominent as the fueling rate, and thus the equivalence ratio, increases showing that the current cycle is impacting this next cycle. It is also pertinent to note that the molar amount of carbon monoxide present at this lower fueling rate is approximately half of the higher fueling rate. In order to test how much of this effect is due directly to the amount of carbon monoxide present, the multiplier on the CO will be altered from the amount of 5,000 to a lower quantity and a higher quantity on the 9 gpm set point and the new return maps will be examined.

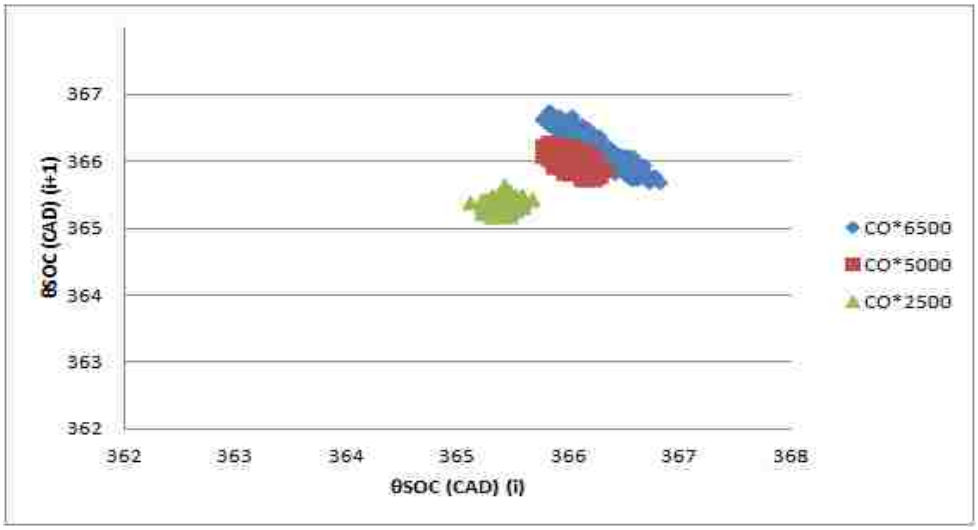

Figure 6.13. Return Map of θ_{SOC} for T_{in}=468 K and 9 gpm with Various Multipliers

The lower residual multiplier creates a return map in Figure 6.13 that shows a pattern that is bordering on stochastic. The return map generated for the higher multiplier of 6,500 displays a very deterministic trend. This helps to reaffirm the supposition that the determinism present in the previous two figures is dependent upon the amount of carbon monoxide in the system. With the effect of CO on θ_{SOC} during partial burn now reviewed, the effect on other terms can now be examined.

One of the most important outputs that an engine has is how much work it can accomplish. With other parameters being easily related to the work through the inclusion of a constant factor, as the indicated gross efficiency does by normalizing the work by the fuel energy input and with the Indicated Mean Effective Pressure (IMEP) by dividing the work by the displacement volume, it was determined that work was an important factor to consider when examining the effect of carbon monoxide within the engine. Thus Figure 6.14 was created for the set point with the intake temperature at 468 K, flow rate at 9 gpm (equivalence ratio of 0.44), and the original carbon monoxide multiplier of 5,000.

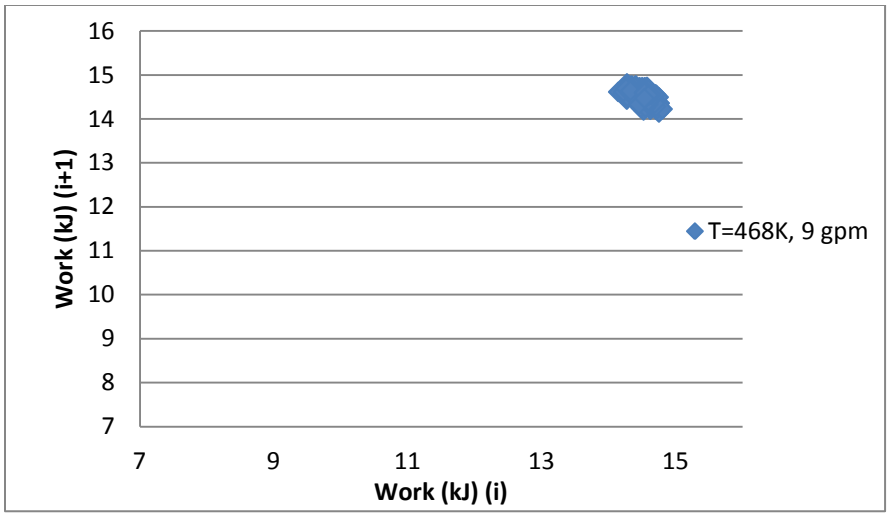

Figure 6.14. Return Map of Work for T_{in}=468 K and 9 gpm

Figure 6.14 shows that when the increased amount of carbon monoxide is varied, a deterministic trend appears in the return map for the amount of work output from the engine. Again, this corroborates what the experimental data gathered by Attebery [3] shows. The data collected displayed that the larger amount of unburned residual that was present, the more prominent the determinism. Thus, the trend should show less determinism for the 6 gpm set point, as Figure 6.15 confirms.

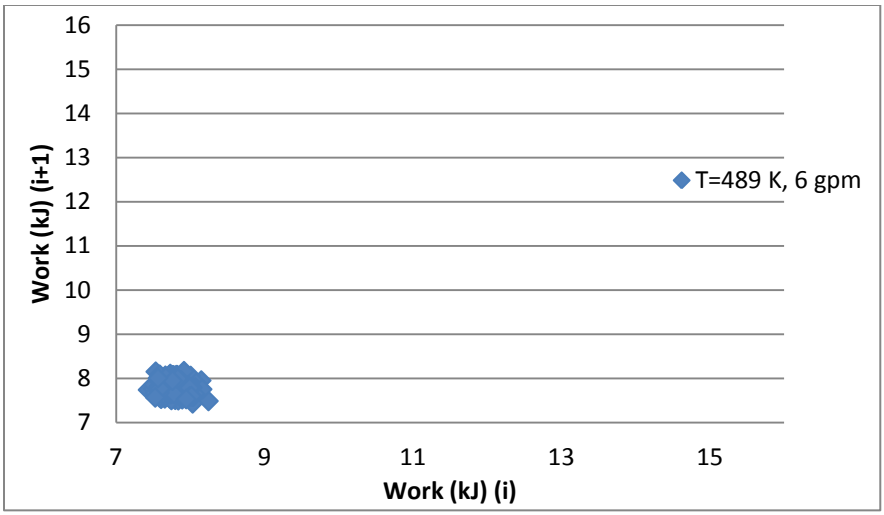

Figure 6.15. Return Map of Work for T_{in}=489 K and 6 gpm

Figure 6.15 shows that the model results follow the same trends with pure CO addition that the experiments completed by Attebery [3] with increased residual gas displayed. When less unburned residual/CO is present, the deterministic trend is weaker. Of course, if too much unburned residual was present, combustion could fail due to the insufficient chemical balance of fuel and air species within the cylinder, so there is a limit as to how much can be present as well. As stated in the beginning of this section, these results can be also used to extrapolate the behavior of the efficiency and the IMEP because each of these values are related to the work by a constant factor that simply shifts the fully intact trend to the newly desired position.

Now that the work parameter, and by extension the efficiency and the IMEP, have been evaluated for cyclic dynamics, the exhaust temperature can be examined. The exhaust temperature is an important factor to review because of the implications that a couple other studies have made that the temperature could play a larger role on the

location of combustion than the internal residual. Attebery tried to demonstrate this temperature effect and arrived at the conclusion that the internal residual has a greater impact. Thus, the carbon monoxide focused on in this study was varied by the Gaussian random number generator to produce the return map for exhaust temperature. Figure 6.16 shows the outcome for when the intake temperature is 468 K, the fuel flow rate is 9 gpm, and the molar amount of carbon monoxide has a multiplier of 5,000.

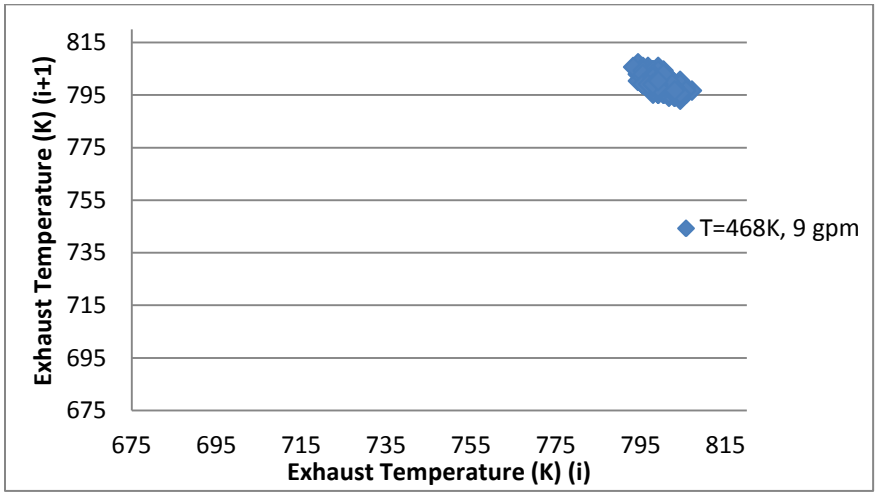

Figure 6.16. Return Map of Exhaust Temperature for T_{in}=468 K and 9 gpm

Figure 6.16 shows clearly that determinism is present in the exhaust temperature when the amount of carbon monoxide within the cylinder is varied. The strong trend suggests that a low temperature cycle is immediately followed by a high temperature cycle. This is more clearly delineated in Figure 6.17.

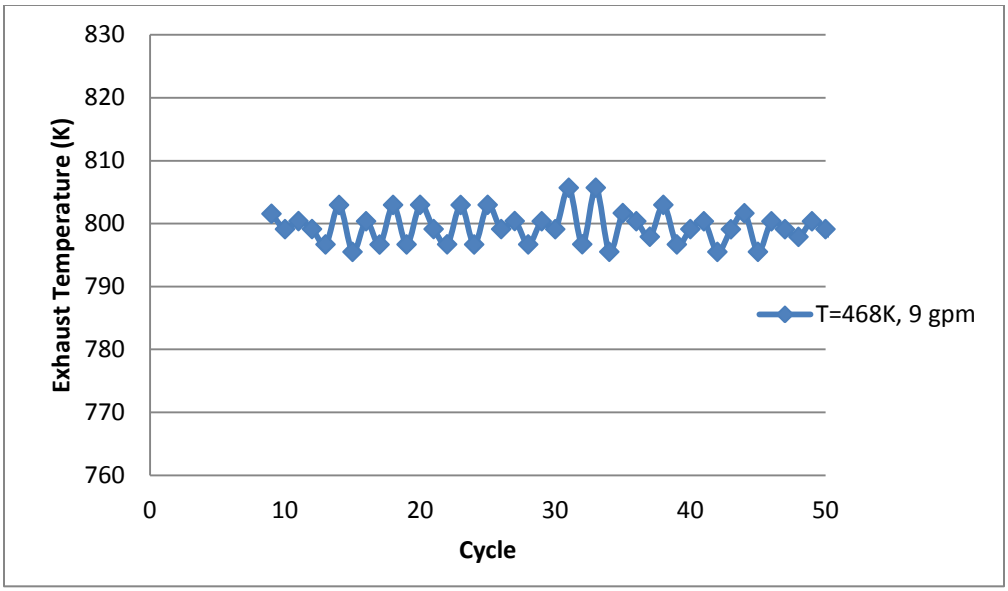

Figure 6.17. Exhaust Temperature Versus Cycle for T_{in}=468 K and 9 gpm

Figure 6.17 shows that with increased residual, the exhaust temperature oscillates between a cycle of lower temperature followed by a cycle with a higher temperature. This oscillation follows the same trend that the location of the start of combustion followed, thus affecting how complete the combustion was for that cycle. The same trend can be seen in a weaker fashion for the 6 gpm set point in Figure 6.18.

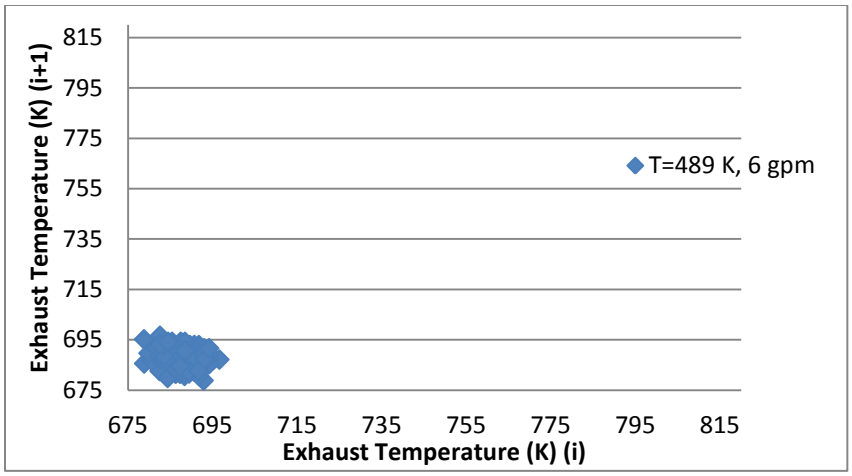

Figure 6.18. Return Map of Exhaust Temperature for T_{in}=489 K and 6 gpm

The deterministic trend in Figure 6.18 is still apparent, and it follows the results that have occurred for the other parameters, that it is less defined for the lower fuel flow rate. Since this is the lowest flow rate of the data that was experimentally tested on this engine, it is important to note that the trends do still appear, albeit weaker, for the parameters that have been delineated above at this minimum set point where the amount of carbon monoxide carry over between cycles is lowest.

6.3.2. Variation of Intake Temperature during Partial Burn. In order to validate the claims that the determinism seen in the parameters evaluated above is due to the variation in carbon monoxide, it was determined to examine the effects of the variation of the intake temperature during the partial burn regime for the higher fueling rate of 9 gpm. The amount of molar carbon monoxide was not increased by a multiplier; instead it was left as originally derived in §3.2.4. The intake temperature was varied using a Gaussian random number generator in the MATLAB model with a mean of 468

K which was the temperature that the set points in the previous section were evaluated at. The standard deviation parameter σ was set to one to ensure that most of the partial burn regime was captured. The effects of this variation will again be presented in the form of return maps and it will include all of the same parameters used above, i.e. the location of the start of combustion, the cyclic work output, and the exhaust temperature.

The trend predicted by the model for the location of the start of combustion at this set point can be seen in Figure 6.19.

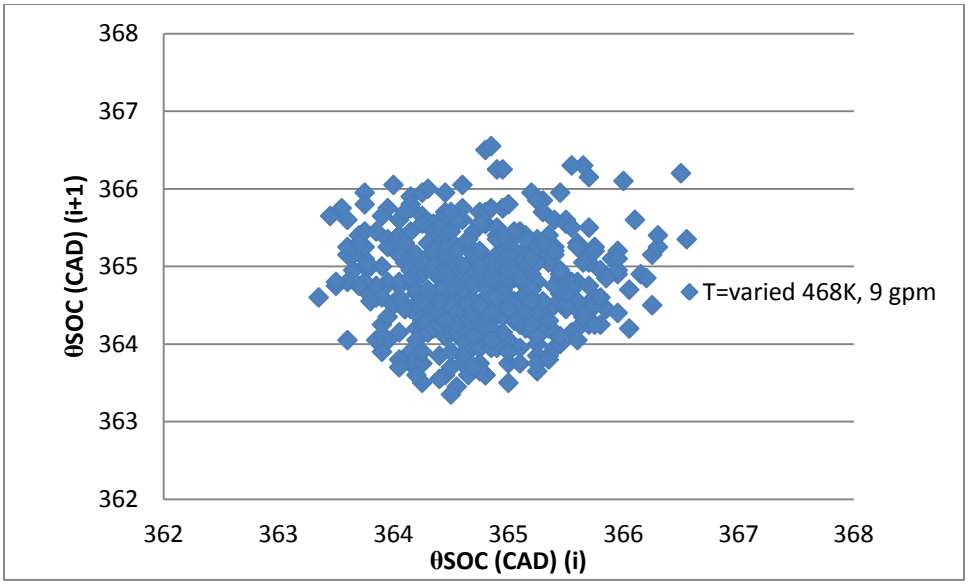

Figure 6.19. Return Map of θ_{SOC} for Varied T_{in} and 9 gpm

As can be seen in Figure 6.19, the prominent determinism that was present for the same parameter when the carbon monoxide value was varied is lacking here. There is a slight

determinism present, so the intake temperature could be responsible for part of the effect, but it is certainly not the dominating factor. In order to examine what role the intake temperature plays in this relationship, a set point with the lower fueling rate of 6 gpm is considered. With the lower fueling rate, the intake temperature within the Gaussian random number generator was set to 490 K with the same amount of variance to capture the partial burn regime. For this set point virtually all deterministic properties disappear as can be seen in Figure 6.20.

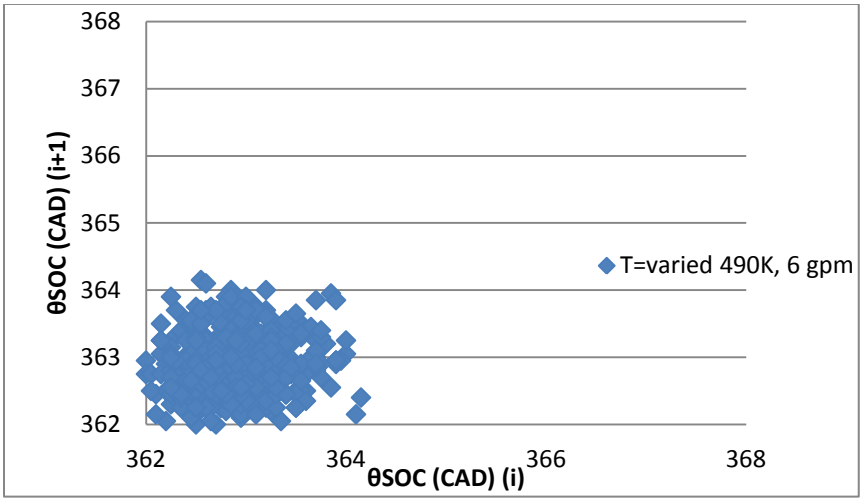

Figure 6.20. Return Map of θ_{SOC} for Varied T_{in} and 6 gpm

Figure 6.20 shows that the outcome from the set point at this lower fueling rate is completely stochastic. When the intake temperature is varied around this set point, there seems to be no pattern that occurs for the location of the start of combustion. So, if the

temperature has an effect on this parameter, it is very slight since it only demonstrates a pattern for the highest flow rate. The next quantity to be inspected is the cyclic work output.

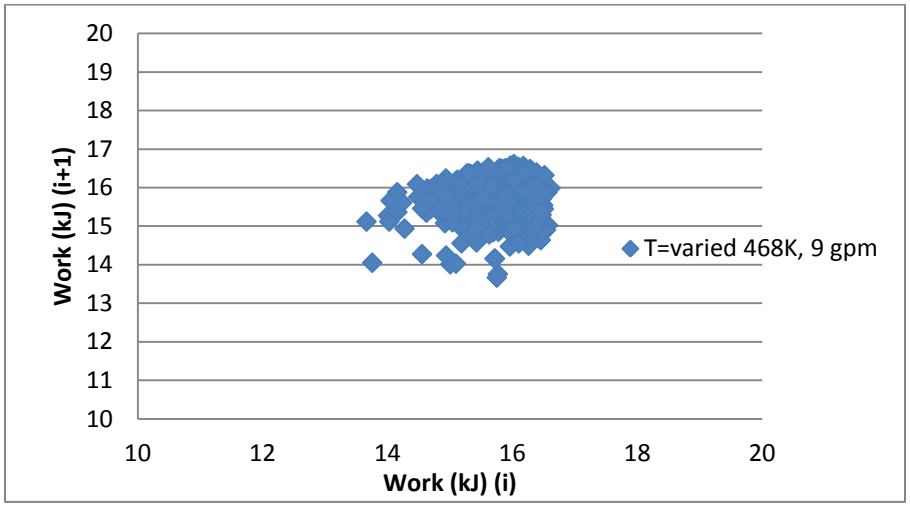

Figure 6.21. Return Map of Work for Varied T_{in} and 9 gpm

Determinism in the cyclic work output can be observed Figure 6.21 when the intake temperature is varied. Thus, the work output is dependent upon intake temperature. Since the chemical kinetic effects and temperature are undoubtedly linked, it is probable that determinism can be caused by more than one parameter. Therefore, it is possible for the work to be affected by both the intake temperature and the amount of carbon monoxide within the system.

The final parameter to be considered is the effect of the intake temperature upon the exhaust temperature. These results can be seen in Figure 6.22 below.

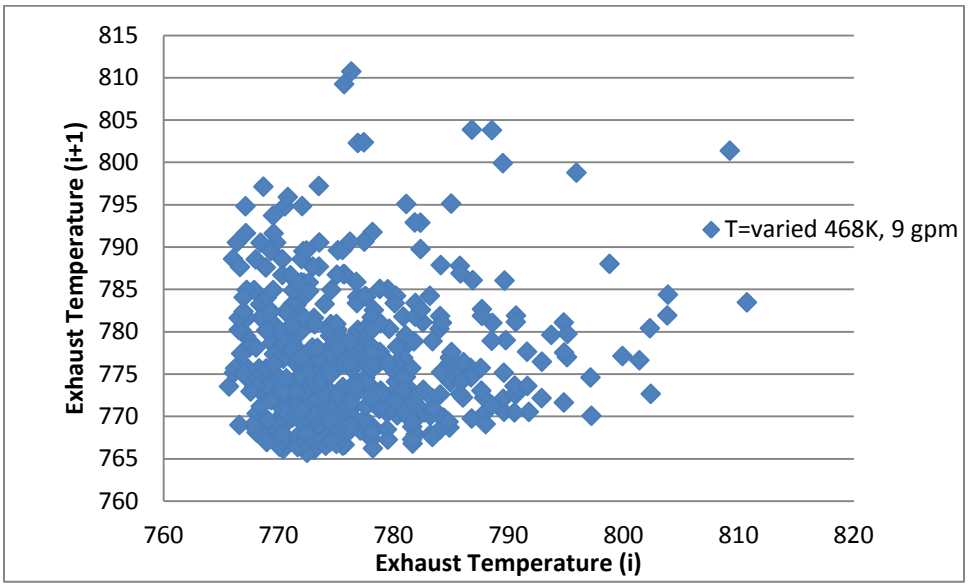

Figure 6.22. Return Map of Exhaust Temperature for Varied T_{in} and 9 gpm

The resulting data trend is fairly deterministic as observed in Figure 6.22. This is expected because the equation set relating the intake and exhaust temperatures was derived with the assumption of an ideal thermodynamic cycle, making the equation for the exhaust temperature ultimately dependent upon the intake temperature. Thus, the exhaust temperature of state five is also affected by multiple variables, the intake temperature and the amount of carbon monoxide present within the cylinder.

6.3.3. Variation of Artificially Increased Carbon Monoxide during Complete Combustion. Now that the effect of carbon monoxide during partial burn has been discussed, its effect during complete combustion can be quickly evaluated. The same parameters used for creating the return maps above will be examined here. It is expected that the results will be entirely stochastic, because there isn't much cyclic variation that

occurs during the stability of complete combustion. The complete combustion regime will be tested by increasing the temperature at the 9 gpm set point by a few degrees Kelvin to shift combustion from partial burn to stable. The first of these parameters, the location of the start of combustion is shown in Figure 6.23.

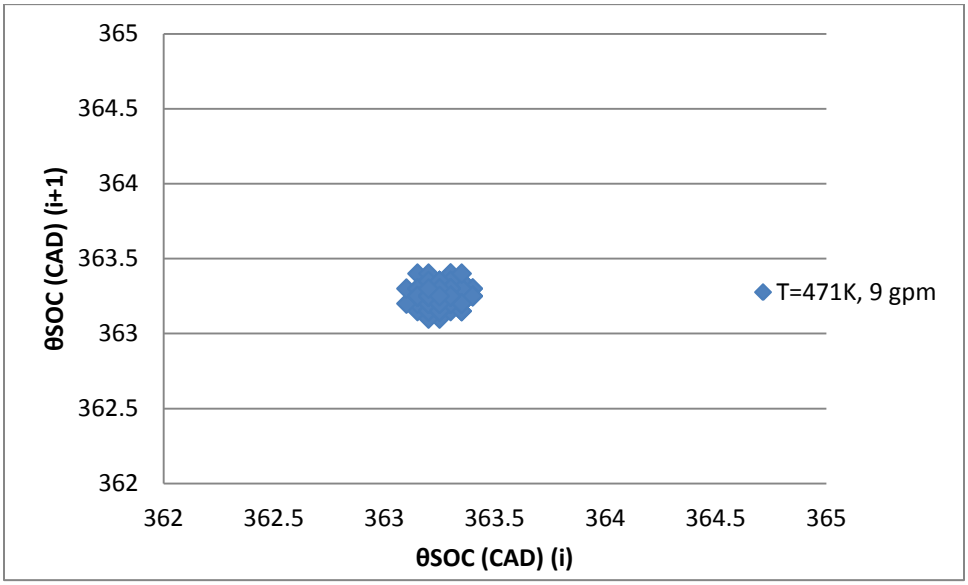

Figure 6.23. Return Map of θ_{SOC} for T_{in}=471K and 9 gpm

Figure 6.23 is created by artificially increasing the molar amount of carbon monoxide present in the system by the same value as used previously, 5,000. The amount of CO was also varied by the same Gaussian random number generator used previously with a mean of zero. It can be seen for this complete combustion case that there is no specific

effect caused by the variation of the CO. This is anticipated due to little cyclic variation being present when complete combustion occurs.

Next to be examined is the effect of the variation of an artificially increased amount of carbon monoxide on the cyclic behavior of the work output per cycle. This can be observed in Figure 6.24.

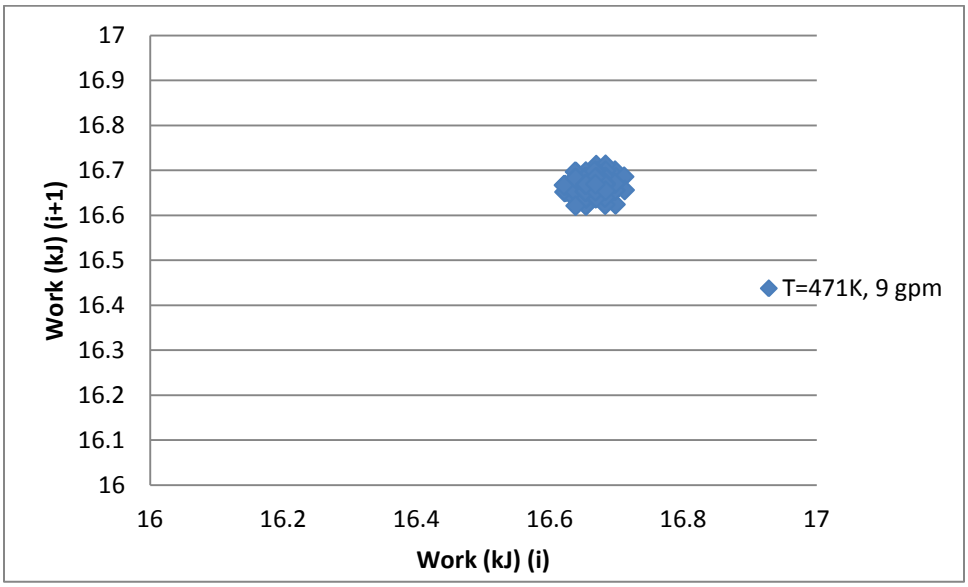

Figure 6.24. Return Map of Work for T_{in}=471K and 9 gpm

Figure 6.24 shows that again there is an entirely stochastic relationship between the work produced in one cycle when compared to the next during complete combustion. Thus, carbon monoxide isn't affecting the work during complete combustion even with artificially increased amounts.

The final parameter from the model to be evaluated is the exhaust temperature. Using the exact same set point as for the other complete combustion cases, the return map in Figure 6.25 was created.

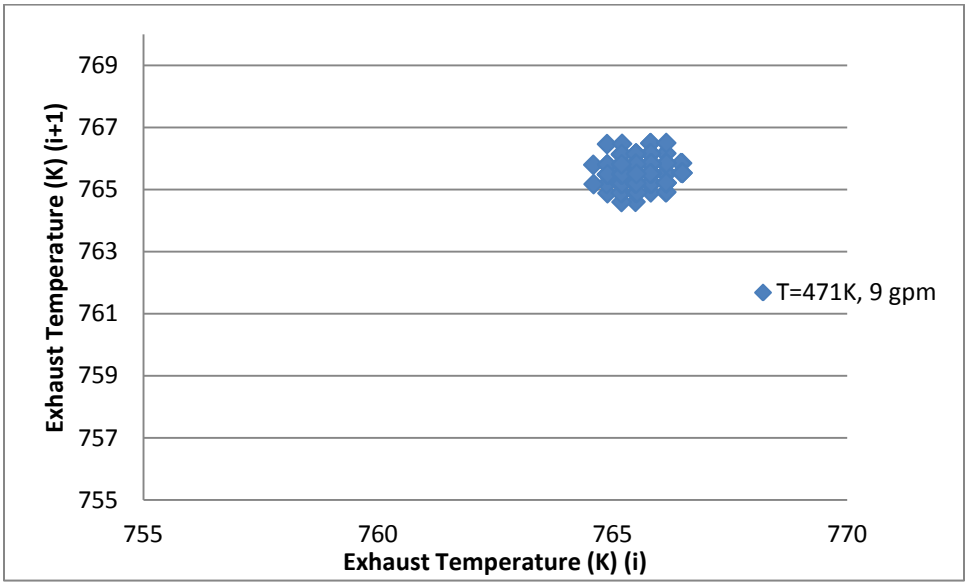

Figure 6.25. Return Map of Exhaust Temperature for T_{in}=471K and 9 gpm

The exhaust temperature also behaves in a stochastic manner as the amount of artificially increased carbon monoxide is varied as can be observed in Figure 6.25. This demonstrates that the carbon monoxide has little to no effect on the operation of the engine during complete combustion.

7. CONCLUSIONS

HCCI has the potential to become a method for beating the ever increasing regulations on emissions and efficiency if the issues surrounding its stability can be addressed. Review of the most recent studies suggests that chemical compounds within the residual could be used as a control mechanism. The species of carbon monoxide was tested in this study to determine its effects, especially during the unstable partial burn regime that occurs when the engine load is changed and also when the intake temperature is lowered for a specific fueling rate. In order to examine these effects a five-state thermodynamic model was created, based on the one used by Bettis [4]. The methodology for determining the location of the start of combustion was altered to be dependent upon the amount of carbon monoxide present within the cylinder. In this manner, the molar amount of carbon monoxide within the system would have a direct effect on parameters in the model. A simplified chemical kinetic model created by Ernst [7] was coupled to the thermodynamic model so that the conditions calculated within the latter model would act as inputs to the former model to compute how much carbon monoxide was present in the current cycle and what quantity would be fed forward into the next cycle by being trapped by the valve timing. The verification of this model was performed on a Hatz 1D50Z engine modified to run in HCCI mode in the Internal Combustion Engines Laboratory at Missouri S&T. The fuel chosen for the verification experiments was PRF96, due to it having a similar octane index as fuels successfully run on the engine before and because the fuel chemistry was able to be analyzed with the chemical kinetic model selected for this study. After the model was verified, the effects of carbon monoxide could be observed in the form of return maps generated by data from

the model. These return maps displayed that although the amount of carbon monoxide naturally produced within the engine had little effect, if the amount was increased artificially by a multiplier then deterministic trends appeared. These trends were noticeably stronger for a higher fueling rate/equivalence ratio, but were still present for the set points with the lower fueling rate. The results produced by the model for the increased amount of carbon monoxide were also consistent with experimental results obtained by Attebery for increased residual gas [3]. Even though the results in [3] were obtained using indolene instead of PRF96, the octane number is similar and the experimental set up was identical. However, the model is failing to capture that carbon monoxide at amounts close to those naturally produced in the engine have been shown in other studies to have an effect. This could be due to the Arrhenius integration that defines the start of combustion, or to the simplifications made to the chemical kinetic model when it was coupled to the five-state model.

The effect of the intake temperature was also considered, as some studies suggest that it also has potential to be used as a control, but it has a much lesser effect on the location of the start of combustion as shown by the return maps. It did have some effect on the work and exhaust temperature cyclic dynamics though. Finally, the effect of carbon monoxide during a steady state of complete combustion was examined. Although little to no effect of the carbon monoxide variation can be seen during complete combustion as presented by the results of the evaluated parameters above, the carbon monoxide variation at these same levels produces some determinism when the engine is operating in a partial burn state. Thus, because of the determinism displayed in the partial burn regime when the artificially increased carbon monoxide is varied by a Gaussian

random number generator it can be concluded that carbon monoxide has some potential to be used as a control mechanism for HCCI during regions of unstable combustion. However, until a more direct relationship of how carbon monoxide in the prior cycle residual effects cyclic dynamics is established, the extent of its effects is to be determined.

APPENDIX A
RESIDUAL GAS INJECTOR DRAWINGS

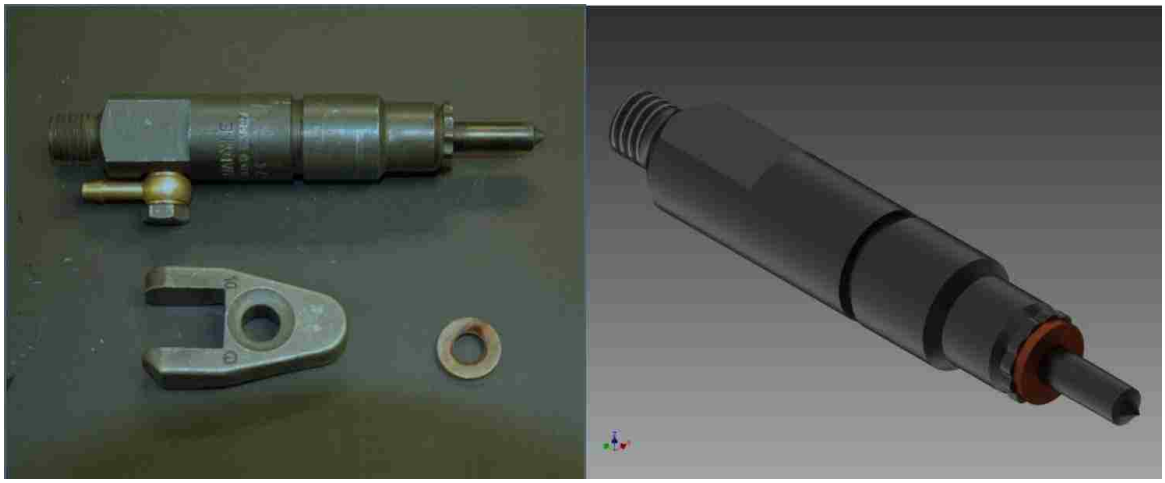

Figure A.1. OEM Diesel Injector, Actual and Solid Model

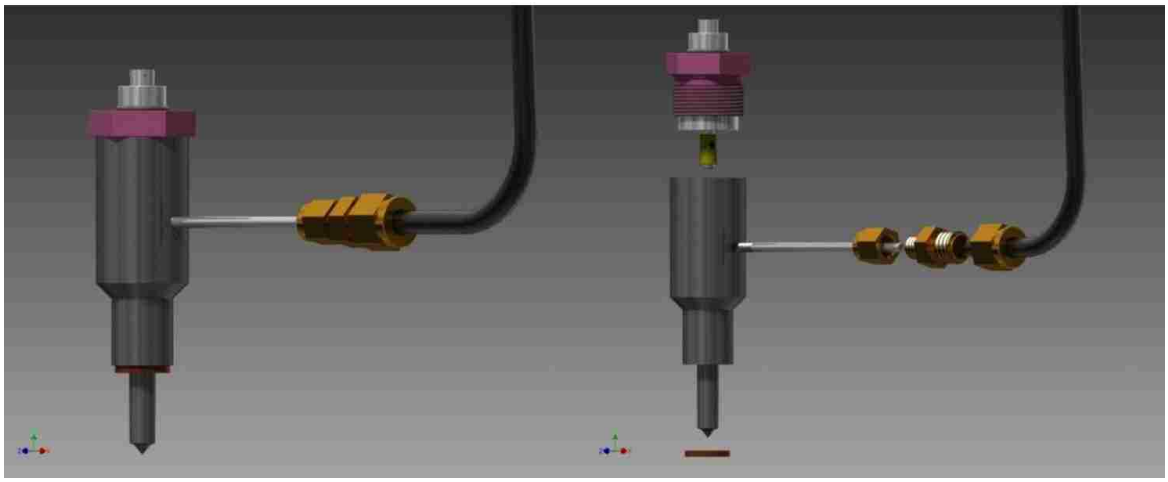

Figure A.2. Residual Gas Injector Solid Model, Assembled and Exploded View

Figure A.3 Residual Gas Injector Prototype, Assembled and Exploded

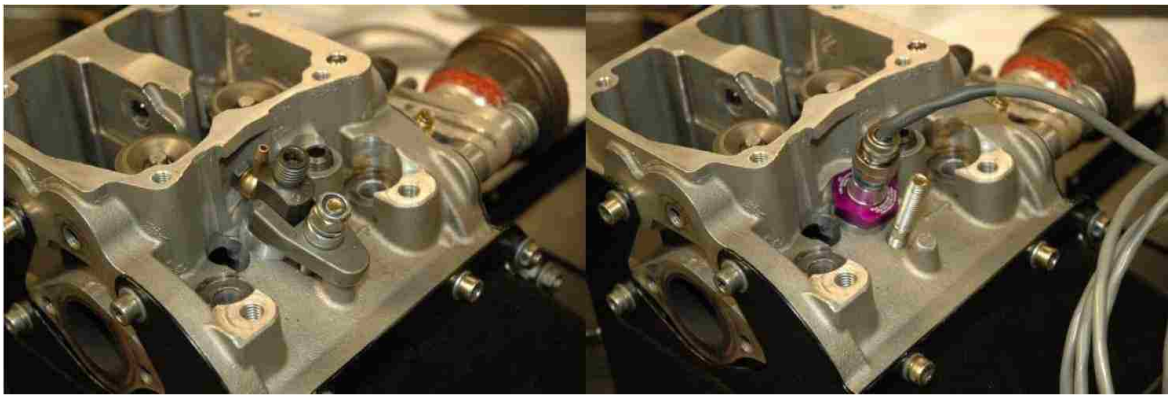

Figure A.4. Head/ Injector Installation, OEM Diesel Injector and RGI

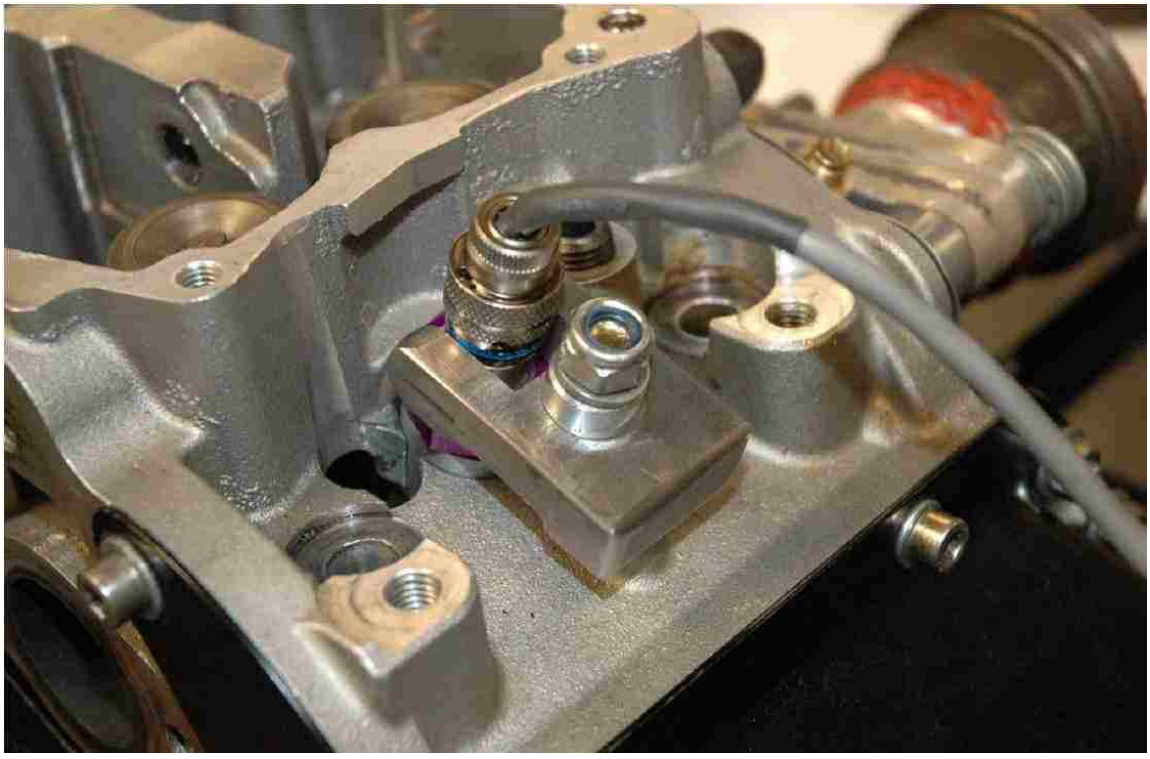

Figure A.5. RGI Installed in Hatz Engine Head with Fabricated Clamp

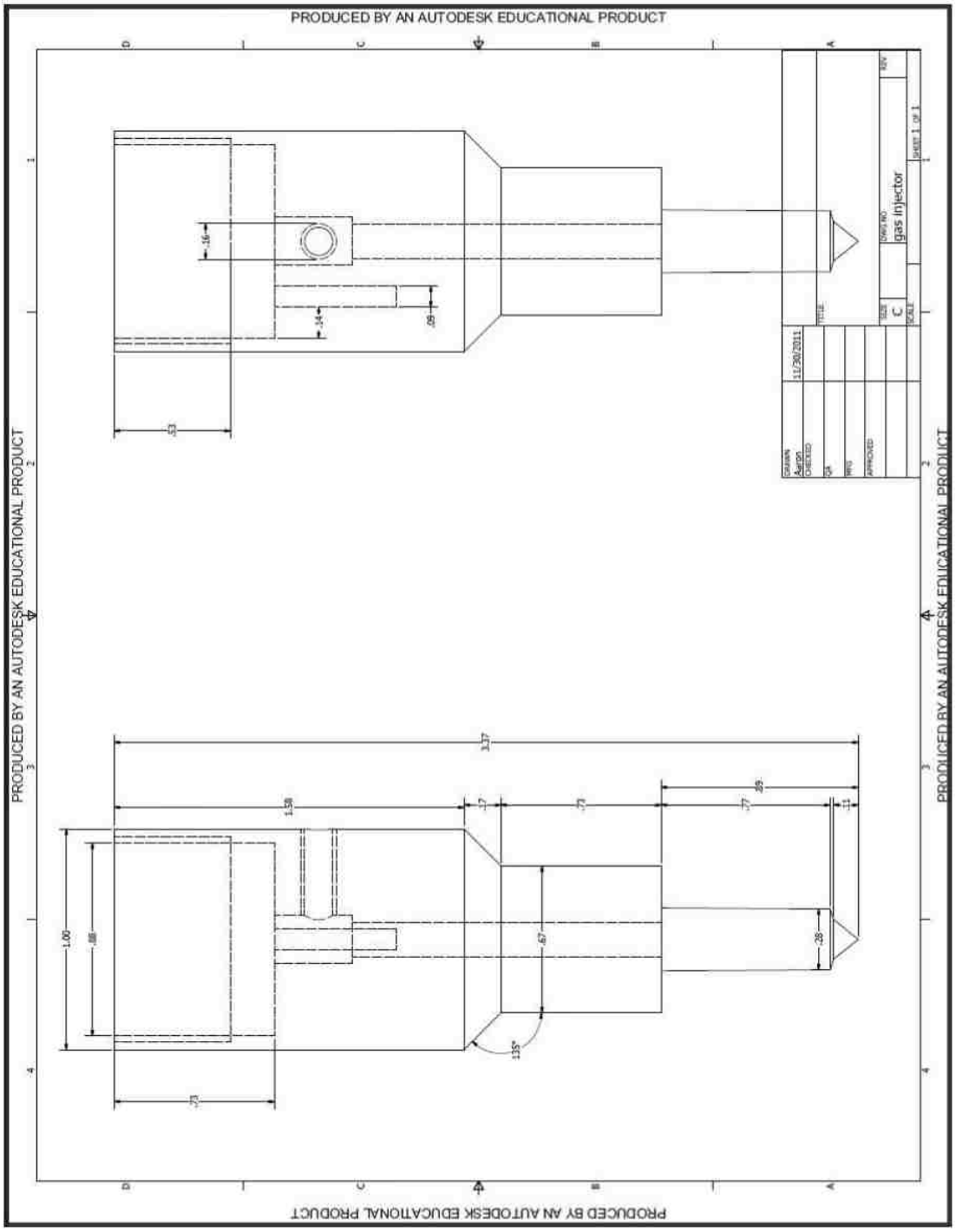

Figure A.6. Solid Model Sheet for RGI Fabrication

APPENDIX B

HCCI THERMODYNAMIC AND CHEMICAL KINETIC CODE

```
%% This is the Ridenhour Modified Model (Engine Geometry MS&T Hatz, running
% PRF96)
% This code uses the modified integrated arrhenius rate combustion model
% and its parameters.
%
% This code includes heated internal EGR (alphai), cooled external
% EGR (alphae) and carryover air from misfires (alphaunb). Carryover fuel
% is neglected because it is such a small amount compared to other
% residual species and residual fuel has been shown to have a negligible
% impact on the start of combustion.
%
% Also included is residual CO to determine the impact on start of
% combustion. The CO value is brought in from spreadsheets generated by
% Allen Ernst's CHEMKIN code.
%
% This code uses PRF 96 as the operating fuel.
%
% The combustion parameters are calculated using information from Turns,
% and from the Technical Data Book of Petroleum Refining from the American
% Petroleum Institue.
%
% The derivation of this code is explained in detail in the Ridenhour 2015
% thesis from Missouri S&T.


%% Control Model Code

cycles=25;      % # times to loop program

%----------Define Variable Matrices-------------

P1=zeros(1, cycles);       % state 1 is at IVC, the end of intake
V1=zeros(1, cycles);
T1=zeros(1, cycles);
P2=zeros(1, cycles);       % state 2 is at the end of compression,...
T2=zeros(1, cycles);       % immediately before combustion
T3=zeros(1, cycles);       % state 3 is after instantaneous combustion
P3=zeros(1, cycles);       % P3 in cycle, as opposed to output
V4=zeros(1, cycles);       % state 4 is end of expansion right at EVO
T4=zeros(1, cycles);
P4=zeros(1, cycles);
T5=zeros(1, cycles);       % state 5 is after blowdown, right at IVO
P5=zeros(1,cycles);
T6=zeros(1, cycles);       % state 6 serves as update variables for the...
P6=zeros(1,cycles);        % next cycles state 1 parameters

alphae=zeros(1,cycles);    % input variable, mass fraction of external EGR
alphai=zeros(1,cycles);    % mass fraction of internal EGR (iEGR)
alphaunb=zeros(1, cycles); % mass fraction of unburned residual
alphatot=zeros(1, cycles); % mass fraction total of EGR, iEGR, and unburned
alphacheck=zeros(1, cycles);%check variable for alphatot
gpm=zeros(1, cycles);      % input variable, fuel flow in grams/minute
Tin=zeros(1,cycles);       % input variable, intake temperature
C1=zeros(1,cycles);        % "spec. heat average" of reactants
C2=zeros(1,cycles);        % "spec. heat average" of products
C3=zeros(1,cycles);        % "heat of formation average" of combustion rxn
C4=zeros(1,cycles);        % secondary "spec. heat average" of products
C5=zeros(1,cycles);        % "spec. heat average" of remaining terms
Cunb=zeros(1,cycles);      % "spec. heat average" of unburned reactants
```

```
Cegr=zeros(1,cycles);      % "spec. heat average" of cooled EGR
Gamma=zeros(1,cycles);     % scaled molar amount of CO
Gamma_raw=zeros(1,cycles); % molar amount of CO from CHEMKIN spreadsheets
Gamma1=zeros(1,cycles);
Sigma=zeros(1,cycles);     % fraction amount of CO from previous cycle
Epsilon=zeros(1,cycles);   % amount of O2 from CHEMKIN to normalize CO
N2=zeros(1, cycles);       % number of moles prior to combustion
N3=zeros(1, cycles);       % number of moles post-combustion
Nt=zeros(1, cycles);       % total number of moles by Ideal Gas Law
Xegr=zeros(1, cycles);     % mole fraction of EGR
Negr=zeros(1, cycles);     % number of moles of EGR
Xunb=zeros(1, cycles);     % mole fraction of unburned residual
Nunb=zeros(1, cycles);     % number of moles of unburned residual
Niegr=zeros(1, cycles);    % number of moles of iEGR
Nfs=zeros(1, cycles);      % number of moles for stoichiometric F/A ratio
Xa=zeros(1, cycles);       % mole fraction of air
Xf=zeros(1, cycles);       % mole fraction of fuel (actual)
Xiegr=zeros(1, cycles);    % mole fraction of iEGR
Xcheck=zeros(1,cycles);    % check variable to show mole fraction total = 1
z=zeros(1, cycles);        % ratio of moles: N3/N2
Psoc=zeros(1,cycles);      % pressure at SOC (start of combustion)
Tsoc=zeros(1,cycles);      % temperature at SOC
T1up=zeros(1, cycles);     % state update variable of T1
alphaiup=zeros(1,cycles);  % state update variable of alphai
V23=zeros(1, cycles);      % volume at combustion
P3op=zeros(1, cycles);     % output P3, as opposed to in cycle
PRR=zeros(1, cycles);      % pressure rise rate
PRRop=zeros(1,cycles);

nCO2=zeros(1,cycles);

dtheta=zeros(1,cycles);
dtheta1=zeros(1,cycles);
theta23=zeros(1, cycles);  % angle where peak pressure occurs (radians)
theta23op=zeros(1,cycles); % output theta23 (radians)
thetaSOC1=zeros(1,cycles);
thetaSOC2=zeros(1,cycles);
m=zeros(1,cycles);
W34op=zeros(1, cycles);    % gross indicated work output
W34op2=zeros(1,cycles);
Wigef=zeros(1, cycles);    % indicated gross efficiency

Mass=zeros(1,cycles);
ER=zeros(1,cycles);
no2=zeros(1,cycles);
Ii=zeros(1,cycles);

%-----------Constants-----------
MWf=113.60;              % molecular weight of fuel (g/mol)
MWa=29;                  % molecular weight of air (g/mol)
FAs=1/15.138;            % stoichiometric fuel/air ratio
LHV2=44.658;             % LHV of PRF96 (KJ/g fuel)
LHV=LHV2*MWf;            % LHV of PRF96 (kJ/mol fuel)
ES=1800;                 % engine speed (rpm)
N=ES*6*pi/180;           % engine speed (rad/sec)
s=7.0;                   % stroke (cm)
l=11.042;                % connecting rod length (cm)
bore=9.6999;             % bore diamater (cm)
crank=3.5;               % crank radius (cm)
R=l/crank;
```

```
rc=14.5;                % compression ratio
thetaEVO=476*pi/180;    % radians
thetaTDC=360*pi/180;    % radians
thetaIVO=705*pi/180;    % radians
thetaIVC=227*pi/180;    % radians

Tref=298;           % reference temp corresponding to heat of formation (K)
Tegr=300;           % temperature of cooled EGR (K)
Pin=.0101;          % atmospheric pressure (kN/cm^2)

Vd=pi()*(bore^2)*0.25*s;% disp vol (cm^3)
Vc=Vd/(rc-1);           % clearance vol=V(TDC)=V(360) (cm^3)
Vivc=(Vc*(1+0.5*(rc-1)*(R+1-cos(thetaIVC)-(R^2-
sin(thetaIVC)^2)^.5)));%(cm^3)
Vevo=(Vc*(1+0.5*(rc-1)*(R+1-cos(thetaEVO)-(R^2-
sin(thetaEVO)^2)^.5)));%(cm^3)
Vivo=(Vc*(1+0.5*(rc-1)*(R+1-cos(thetaIVO)-(R^2-
sin(thetaIVO)^2)^.5)));%(cm^3)
Vbdc=Vd+Vc;             % (cm^3)
Vtdc=Vc;

Cpprf96R=.255172;     % spec. heat of fuel in reactants (kJ/molfuel*K)
Cpo2R=.030481;        % spec. heat of O2 in reactants (kJ/molO2*K)
Cpn2R=.029414;        % spec. heat of N2 in reactant (kJ/molN2*K)
CpcoP=.0314745;       % spec heat of CO in reinducted products (kJ/molCO*K)
Cpco2P=.050523;       % spec heat of CO2 in reinducted products
(kJ/molCO2*K)
Cph2oP=.0381;         % spec heat of H2O in reinducted products
(kJ/molH2O*K)
Cpn2P=.031091;        % spec heat of N2 in reinducted products (kJ/molN2*K)
Cpo2P=.033376;        % spec heat of O2 in reinducted products (kJ/molO2*K)
Cpn2E=.029075;        % spec heat of N2 in cooled external EGR (kJ/molN2*K)
Cpprf96U=.369575;     % spec. heat of fuel in carryover (kJ/molfuel*K)
Cpo2U=.033376;        % spec. heat of O2 in carryover (kJ/molO2*K)
Cpn2U=.031091;        % spec heat of N2 in carryover (kJ/molN2*K)

Hfprf96=-222.500;     % heat of formation of PRF96 (kJ/molfuel)
Hfco2=-393.500;       % heat of formation of CO2 (kJ/molCO2)
Hfh2o=-241.800;       % heat of formation of H2O (kJ/molH2O)
Hfco=-110.500;        % heat of formation of CO (kJ/molCO)

gamma=1.3;      % spec. heat ratio of fuel

A=4.6e11;       % Arrhenius rate pre-exponential factor (gmol/cm^3)^1-a-b/s
Ea=15098;       % activation energy (K)
a=0.25;         % Arrhenius rate parameter (unitless)
b=1.5;          % Arrhenius rate parameter (unitless)
Kth=0.00334;    % Arrhenius threshold value (gmol/cm^3) (X=0.56)

theta=(228:0.05:720).*pi/180;  % Arrhenius integration limits in radians
thetad=(228:0.05:720);         % Arrhenius integration limits in degrees

Ru1=.008314472;         % universal gas constant (KJ/mol*K)
Ru2=.8314472;           % universal gas constant (Kn-cm/mol*K)

X=0.56;            % relationship between temperature of reinducted...
                   % products and exhaust temperature of last cycle...
                   % where Treinduct=XTex
```

```
beta=0.1;          % fraction of LHV representing heat loss due to
combustion


%-----------Initializations-----------

T6(1,2)=215+273;
% temp of inducted products and reactants from "zeroth" cycle (K)
thetaSOC(1,3)=354*pi/180;
% angle at which combustion initiates (radians)
Vsoc(1,2)=Vtdc;
Vsoc(1,3)=(Vc*(1+0.5*(rc-1)*(R+1-cos(thetaSOC(1,2))-(R^2-
sin(thetaSOC(1,2))^2)^.5))); % combustion to 50% burn
dtheta(1,3)=11*pi/180;
% combustion duration
theta23(1,3)=365*pi/180;
% angle at which peak pressure is assumed to occur (radians)
V23(1,3)=(Vc*(1+0.5*(rc-1)*(R+1-cos(theta23(1,2))-(R^2-
sin(theta23(1,2))^2)^.5)));    % cylinder vol at peak pressure (cm^3)

PHI(1,1)=.35;           % initializes the equivalence ratio
PHI(1,2)=.35;

Nf(1,2)=.000058;        % initializes molar amount of fuel
Na(1,2)=.003;           % initializes molar amount of air
alphai(1,3)=.0299;      % initializes the internal EGR(valve overlap and
                          trapped residual)
alphae(1,1)=0;          % initializes the external EGR
alphae(1,2)=0;
alphae(1,3)=0;
alphaunb(1,2)=0;        % initializes the unburned residual
alphaunb(1,3)=0;
C1(1,2)=1.8433;         % initializes "averaged" values
C2(1,2)=1.9832;
Cegr(1,2)=1.7308;
Cunb(1,2)=1.9977;
C3(1,2)=1598.0;
C4(1,2)=1.983;
C5(1,2)=0.17077;
Gamma(1,2)=0;           % initializes variables retrieved from spreadsheets
Gamma(1,3)=0;
Epsilon(1,2)=0;
Epsilon(1,3)=0;
Sigma(1,2)=0;
Sigma(1,3)=0;

%-----------Begin Looping the Program--------------

for i=3:cycles;

    % Tin, alphae, and gpm are the 3 inputs that are manually changed.

    % Gives gaussian distributed random values for the intake temperature

    %   Tin(1,i) = normrnd(483,1);
        Tin(1,i)=507.6711;

    % Gives gaussian disributed random values for the external EGR

    %   alphae(1,i) = normrnd(.007,.0015);
```

```
    alphae(1,i)=0;

% Gives gaussian disributed random values for the fueling rate

%   gpm(1,i) = normrnd(7.5,.03);
    gpm(1,i)=6;

%-----------1: Adiabatic Induction, Instant Mixing-----------
P1(1,i)=Pin; % intake pressure is kN/cm^2
V1(1,i)=(Vc*(1+0.5*(rc-1)*(R+1-cos(thetaIVC)-(R^2-
        sin(thetaIVC)^2)^.5)));
                        % volume is found using the engine geometry
if i==3;
    T1(1,i)=T6(1,2);    % T6 is equivalent to the next cycle's T1
else
    T1(1,i)=T6(1,i-1);
end

%-----------1-2: Isentropic Compression-----------
% use isentropic relationships
P2(1,i)=(P1(1,i)*((V1(1,i)/V23(1,i))^gamma));
T2(1,i)=(T1(1,i)*((V1(1,i)/V23(1,i))^(gamma-1)));
Psoc(1,i)=(P1(1,i)*((V1(1,i)/Vsoc(1,i))^gamma));
Tsoc(1,i)=(T1(1,i)*((V1(1,i)/Vsoc(1,i))^(gamma-1)));

%-----------Intermediate Calculations-----------------
% calculate the amount of moles before and after combustion and their
% ratio
N2(1,i)=(PHI(1,i-1)+59.1787+(alphai(1,i)*((4.4775*PHI(1,i-
2))+59.1787+(Sigma(1,i-2)*PHI(1,i-2))/2))+(alphae(1,i-1)*(PHI(1,i-
1)+59.1787))+(alphaunb(1,i-1)*(PHI(1,i-2)+59.1787)));
% number of moles before combustion
N3(1,i)=((4.4775*(PHI(1,i-1)+(PHI(1,i-2)*alphai(1,i))))+(59.1787)*
(1+alphai(1,i))+(alphae(1,i-1)*(PHI(1,i-1)+59.1787))+(alphaunb(1,i-
 1)*(PHI(1,i-2)+59.1787))+(Gamma(1,i-1)/2));
% number of moles after combustion
z(1,i)=N3(1,i)/N2(1,i);
% product to reactant molar ratio for combustion reaction

%-----------2-3: Isochoric Combustion-----------
% Assume instantaneous, constant volume combustion
% properties after combustion determined by a first law analysis
T3(1,i)=((C3(1,i-1)+((C1(1,i-1)+(C2(1,i-1)*alphai(1,i))+(Cegr(1,i-
1)*alphae(1,i-1))+(Cunb(1,i-1)*alphaunb(1,i-1))-
(Ru1*N2(1,i)))*T2(1,i))+(C5(1,i-1)*Tref))/...
((C2(1,i-1)*(alphai(1,i)))+(Cegr(1,i-1)*alphae(1,i-1))+(Cunb(1,i-
 1)*alphaunb(1,i-1))+C4(1,i-1)-(Ru1*N3(1,i))));

P3(1,i)=(z(1,i)*((V1(1,i)/V23(1,i))^gamma)*Pin*T3(1,i)*((C1(1,i-
1)+(C2(1,i-1)*alphai(1,i))+(Cegr(1,i-1)*alphae(1,i-1))+(Cunb(1,i-
1)*alphaunb(1,i-1))-(Ru1*N2(1,i)))/...
((((C2(1,i-1)*(alphai(1,i)))+(Cegr(1,i-1)*alphae(1,i-1))+(Cunb(1,i-
1)*alphaunb(1,i-1))+C4(1,i-1)-(Ru1*N3(1,i)))*T3(1,i))-C3(1,i-1)-
(C5(1,i-1)*Tref))));

%------------Pressure Rise Rate---------------
% change in pressure over change in angle
PRR(1,i)=((P3(1,i)-Psoc(1,i))*2*pi*100)/(dtheta(1,i)*360);
% bar/CAD
```

```
%-----------3-4: Isentropic Expansion-----------
% use isentropic relationships
V4(1,i)=(Vc*(1+0.5*(rc-1)*(R+1-cos(thetaEVO)...
    -sqrt(R^2-sin(thetaEVO)^2))));

T4(1,i)=(T3(1,i)*((V23(1,i)/V4(1,i))^(gamma-1)));
P4(1,i)=(P3(1,i)*((V23(1,i)/V4(1,i))^gamma));

%-----------4-5: Isentropic Exhaust-----------
% use isentropic relations and use exhaust pressure as atmospheric
T5(1,i)=(T4(1,i)*((Pin/P4(1,i))^((gamma-1)/gamma)));
P5(1,i)=Pin;

               %%---------This section calculates the residual mass
                %---------- fraction trapped in the cylinder

                   w=ES/60;          % engine speed (rev/sec)
                   rc=14.5;          % compression ratio
                   Pi=0.949;         % intake pressure
                   Pe=1.235;         % exhaust pressure
                   B=96.999;         % bore diamater (mm)
                   Dv=32;            % average valve seat diameter (mm)
                   Lv=8.912;         % average valve lift (mm)
                   IVO=705;          % intake valve opening (CAD)
                   EVC=18;           % exhaust valve closing (CAD)
                   thetaoverlap=33; % valve overlap EVC-IVO (CAD)


   %---------------- Calculate the Overlap Factor OF--------
   % relationship described in thesis (Bettis and
   % Ridenhour)
   OF = (1.45/B)*(107+7.8*thetaoverlap+(thetaoverlap^2))*((Lv*Dv)/B^2);


%---------------- Calculate the residual mass fraction -------------

alphai(1,i+1) = ((.401*(OF/w)*(1-exp((-4.78*(1-((Pi/Pe)^.7)))-(153.8*(1
  -((Pi/Pe)^4.5)))))*(Pe/Pi)*(Tin(1,i)/T5(1,i)))+((Pe*Tin(1,i))/
  (rc*Pi*T5(1,i))));
alphatot(1,i)= alphai(1,i+1);    % Total amount of exhaust residual

 if theta23(1,i)<=(373*pi/180);   % angle cutoffs determined in thesis
    alphaunb(1,i)=0;              % fraction of unburned reactants
 elseif theta23(1,i)>=(390*pi/180);
    alphaunb(1,i)=alphatot(1,i);
    alphai(1,i+1)=alphatot(1,i);
 else
    alphaunb(1,i)=(1-((390-(theta23(1,i)*180/pi))/(390-373))))
  *alphatot(1,i);
    alphai(1,i+1)=alphatot(1,i)-alphaunb(1,i)-alphae(1,i);
 end


%-----------1: Adiabatic Induction, Instant Mixing-----------
% state 6 represents the next cycle's state 1
P6(1,i)=Pin;
T6(1,i)=((C1(1,i-1)*Tin(1,i)+(C2(1,i-
1)*alphai(1,i+1)*X*T5(1,i))+(Cegr(1,i-1)*alphae(1,i)*Tegr)+(Cunb(1,i-
1)*alphaunb(1,i)*X*T5(1,i)))/(C1(1,i-1)+(C2(1,i-1)*alphai(1,i+1))
+(Cegr(1,i-1)*alphae(1,i))+(Cunb(1,i-1)*alphaunb(1,i))));
```

```
%-----------Calculate Air Inducted and Equivalence Ratio------------
     % use of ideal gas law and molar properties
     Nf(1,i)=((gpm(1,i)*4*pi)/(MWf*N*60));  % moles of fuel
     Nt(1,i)=(Pin*(Vd+Vc))/(Ru2*Tin(1,i));
     Xegr(1,i)=(alphae(1,i)*(PHI(1,i-1)+59.1787))/((PHI(1,i-
     1)+59.1787)*(1+alphae(1,i))+(alphai(1,i)*((4.4775*PHI(1,i-
     2))+59.1787+(Sigma(1,i-2)*PHI(1,i-2))/2))+(alphaunb(1,i)*(PHI(1,i-
     2)+59.1787)));
     Negr(1,i)=Xegr(1,i)*Nt(1,i);
     Xunb(1,i)=(alphaunb(1,i)*(PHI(1,i-2)+59.1787))/((PHI(1,i-
     1)+59.1787)*(1+alphae(1,i))+(alphai(1,i)*((4.4775*PHI(1,i-
     2))+59.1787+(Sigma(1,i-2)*PHI(1,i-2))/2))+(alphaunb(1,i)*(PHI(1,i-
     2)+59.1787)));
     Nunb(1,i)=Xunb(1,i)*Nt(1,i);
     Niegr(1,i)=alphai(1,i+1)*(Nt(1,i));
     Na(1,i)=Nt(1,i)-Negr(1,i)-Niegr(1,i)-Nunb(1,i)-Nf(1,i);
     % air moles are what is left over
     Nfs(1,i)=(Na(1,i)*MWa*FAs)/(MWf);
     % stoich moles of fuel
     PHI(1,i)=Nf(1,i)/Nfs(1,i);           % equiv. ratio
     Xa(1,i)=Na(1,i)/Nt(1,i);
     Xf(1,i)=Nf(1,i)/Nt(1,i);
     Xiegr(1,i)=Niegr(1,i)/Nt(1,i);
     Xcheck(1,i)=Xa(1,i)+Xf(1,i)+Xiegr(1,i)+Xegr(1,i)+Xunb(1,i);
     % check to verify moles fractions of the reactants
     alphacheck(1,i)=alphae(1,i)+alphai(1,i+1)+alphaunb(1,i);
     %check variable for alphatot
 %-----------Feed Forward Mechanism-----------

        %-----------Estimate Percent Energy Released-----------
        %this assumes that complete combustion is equivalent
        %to 99 percent energy release, misfire is equal to
        %0 percent energy release and that between those
        %two a linear progression occurs
        if theta23(1,i)<=(373*pi/180);
               % angle cutoffs determined in Attebery thesis
           ER(1,i)=99.0;
        elseif theta23(1,i)>=(390*pi/180);%(381*pi/180);
           ER(1,i)=0;
             % .001 allows for the first cycle (which =0) to be ignored
        else
           ER(1,i)=((390-(theta23(1,i)*180/pi))/(390-373))*100;
        end


        EnergyReleased=ER(1,i-1);
        EnergyReleasedCurrent=ER(1,i);
        gpmCurrent=gpm(1,i);
        Alphaunb=alphaunb(1,i);


        %------ Select the Spreadsheet for use on this run--------
        if gpmCurrent==6;
           if (EnergyReleased==99)||(Alphaunb==0)
               ActiveSpreadsheet = 'F6T990';
               Mass(1,i)=0.366880662533115;
           elseif (EnergyReleased >= 85) || (EnergyReleased < 20)
                   ActiveSpreadsheet = 'F6T990ER20';
                   Mass(1,i)=0.371816662533115;
```

```
  elseif (EnergyReleased >= 20) && (EnergyReleased < 50)
          ActiveSpreadsheet = 'F6T990ER50';
          Mass(1,i)=0.377873662533115;
  elseif (EnergyReleased >= 50) && (EnergyReleased < 65)
          ActiveSpreadsheet = 'F6T990ER57';
          Mass(1,i)=0.378763662533115;
  elseif (EnergyReleased >= 65) && (EnergyReleased < 85)
          ActiveSpreadsheet = 'F6T990ER50';
          Mass(1,i)=0.377873662533115;
  end
elseif gpmCurrent==7.5;
      if (EnergyReleased==99)||(Alphaunb==0)
          ActiveSpreadsheet = 'F75T975';
          Mass(1,i)=0.368547329199782;
      elseif (EnergyReleased >= 85) || (EnergyReleased < 20)
              ActiveSpreadsheet = 'F75T975ER20';
              Mass(1,i)=0.374747329199781;
      elseif (EnergyReleased >= 20) && (EnergyReleased < 50)
              ActiveSpreadsheet = 'F75T975ER50';
              Mass(1,i)=0.382373329199782;
      elseif (EnergyReleased >= 50) && (EnergyReleased < 65)
              ActiveSpreadsheet = 'F75T975ER57';
              Mass(1,i)=0.383514329199782;
      elseif (EnergyReleased >= 65) && (EnergyReleased < 85)
              ActiveSpreadsheet = 'F75T975ER50';
              Mass(1,i)=0.382373329199782;
      end
 elseif gpmCurrent==9;
      if (EnergyReleased==99)||(Alphaunb==0)
          ActiveSpreadsheet = 'F9T945';
           Mass(1,i)=0.370213995866448;
       elseif (EnergyReleased < 20)
               ActiveSpreadsheet = 'F9T945ER20';
               Mass(1,i)=0.377598995866448;
       elseif (EnergyReleased >= 85) || (EnergyReleased < 20)
               ActiveSpreadsheet = 'F9T945ER20';
               Mass(1,i)=0.377598995866448;
       elseif (EnergyReleased >= 20) && (EnergyReleased < 50)
               ActiveSpreadsheet = 'F9T945ER50';
               Mass(1,i)=0.386877995866448;
       elseif (EnergyReleased >= 50) && (EnergyReleased < 65)
               ActiveSpreadsheet = 'F9T945ER57';
               Mass(1,i)=0.388206995866448;
       elseif (EnergyReleased >= 65) && (EnergyReleased < 85)
               ActiveSpreadsheet = 'F9T945ER50';
               Mass(1,i)=0.386877995866448;
       end
     end

  Energy = xlsread(ActiveSpreadsheet, 'FC', 'E:E'); %these
  commands find the correct columns of data from the selected
  spreadsheet for Energy, O2, and CO
  OO = xlsread(ActiveSpreadsheet, 'MassFR', 'C:C');
  CO = xlsread(ActiveSpreadsheet, 'MassFR', 'G:G');
  I=find(Energy>=EnergyReleasedCurrent,1);
  %this searches energy for the index of the correct Energy
   Released value
  Ii(1,i)=I;
```

```
        %-----------Calculate C values-----------
        C1(1,i)=PHI(1,i)*Cpprf96R+12.4325*Cpo2R+46.7462*Cpn2R;
        % "specific heat" of reactants
        C2(1,i)=(7.955*PHI(1,i-1)-Sigma(1,i-1)*PHI(1,i-1))*Cpco2P
        +8.955*PHI(1,i-1)*Cph2oP+46.7462*Cpn2P+(12.4325*(1-PHI(1,i-
        1))+(Sigma(1,i-1)*PHI(1,i-1))/2)*Cpo2P+Sigma(1,i-1)*PHI(1,i-
        1)*CpcoP;  % "specific heat" of products
        Cegr(1,i)=(PHI(1,i)+59.1787)*Cpn2E;
        % "specific heat" of cooled EGR
        C3(1,i)=PHI(1,i)*Hfprf96+(Gamma(1,i)-7.955*PHI(1,i)-
        alphai(1,i+1)*Sigma(1,i-1)*PHI(1,i-1))*Hfco2+(alphai(1,i+1)*
        Sigma(1,i-1)*PHI(1,i-1)-Gamma(1,i))*Hfco-8.955*PHI(1,i)
        *Hfh2o-LHV*beta;
        C4(1,i)=(7.955*PHI(1,i)-Gamma(1,i)+Sigma(1,i-1)*PHI(1,i-
        1)*alphai(1,i+1))*Cpco2P+8.955*PHI(1,i)*Cph2oP+46.7462*Cpn2P
        +(12.4325*(1-PHI(1,i))-(Sigma(1,i-1)*PHI(1,i-1)*alphai(1,i+1))/2
        +Gamma(1,i)/2)*Cpo2P+(Gamma(1,i)-Sigma(1,i-1)*PHI(1,i-
        1)*alphai(1,i+1))*CpcoP;
        Cunb(1,i)=PHI(1,i-1)*Cpprf96U+12.4325*Cpo2U+46.7462*Cpn2U;
        % "specific heat" of carryover
        C5(1,i)=-PHI(1,i)*Cpprf96R+(7.955*PHI(1,i)-Gamma(1,i)+
        Sigma(1,i-1)*PHI(1,i-1)*alphai(1,i+1))*Cpco2P+8.955*PHI(1,i)
        *Cph2oP+(-(Sigma(1,i-1)*PHI(1,i-1)*alphai(1,i+1))/2+Gamma(1,i)/2)
        *Cpo2P+(Gamma(1,i)-Sigma(1,i-1)*PHI(1,i-1)*alphai(1,i+1))*CpcoP;
%-----------State Update Equations-----------

 T1up(1,i+1)=(((C1(1,i)*Tin(1,i)+(Cegr(1,i)*alphae(1,i)*Tegr)+((C2(1,i)
        *alphai (1,i+1)+(Cunb(1,i)*alphaunb(1,i)))*X*((((((C2(1,i-1)
        *(alphai(1,i)))+(Cegr(1,i-1)*alphae(1,i-1))+(Cunb(1,i-1)*
        alphaunb(1,i-1))+C4(1,i-1)-(Ru1*N3(1,i)))*T1(1,i))/(z(1,i)*
        (V1(1,i)/V23(1,i))*(C3(1,i-1)+((C1(1,i-1)+(C2(1,i-1)*alphai(1,i))
        +(Cegr(1,i-1)*alphae(1,i-1))+(Cunb(1,i-1)*alphaunb(1,i-1))-
        (Ru1*N2(1,i)))*(T1(1,i)*((V1(1,i)/V23(1,i))^(gamma-1))))+C5(1,i-
        1)*Tref))))^((gamma-1)/gamma))*((C3(1,i-1)+((C1(1,i-1)+(C2(1,i-
        1)*alphai(1,i))+(Cegr(1,i-1)*alphae(1,i-1))+(Cunb(1,i-1)
        *alphaunb(1,i-1))-(Ru1*N2(1,i)))*(T1(1,i)*((V1(1,i)/V23(1,i))
        ^(gamma-1))))+((C5(1,i-1))*Tref))/((C2(1,i-1)*(alphai(1,i)))
        +(Cegr(1,i-1)*alphae(1,i-1))+(Cunb(1,i-1)*alphaunb(1,i-1))
        +C4(1,i-1)-(Ru1*N3(1,i)))))))/(C1(1,i)+(C2(1,i)*alphai(1,i+1))
        +(Cegr(1,i)*alphae(1,i))+(Cunb(1,i)*alphaunb(1,i))));
        % update equation in terms of state variables T1, theta23 &alphai

 V=Vc*(1+(0.5*(rc-1)*(R+1-(cos(theta))-(((R^2)-(sin(theta)).^2).^.5))));

        v = Vivc./V;
        Nr = ((Pin*Vivc)./(Ru2*(T1up(1,i+1).*N2(1,i))));
        %-----------Import Data from Spreadsheets-----------
        %column         (row)                   / constant
            m(1,i)=CO(I);
            no2(1,i)=((((12.4325*((alphai(1,i+1)*(1-PHI(1,i-1)))+
                alphaunb(1,i)+1))+alphai(1,i+1)*(Sigma(1,i-1)*
                PHI(1,i-1))/2)*Nr)./Vtdc);
            Epsilon(1,i)=OO(I)*(Mass(1,i)/32);
            Gamma_raw(1,i)=CO(I)*(Mass(1,i)/28);
            Gamma(1,i)=Gamma_raw(1,i)*(no2(1,i)/Epsilon(1,i));
            Sigma(1,i-1)=Gamma(1,i)/(PHI(1,i-1)*alphai(1,i+1));
            nco=((alphai(1,i+1)*(Sigma(1,i-1)*PHI(1,i-1)))./V);
            nf=(((PHI(1,i)+alphaunb(1,i)*PHI(1,i-1))*Nr)./V);
            No2=((((12.4325*((alphai(1,i+1)*(1-PHI(1,i-1)))
               +alphaunb(1,i)+1))+alphai(1,i+1)*(Sigma(1,i-1)*
```

```
            PHI(1,i-1))/2)*Nr)./V);
        nh2o=(((8.955*alphai(1,i+1)*(PHI(1,i-1)))*Nr)./V);
        CO2 = (A.*exp(-Ea./(T1up(1,i+1).*(v.^(gamma-1))))).*
            (((7.955*(PHI(1,i)+alphai(1,i+1)*PHI(1,i-1))-Gamma(1,i))
            *Nr)./V))./N;
    [Ix,IF,Itotal]=TrapezoidalIntegrationSimplefxn(CO2,theta); clear Ix
        ind=find(IF>=Kth,1);
        thetaSOC(1,i+1)=theta(ind)      % SOC for unsimplified integral
        Vsoc(1,i+1)=(Vc*(1+0.5*(rc-1)*(R+1-cos(thetaSOC(1,i+1))
             -(R^2-sin(thetaSOC(1,i+1))^2)^.5)));

        nCO2(1,i)=(((7.955*(PHI(1,i)+alphai(1,i+1)*PHI(1,i-1))
                 -Gamma(1,i))*Nr)./Vsoc(1,i+1));

% variable combustion duration for 10-90% MFB
      dtheta1(1,i+1)=((3.38031170622534e-55)*
          (.0001665217021832O6^PHI(1,i))*(.998447810361586^(((V1(1,i)/
          Vsoc(1,i+1))^(gamma-1))*T1up(1,i+1)))*
          (1.43866188620208^(thetaSOC(1,i+1)*(180/pi))))*(pi/180);
         % predicts the combustion duration using equivalence ratio,
          thetaSOC and temperature at SOC
      if dtheta1(1,i+1)>.75;
         dtheta(1,i+1)=25*pi/180;
      else
         dtheta(1,i+1)=dtheta1(1,i+1);
      end

    theta23(1,i+1)=thetaSOC(1,i+1)+dtheta(1,i+1);   %radians
    % update equation for unsimplified integral
      V23(1,i+1)=(Vc*(1+0.5*(rc-1)*(R+1-cos(theta23(1,i+1))-
      (R^2-sin(theta23(1,i+1))^2)^.5)));

      alphaiup(1,i+1) =(.1010700925*Tin(1,i))/((((((C2(1,i-
          1)*(alphai(1,i)))+(Cegr(1,i-1)*alphae(1,i-1))+(Cunb(1,i-1)
          *alphaunb(1,i-1))+C4(1,i-1)-(Ru1*N3(1,i)))*T1(1,i))/(z(1,i)*
          (V1(1,i)/V23(1,i))*(C3(1,i-1)+((C1(1,i-1)+(C2(1,i-1)
          *alphai(1,i))+(Cegr(1,i-1)*alphae(1,i-1))+(Cunb(1,i-1)
          *alphaunb(1,i-1))-(Ru1*N2(1,i)))*(T1(1,i)*((V1(1,i)/V23(1,i))
          ^(gamma-1))))+(C5(1,i-1))*Tref)))^((gamma-1)/gamma))*
          ((C3(1,i-1)+((C1(1,i-1)+(C2(1,i-1)*alphai(1,i))+(Cegr(1,i-1)
          *alphae(1,i-1))+(Cunb(1,i-1)*alphaunb(1,i-1))-
          (Ru1*N2(1,i)))*(T1(1,i)*((V1(1,i)/V23(1,i))^(gamma-1))))+
          ((C5(1,i-1))*Tref))/((C2(1,i-1)*(alphai(1,i)))+(Cegr(1,i-1)
          *alphae(1,i-1))+(Cunb(1,i-1)*alphaunb(1,i-1))+C4(1,i-1)
          -(Ru1*N3(1,i)))));
      % update equation in terms of state variables T1, theta23& alphai

%-----------Output Equations-----------
P3op(1,i)=(z(1,i)*(V1(1,i)/V23(1,i))*Pin*((C3(1,i-1)+((C1(1,i-1)+
    (C2(1,i-1)*alphai(1,i))+(Cegr(1,i-1)*alphae(1,i-1))+
    (Cunb(1,i-1)*alphaunb(1,i-1))-(Ru1*N2(1,i)))*(T1(1,i)*((V1(1,i)/
    V23(1,i))^(gamma-1))))+((C5(1,i-1))*Tref))/(((C2(1,i-1)
    *(alphai(1,i)))+(Cegr(1,i-1)*alphae(1,i-1))+(Cunb(1,i-1)
    *alphaunb(1,i-1))+C4(1,i-1)-(Ru1*N3(1,i)))*T1(1,i))));
    % output equation in terms of state variables T1, theta23, alphai
theta23op(1,i)=thetaSOC(1,i)+dtheta(1,i);
    % output equation for unsimplified integral
W34op(1,i)=((P4(1,i)*V4(1,i))-(P3(1,i)*V23(1,i))+(P2(1,i)*V23(1,i))-
     (.01157*V4(1,i))+(.01157*V4(1,i))-(Pin*V1(1,i))+(Pin*(1-gamma)
     *(V1(1,i)-V4(1,i))))/(1-gamma);
```

```
        % output equation for gross work
    W34op2(1,i)=((((V4(1,i)*((V23(1,i)/V4(1,i))^gamma))-V23(1,i))*
        (z(1,i)*(V1(1,i)/V23(1,i))*Pin*(C3(1,i-1)+((C1(1,i-1)+(C2(1,i-1)
        *alphai(1,i))+(Cegr(1,i-1)*alphae(1,i-1))+(Cunb(1,i-1)
        *alphaunb(1,i-1))-(Ru1*N2(1,i)))*(T1(1,i)*((V1(1,i)/V23(1,i))
        ^(gamma-1))))+((C5(1,i-1))*Tref))) + (Pin*((V23(1,i)*
        ((V1(1,i)/V23(1,i))^gamma))-V1(1,i)+((1-gamma)*(V1(1,i)-V4(1,i))))
        *((((C2(1,i-1)*(alphai(1,i)))+(Cegr(1,i-1)*alphae(1,i-1))
        +(Cunb(1,i-1)*alphaunb(1,i-1))+C4(1,i-1)-Ru1*N3(1,i)))*T1(1,i)))))
        /((((C2(1,i-1)*(alphai(1,i)))+(Cegr(1,i-1)*alphae(1,i-1))
        +(Cunb(1,i-1)*alphaunb(1,i-1))+C4(1,i-1)-(Ru1*N3(1,i)))*T1(1,i))
        *(1-gamma)));
    PRRop(1,i)=(((z(1,i)*(V1(1,i)/V23(1,i))*Pin*((C3(1,i-1)+((C1(1,i-1)
         +(C2(1,i-1)*alphai(1,i))+(Cegr(1,i-1)*alphae(1,i-1))+(Cunb(1,i-1)
         *alphaunb(1,i-1))-(Ru1*N2(1,i)))*(T1(1,i)*((V1(1,i)/V23(1,i))^
         (gamma-1))))+((C5(1,i-1))*Tref))/(((C2(1,i-1)*(alphai(1,i)))+
         (Cegr(1,i-1)*alphae(1,i-1))+(Cunb(1,i-1)*alphaunb(1,i-1))
         +C4(1,i-1)-(Ru1*N3(1,i)))*T1(1,i))))-Psoc(1,i))*2*pi*100)
         /(dtheta(1,i)*360);

    Wigef(1,i)=((((V4(1,i)*((V23(1,i)/V4(1,i))^gamma))-V23(1,i))*(z(1,i)
        *(V1(1,i)/V23(1,i))*Pin*(C3(1,i-1)+((C1(1,i-1)+(C2(1,i-1)
        *alphai(1,i))+(Cegr(1,i-1)*alphae(1,i-1))+(Cunb(1,i-1)
        *alphaunb(1,i-1))-(Ru1*N2(1,i)))*(T1(1,i)*((V1(1,i)/V23(1,i))
        ^(gamma-1))))+((C5(1,i-1))*Tref))) + (Pin*((V23(1,i)*
        ((V1(1,i)/V23(1,i))^gamma))-V1(1,i)+((1-gamma)*(V1(1,i)-
        V4(1,i))))*((((C2(1,i-1)*(alphai(1,i)))+(Cegr(1,i-1)*alphae(1,i-1))
        +(Cunb(1,i-1)*alphaunb(1,i-1))+C4(1,i-1)-(Ru1*N3(1,i)))*T1(1,i)))))
        /((((C2(1,i-1)*(alphai(1,i)))+(Cegr(1,i-1)*alphae(1,i-1))
        +(Cunb(1,i-1)*alphaunb(1,i-1))+C4(1,i-1)-(Ru1*N3(1,i)))*T1(1,i))
        *(1-gamma)))/((Nf(1,i))*100*LHV);
        % output equation for indicated gross efficiency
 end

% prepare units for graphs
theta23(cycles+1)=[];
theta23=theta23*(180/pi);

dtheta(cycles+1)=[];
dtheta=dtheta*(180/pi);

thetaSOC=thetaSOC*(180/pi);
P3=P3*100;
cycle=1:cycles;

% Volume Pressure and Temperature Traces

%--------Plotting output traces--------

  %------------Plotting Volume trace-------------------

        angle=(1:720);
        V=(1:720);
        thetadeg=(1:720);

        for i=1:720

          angle(1,i)=i*(pi/180);

          V(1,i)=Vc*(1+(0.5*(rc-1)*(R+1-(cos(angle(1,i)))-(((R^2)-
```

```
                (sin(angle(1,i)))^2)^.5))));

        end

        figure
        plot(thetadeg,V)
        title('Cylinder Volume vs CAD')
        xlabel('CAD'); ylabel('Cylinder Volume (cm^3)')
        axis([0 720 20 600])
        grid on


%------------Plotting Pressure trace-------------------

        P(1:228)=Pin*100;
                % atmospheric pressure during induction
        for i=229:round((theta23op(1,cycles)-(pi/180))*(180/pi))
           P(1,i)=(Pin*(V1(1,cycles)/V(1,i))^gamma)*100;
                % pressure rise during compression
        end

        P(1,round(theta23op(1,cycles)*(180/pi)))=100*(z(1,cycles)
             *((V1(1,cycles)/V23(1,cycles))^gamma)*((C1+(C2*
             alphai(1,cycles))+(Cegr*alphae(1,cycles-1))+(Cunb*alphaunb
             (1,cycles-1))-(Ru1*N2(1,cycles)))/((((C2*(alphai(1,cycles)))
             +(Cegr*alphae(1,cycles-1))+(Cunb*alphaunb(1,cycles-1))
             +C4(1,cycles-1)-(Ru1*N3(1,cycles)))*T3(1,cycles))-C3-
             (C5*Tref)))*Pin*T3(1,cycles));
        for i=round((theta23op(1,cycles)+(pi/180))*(180/pi)):476
          P(1,i)=(P3(1,cycles)*((V23(1,cycles)/V(1,i))^gamma));
                % pressure fall during expansion
        end

        for i=477:704
          P(1,i)=Pin*100;
        end

        P(704:720)=Pin*100;     % atmospheric pressure during exhaust

        figure
        plot(thetadeg,P)
        title('Pressure vs CAD')
        xlabel('CAD'); ylabel('Pressure (bar)')
        axis([0 720 0 62])
        grid on

  %------------Plotting Temperature trace-------------------
          T=zeros(1,720);

        for i=1:228
           T(1,i)=((C1*Tin(1,cycles)+(C2*alphai(1,cycles)*X*T5(1,cycles))
           +(Cegr*alphae(1,cycles)*Tegr)+(Cunb*alphaunb(1,cycles)*X
           *T5(1,cycles)))/(C1+(C2*alphai(1,cycles))+(Cegr*alphae(1,
           cycles))+(Cunb*alphaunb(1,cycles))));
        end

        for i=229:round((theta23op(1,cycles))*(180/pi))
          T(1,i)=T1(1,cycles)*(V1(1,cycles)/V(1,i))^(gamma-1);
                % temperature rise during compression
        end
```

```
            T(1,round(theta23op(1,cycles)*(180/pi)))=((C3+((C1+(C2
               *alphai(1,cycles-1))+(Cegr*alphae(1,cycles-1))
               +(Cunb*alphaunb(1,cycles-1))-(Ru1*N2(1,cycles)))
               *T2(1,cycles))+(C5*Tref))/((C2*(alphai(1,cycles-1)))
               +(Cegr*alphae(1,cycles-1))+(Cunb*alphaunb(1,cycles-1))+
               C4-(Ru1*N3(1,cycles))));
        for i=round((theta23op(1,cycles)+(pi/180))*(180/pi)):476
            T(1,i)=T3(1,cycles)*((V23(1,cycles)/V(1,i))^(gamma-1));
            % temperature fall during expansion
        end

        for i=477:720
            T(1,i)=T4(1,cycles)*(Pin/P4(1,cycles))^((gamma-1)/gamma);
            % temperature during exhaust
        end

        figure
        plot(thetadeg,T)
        title('Temperature vs CAD')
        xlabel('CAD'); ylabel('Temperature (K)')
        axis([0 720 400 2300])
        grid on

        save('HCCI_ExhaustTempRUN_Tin460_gpm7.5_X56_ES_1800', 'T1', 'T5',
             'alphai', 'alphae', 'alphaunb', 'P3', 'theta23', 'thetaSOC',
             'Tin', 'cycle', 'gpm', 'PRR', 'dtheta','PHI', 'Wigef',
             'W34op','P')
```

SUBROUTINE

```
% Trapezoidal Rule Algorithm for numerical integration
function [Ix,Ifcumulative,Itotal]=TrapezoidalIntegrationSimplefxn(f,x)
% f=input('Enter the y-data vector (or function values): ');
% x=input('Enter the x-data vector: ');
clear If Ix Ifcumulative Itotal
n=length(f);
If=zeros(length(f),1);
Ifcumulative=zeros(length(f),1);
Ix=x;
if n>=3
% Calculates Integral Using Trapazoidal Integration
for k=1:n-1;
    h=abs(x(k+1)-x(k));
    If(k+1)=h/2*(f(k)+f(1+k));
    if k==1
        Ifcumulative(k+1)=If(k+1);
    else
        Ifcumulative(k+1)=Ifcumulative(k)+If(k+1);
    end
end
else
   h=x(2)-x(1);
    If(2)=h/2*(f(1)+f(2));
    Ifcumulative(2)=If(2);
end
Itotal=sum(If);
clear n k h f
```

APPENDIX C
HCCI TEST CASES

MODEL OPERATION INSTRUCTIONS

These instructions are given to provide clarity to the operation of the model attached in Appendix B. First, the number of engine cycles to be considered should be entered next to the variable *cycles.* The engine geometry, fuel properties, and similar parameters can be adjusted in the Constants section if a Hatz1D50Z engine operating on PRF96 fuel is not desired. If the engine geometry and valve timing is altered, then values in the 4-5: Isentropic Exhaust section will need to be updated as well. With these parameters defined, the inlet conditions can be entered in the main for loop of the code. These input variables are the intake temperature (*Tin),* external EGR fraction (*alphae),* and fueling rate (*gpm).* Perturbations can be added by un-commenting the Gaussian random number terms that are immediately above or below the respective input. The code can then be run to produce the output values. It must be noted that the subroutine at the end of Appendix B must be in the same folder as the main code in order for it to compile. Additionally, if the use of the residual feed forward mechanism is desired, the spreadsheets must also be in the same folder. The following test cases are provided with sample outputs from the code for a few cases to ensure that the model is operating correctly.

CASE 1:

Inputs:

- Tin = 490 K
- alphae = 0
- gpm = 6 grams/min

Outputs:

- thetaSOC = 362.9 CAD
- T5 = 668.9041 K
- W34op = 8.775014 KN-cm
- Wigef = 0.294741
- PRR = 0.164561 bar/CAD
- Gamma = 1.97E-05 moles
- ER = 81.94699 %

CASE 2:

Inputs:

- Tin = 478 K
- alphae = 0
- gpm = 7.5 grams/min

Outputs:

- thetaSOC = 363.65 CAD
- T5 = 721.6166 K
- W34op = 12.44575 KN-cm
- Wigef = 0.334428
- PRR = 0.810691 bar/CAD
- Gamma = 1.14E-05 moles
- ER = 91.64658 %

BIBLIOGRAPHY

[1] McCuen, M. J., Z. Sun, and G. Zhu. "Chemical Composition Modeling of a Two-Zone Control-Oriented Mixing Model for Homogeneous Charge Compression Ignition Engines." *Proceedings of the 2010 ASME Dynamic Systems and Control Conference* (2010).

[2] Yao, M., Z. Zhang, and H. Liu. "Progress and Recent Trends in Homogeneous Charge Compression Ignition (HCCI) Engines." *Progress in Energy and Combustion Science* 35 (2009): 398-437.

[3] Attebery, A. D. "Investigating the Effects of Internally Trapped Residuals on the Performance of a Homogeneous Charge Compression Ignition (HCCI) Engine." Thesis. Missouri University of Science and Technology, 2012.

[4] Bettis, J. B. "Thermodynamic Based Modeling for Nonlinear Control of Combustion Phasing in HCCI Engines." Thesis. Missouri University of Science and Technology, 2010.

[5] Anderlohr, J. M, A. Pires da Cruz, R. Bounaceur, and F. Battin-Leclerc. "Thermal and Kinetic Impact of CO, CO_2, and H_2O on the Postoxidation of IC-Engine Exhaust Gases." *Combustion Science and Technology* 182 (2010): 39-59.

[6] Subramanian, G., A. Pires da Cruz, R. Bounaceur, and L. Vervisch. "Chemical Impact of CO and H_2 Addistion on the Auto-Ignition Delay of Homogeneous n-Heptane/Air Mixtures." *Combustion Science and Technology* 179 (2007): 1937-1962.

[7] Ernst, A. C. Personal Communication. 2013-2015.

[8] Tsurushima, T. "A New Skeletal PRF Kinetic Model for HCCI Combustion." *Proceedings of the Combustion Institute* 32 (2007): 2835-2841.

[9] Heywood, J. B. "Internal Combustion Engine Fundamentals." McGraw-Hill, 1988.

[10] Onishi, S., S. H. Jo, K. Shoda, P. D. Jo, and S. Kato. "Active Thermo-Atmosphere Combustion (ATAC)- A New Combustion Process for Internal Combustion Engines". *SAE Technical Papers* (1979).

[11] Najt, P. M., and D. E. Foster. "Compression-Ignited Homogeneous Charge Combustion." *SAE Technical Papers* (1983).

[12] Olesky, L. M., J. Vavra, D. Assanis, and A. Babajimopoulos. “Effects of Charge Preheating Methods on the Combustion Phasing Limitations of an HCCI Engine With Negative Valve Overlap.” *Journal of Engineering for Gas Turbines and Power* (2012).

[13] Hellström, E., J. Larimore, A. Stefanopoulou, J. Sterniak, and L. Jiang. “Quantifying Cyclic Variability in a Multicylinder HCCI Engine With High Residuals.” *Journal of Engineering for Gas Turbines and Power* (2012).

[14] Zhao, H., Z. Peng, and N. Ladommatos. “Understanding of Controlled Autoignition Combustion in a Four-Stroke Gasoline Engine.” *Proceedings of the Institution of Mechanical Engineers* (2001).

[15] Yang, X., and G. Zhu. “SI and HCCI Combustion Mode Transition Control of an HCCI Capable SI Engine.” *IEEE Transaction on Control Systems Technology* 21 (2013).

[16] Saxena, S., and I. D. Bedoya. “Fundamental Phenomena Affecting Low Temperature Combustion and HCCI Engines, High Load Limits, and Strategies for Extending These Limits.” *Progress in Energy and Combustion Science* (2013).

[17] Xie, H., Lu, J., Chen, T., Li, L., Li, C., and H. Zhao. “Chemical Effects of the Incomplete-Oxidation Products in Residual Gas on the Gasoline HCCI Auto-Ignition.” *Combustion Science and Technology* 186 (2014): 273-296.

[18] He, X., M. T. Donovan, B. T. Zigler, T. R. Palmer, S. M. Walton, M. S. Wooldridge, and A. Atreya. “An Experimental and Modeling Study of Iso-Octane Ignition Delay times Under Homogeneous Charge Compression Ignition Conditions.” *Combustion and Flame* 142 (2005): 266-275.

[19] Shaver, G. M. “Physics-Based Modeling and Control of Residual-Affected HCCI Engines Using Variable Valve Actuation.” Dissertation. Stanford University, (2005).

[20] Eaton, S. and B. Bunting. “Hatz HCCI Engine Pistons –New Design-.” Oak Ridge National Laboratory. 2009. *PowerPoint* file.

[21] Vance, J., P. He, B. Kaul, S. Jagannathan, and J. Drallmeier. “Neural Network-Based Output Controller for Lean Operation of Spark Ignition Engines.” *Proceedings of the American Controls Conference* (2006): 1898-1905.

[22] Bettis, J. B., J. A. Massey, J. A. Drallmeier, J. Sarangapani. “Thermodynamic Based Modeling for Nonlinear Control of Combustion Phasing in HCCI Engines.” *Proceedings of the 2010 Technical Meeting of the Central States Section of the Combustion Institute* (2010).

[23] Subcommittee on Technical Data. “Technical Data Book- Petroleum Refining.” American Petroleum Institute. 1970.

[24] McCuen, M. J., Sun, Z., and G. Zhu. “Control-Oriented Mixing Model for Homogeneous Charge Compression Ignition Engines.” *American Control Conference* (2010).

[25] Fox, J. W., Wai, K. C., and J. B. Heywood. “A Model for Predicting Residual Gas Fraction in Spark-Ignition Engines.” *SAE Paper* 931025

[26] Waero, R. R. “The Effect of Spark Timing on Residual Gas Fraction.” Thesis. University of Michigan, Ann Arbor. 1997.

[27] Shaver, G., Roelle, M., Caton, P., Kaahaaina, N., Ravi, N., Hathout, J., et al. “A physics-based approach to the control of homogeneous charge compression ignition engines with variable valve actuation.” *International Journal of Engine Research* (2005): 361-375.

[28] Turns, S. R. “An Introduction to Combustion: Concepts and Application.” McGraw-Hill, 2nd edition, 2000.

[29] Kee, R. J., Miller, J. A., and T. H. Jefferson. “CHEMKIN: A General-Purpose, Problem-Independent, Transportable, Fortran Chemical Kinetics Code Package.” Sandia Laboratories. 1980.

[30] Massey, J. A. “Development of a Simple Vibration Model for Predicting the Structural Dynamics of an HCCI Engine.” Dissertation. Missouri University of Science and Technology, 2011.

[31] N.p. *How Auto Work*. <http://howautowork.com/3.Engine_Performance_and_Driveablity/ch_2/Geometrical_Properties_of_Reciprocating_Engines_2.html>

[32] Chapra, S., and R. Canale. *Numerical Methods for Engineers*. McGraw-Hill Science, 2009. Print.

[33] Primary Reference Fuels (PRF): iso-Octane/ n-Heptane Mixtures. <https://combustion.llnl.gov/archived-mechanisms/surrogates/prf-isooctane-n-heptane-mixture>

VITA

Krishawn Michele Ridenhour Goodwin was born in St. Louis, Missouri on April 29, 1990. She graduated from Eureka High School in Eureka, Missouri in May 2008. She worked as an Engineering Intern for Ameren UE at Callaway Nuclear Power Plant in Fulton, Missouri. In May 2012, she received her B.S. in Mechanical Engineering from Missouri University of Science and Technology (formerly known as University of Missouri-Rolla).

During the summer of 2012, she worked as a Mechanical Engineering Intern at Holcim Inc. in Ste. Genevieve, Missouri. In 2014 she worked as a Process Engineer for Ford Motor Company in Claycomo, Missouri while finishing the research for this study. She was wed in June of 2014 to Brandon Goodwin. She began work as an Account Manager at Air Fixture, LLC just prior to receiving her M.S. degree in Mechanical Engineering from Missouri University of Science and Technology in August of 2015.